INFORMATION TO USERS

This material was produced from a microfilm copy of the original document. While the most advanced technological means to photograph and reproduce this document have been used, the quality is heavily dependent upon the quality of the original submitted.

The following explanation of techniques is provided to help you understand markings or patterns which may appear on this reproduction.

1. The sign or "target" for pages apparently lacking from the document photographed is "Missing Page(s)". If it was possible to obtain the missing page(s) or section, they are spliced into the film along with adjacent pages. This may have necessitated cutting thru an image and duplicating adjacent pages to insure you complete continuity.

2. When an image on the film is obliterated with a large round black mark, it is an indication that the photographer suspected that the copy may have moved during exposure and thus cause a blurred image. You will find a good image of the page in the adjacent frame.

3. When a map, drawing or chart, etc., was part of the material being photographed the photographer followed a definite method in "sectioning" the material. It is customary to begin photoing at the upper left hand corner of a large sheet and to continue photoing from left to right in equal sections with a small overlap. If necessary, sectioning is continued again – beginning below the first row and continuing on until complete.

4. The majority of users indicate that the textual content is of greatest value, however, a somewhat higher quality reproduction could be made from "photographs" if essential to the understanding of the dissertation. Silver prints of "photographs" may be ordered at additional charge by writing the Order Department, giving the catalog number, title, author and specific pages you wish reproduced.

5. PLEASE NOTE: Some pages may have indistinct print. Filmed as received.

University Microfilms International
300 North Zeeb Road
Ann Arbor, Michigan 48106 USA
St. John's Road, Tyler's Green
High Wycombe, Bucks, England HP10 8HR

Downloaded from SHAREOK. Persistent Handle URL: https://hdl.handle.net/11244/4277

77-21,378

HENDRICKSON, Paul Edwin, 1941-
MEASUREMENT OF THE THERMODYNAMIC DERIVATIVE SPECTRA OF THE 6.3 μm WATER VAPOR BAND.

The University of Oklahoma, Ph.D., 1977
Physics, optics

Xerox University Microfilms, Ann Arbor, Michigan 48106

THE UNIVERSITY OF OKLAHOMA

GRADUATE COLLEGE

MEASUREMENT OF THE THERMODYNAMIC DERIVATIVE SPECTRA OF THE 6.3 μm WATER VAPOR BAND

A DISSERTATION

SUBMITTED TO THE GRADUATE FACULTY

in partial fulfillment of the requirements for the

degree of

DOCTOR OF PHILOSOPHY

BY

PAUL EDWIN HENDRICKSON

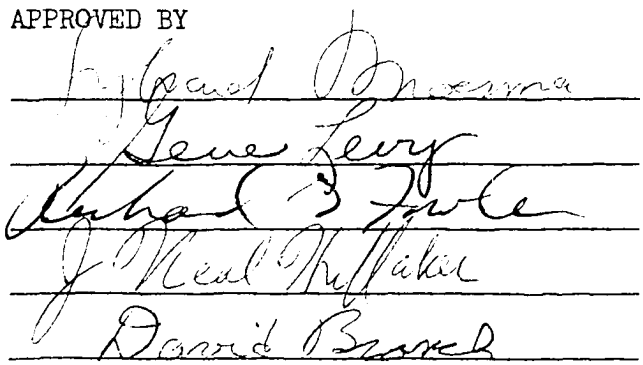
Norman, Oklahoma

1977

MEASUREMENT OF THE THERMODYNAMIC DERIVATIVE SPECTRA OF THE

6.3 μm WATER VAPOR BAND

APPROVED BY



DISSERTATION COMMITTEE

ACKNOWLEDGEMENT

I sincerely acknowledge Dr. Sybrand Broersma for his invaluable contributions throughout this research. His dedication and guidance have been superb.

I am grateful to Larry Walls for his technical advice during the experiment and for his contribution to the computer program which handled the data.

I also thank Dr. David Wilson for his advice and for being a source of encouragement.

I acknowledge Dr. Fritz Krause for financial support via the NASA contract.

To my family, Patricia, Brian and Cynthia, I will always be indebted for their understanding.

TABLE OF CONTENTS

Page

ACKNOWLEDGEMENT iii

LIST OF TABLES vi

LIST OF FIGURES vii

ABSTRACT xi

Chapter

I. Introduction 1

A. Problem Perspective 1

B. Calculation 6

C. Experiment 6

II. Calculation 11

A. Introduction 11

B. Calculation Method 12

III. Experiment 26

A. Basic Experimental Apparatus 26

B. Component Design 35

1. Infrared Absorption Cell Chamber 35

2. Production of Water Vapor 39

3. Determination of Humidity 44

4. Thermal Control 52

5. Pressure Control 54

6. HgCdTe Detector 55

7. Detector Extension Dewar 60

TABLE OF CONTENTS (Cont'd.)

Page

8. General Operating Procedure 63

C. Data Acquisition. 67

IV. Analysis of Results 70

A. General Procedure 70

B. Trends in Reference Spectra 72

C. Absorption. 82

D. Derivative Spectra. 90

E. Conclusions 101

Appendix

I. SPECTROSCOPIC UNITS 103

II. EQUIPMENT LIST. 104

REFERENCES. 106

LIST OF TABLES

TABLE		Page
I.	Data Sequence.	74
II.	Integrated Absorptance for 1.005 m Column.	83
III.	Values of c, p and T for Derivative Spectra.	91

LIST OF FIGURES

Figure		Page
1.	Absorptance as a function of concentration.	15
2.	The partial derivative of the absorptance with respect to concentration.	16
3.	The partial derivative of the absorptance with respect to pressure	17
4.	The partial derivative of the absorptance with respect to temperature.	18
5.	The second partial derivative of absorptance with respect to concentration.	20
6.	The second partial derivative of absorptance with respect to concentration and pressure	21
7.	The second partial derivative of absorptance with respect to concentration and temperature.	22
8.	The second partial derivative of absorptance with respect to pressure	23
9.	The second partial derivative of absorptance with respect to pressure and temperature	24
10.	The second partial derivative of absorptance with respect to temperature.	25
11.	Absorption cell - principle of operation.	28
12.	Thermocouple positions within the absorption cell . . .	32
13.	Absorption cell - cross sectional view.	36

LIST OF FIGURES (Cont'd)

Figure		Page
14.	Absorption cell	37
15.	Absorption cell - flange union area	38
16.	Humidity chamber	40
17.	Humidity chamber - principle of operation	41
18.	Humidity chamber - range of operation	43
19.	Water vapor flow system	45
20.	Dew point hygrometer - principle of operation	47
21.	Dew point hygrometer - gas sampling manifold	50
22.	Absorption cell - temperature equilibrium	53
23.	HgCdTe detector relative spectral response	56
24.	HgCdTe detector bias circuit	57
25.	Infrared detector housing base plate for the elliptical mirror mount	58
26.	Infrared detector housing top plate	59
27.	LWP filter holder	61
28.	Liquid nitrogen extension dewar	62
29.	Liquid nitrogen extension dewar	64
30.	Liquid nitrogen extension dewar in its operating position	65
31.	Absorptance as a function of band pass	73
32.	Apparent absorptance of vacuum vs vacuum reference scans	76

LIST OF FIGURES (Cont'd)

Figure		Page
33.	Apparent absorptance of dry nitrogen vs vacuum reference scans	78
34.	Trends in the 15 °C reference scans	79
35.	Trends in the 40 °C and the 65 °C reference scans	81
36.	Absorptance as a function of concentration	84
37.	Absorptance as a function of pressure	85
38.	Absorptance as a function of temperature	86
39.	Absorptance as a function of concentration and pressure	87
40.	Absorptance as a function of pressure	88
41.	The partial derivative of the absorptance with respect to concentration	92
42.	The partial derivative of the absorptance with respect to pressure	93
43.	The partial derivative of the absorptance with respect to temperature	94
44.	The second partial derivative of the absorptance with respect to concentration	96
45.	The second partial derivative of the absorptance with respect to concentration and pressure	97
46.	The second partial derivative of the absorptance with respect to pressure	98

LIST OF FIGURES (Cont'd)

Figure Page

47. The second partial derivative of the absorptance with respect to pressure and temperature. 99

48. Experimental absorptance curve by Burch, et al. 100

ABSTRACT

In environmental detection techniques one utilizes spectral characteristics that are related to concentration, pressure, and temperature. Appropriately chosen segments of a vibrational absorption band can provide transmission averages over a limited number of rotational lines for which the dependence upon such thermodynamic parameters is meaningful.

Here a medium resolution infrared absorption experiment has been performed to examine these relationships. We have measured the absorption in the 6.3 μm band of a one meter column of water vapor as a function of concentration (c), pressure (p), and temperature (T). From the measured absorption the first derivatives with respect to c, p, and T as well as the second derivatives with respect to cc, pp, cp, and pT have been obtained.

Calculations based on high resolution data were used for comparison. Where the transmission is sufficiently large and the band pass not too narrow, individual rotational lines can be used as a starting base for the calculation.

We used the line parameters of the 720 strongest rotational lines in the band. If the absorptance is less than 0.6, the measured band absorption fits the calculated value within 10%, the spectral absorption fits within 15%, the first derivatives within 20% and the second derivatives, depending upon their size, within 25 - 40%.

Chapter I Introduction

A. Problem Perspective

The purpose of the investigation presented in this dissertation is twofold: experimental and computational. While some technical difficulties had to be solved, on the whole the experimental phase was rather straightforward. It consisted of measuring the infrared absorption of water vapor in the 6.3 μm band as a function of concentration, pressure and temperature. The extent of the effort was considerable and is discussed in detail in chapters III and IV. The computational procedure was designed by Broersma and Walls.[1] For the 6.3 μm band we wished to obtain the derivative spectra using the characteristic values for as many rotational lines as was reasonable. We desired to show the applicability of the theory while omitting details. The computational results agree quite well with our experiment and other published experimental work using 720 of the approximately 5000 rotational lines in this particular water vapor band.

For many years major efforts have been devoted to infrared investigations. Quite recently a new urgency has arisen related to environmental remote sensing. Since water is an extremely important resource, investigators are developing methods of remote sensing that will map vapor concentrations in the troposphere. Remote sensing is only one of several methods making such determinations, but it may ultimately prove to be the most economical.

Any method contributing to the knowledge of atmospheric dynamics or the acquisition of valuable meterological data should be considered. Of the techniques presently used, remote sensing offers major potential advantages:[2]

a. The observations are taken remotely, i.e., no instrumentation needs to be placed in the region of the atmosphere to be measured. Remote sensing instrumentation is usually automatic and can without interruption provide fully processed data with a minimum of manpower.

b. Ideally, remote sensing permits the measurement of the relevant parameters of the atmosphere in one, two, or three spatial dimensions, and as a function of time. Excellent resolution and continuity of data in time and/or space are in principle obtainable.

c. A broad range of parameters and constituents of the atmosphere may be sensed. The measurement system does not perturb the parameter being measured.

d. The remote sensing measurements tend to provide a line, area or volume integration. Thus the observations are more representative for a certain region of the medium than those by a single point sensor.

Of the three types of remote sensing: acoustical, radio, and optical, it is felt by Little that optical techniques will eventually become dominant in making measurements in the clear atmosphere. This is based on the applicability of the many interactions of electromagnetic

waves with the constituents of interest. A full range of sensing measurements is conceptually practicable; relatively few measurement techniques have been tested experimentally. It should be emphasized that much of the detailed spectroscopic information needed for remote sensing is not available, and will have to be obtained if the field is to advance efficiently.(3) This investigation is meaningful since the range of the various thermodynamic parameters were chosen so as to reflect the conditions found in the atmosphere. Furthermore, once the derivative spectra, with regard to concentration, pressure and temperature are obtained for a particular case, one should be able to apply these to the set of conditions found locally.

Of added interest to the meterologist is the problem of heat transfer in the atmosphere by infrared radiation. The absorption bands of water vapor are particularly important because its infrared spectrum consists of a large number of widely spaced lines. The vibration-rotation bands with wavelengths up to 10 μm and the 6.3μm band play a major role in governing the heat balance of the lower atmosphere.(4)

Derivative spectra are also of vital importance in the particular remote sensing technique by optical cross-correlation methods.(5) Here the average thermodynamic properties are obtained by expanding the absorption coefficient in a Taylor series and evaluating the fluctuating components as derivatives of the average absorption coefficient. If $k(x,t,\nu)$ is the generalized extinction coefficient, then the light intensity incident upon a detector is given by the

usual expression

$$I_d = I_{source} \cdot \exp\left[-\int k(x,t,\nu)dl\right] \qquad (1)$$

The detected signal thus measures emission or extinction processes along the entire line of sight. In a cross-beam arrangement the desired local information is retrieved by considering the fluctuation of the integrated detector signal and correlating the response of two sensors with intersecting lines of sight. In the case of ideal detectors, this fluctuation is related to the fluctuation of the extinction coefficient

$$k' = k - \langle k \rangle = k(c,p,T) - \overline{k}(c,p,T) \qquad (2)$$

as caused by a fluctuation δ in the various thermodynamic parameters c, p, and T, where $\delta c = c - \bar{c}$, $\delta p = p - \bar{p}$, and $\delta T = T - \bar{T}$. Thus cross-beam spectroscopy is based on the relationship between optical and thermodynamic fluctuations. This can be expressed as a Taylor series expansion of the general relationship (2) around the average values:

$$k'(c,p,T,\nu) = k'(x,t,\nu) + \qquad (3)$$
$$(\delta c\frac{\partial}{\partial c} + \delta p\frac{\partial}{\partial p} + \delta T\frac{\partial}{\partial T})k +$$
$$\tfrac{1}{2}(\delta c\frac{\partial}{\partial c} + \delta p\frac{\partial}{\partial p} + \delta T\frac{\partial}{\partial T})^2 k$$

Thus the desired thermodynamic properties can in principle be obtained by expressing the measured cross-correlation coefficient in terms of these derivatives.

The technique has been used for studying local turbulence properties in aerodynamic flows.[6] Here two optical beams which interact with the flow through absorption or scattering, are crossed at the point of interest. Cross correlation of the two detector output signals yields the response from the region of intersection of the two beams only. This concept has also been used in atmospheric airglow detection in passive form.[7]

A further concern of this investigation was to employ a spectral resolution that would be most useful to other atmospheric research. Extensive high resolution work has been performed over a period of years. And though data exists for only limited values of c, p, and T, it was not our purpose to extend this to a broader range of values of these parameters. Rather our concern was to explore the fundamental thermodynamic dependence involving absorption and the various derivatives using a simple instrument set for medium resolution. In the final analysis all data was degraded to an equivalent band-pass of 25 cm^{-1}, a value containing several rotational lines but extending only over a part of the vibration band. A search of the literature confirms this as a reasonable choice. For example, in efforts made to determine the relative humidity profile in the troposphere, measurements are used for which the spectral resolution elements are narrow in comparison with the total line width of the absorption band but wide in comparison with a single absorption line.[8]

B. Calculation

For a basis of comparison with experimental results, a technique for calculating infrared absorption as a function of pressure, temperature, and concentration was desirable. Once the technique was developed, we were only limited by the availability of rotational line parameters found in the literature. Thus the results for many vibrational bands may be obtained more quickly using the calculation than changing the equipment as might be necessary for direct measurement.

C. Experiment

For the most part, the technical difficulties which were encountered were not new. Similar problems have been faced by those who endeavored to investigate the behavior of water vapor. To look at the infrared absorption for a very narrow range of thermodynamic parameters would have simplified the problem considerably. However this was not acceptable; our main thrust was to determine the derivative spectra.

The major portion of these problems arises because water is a polar molecule easily giving rise to cell chamber wall contamination. Therefore a major effort was made to accurately determine and continuously monitor the water vapor concentration.

Large errors in the determination of the vapor concentration plagued early investigators whose procedure was to introduce a known volume of distilled water into an evacuated

cell.[9] The water vapor density in the cell was then calculated from the known free volume of the cell. To vary the pressure dry air was then admitted into the cell. As shown by others this procedure produces errors as large as 50%.

More recently, experiments performed by Varanasi and Prasad[10] have indicated that satisfactory results may be obtained by connecting the cell directly to a bottle of liquid water which is maintained at a given temperature. This established the partial pressure of the water in the cell. Sufficiently long times were allowed before a spectral scan to ensure that the water vapor was properly mixed with the broadening gas. The cell was then sealed off from the rest of the experimental set-up. Reproducibility was checked by making spectral scans every day for two or three successive days, thus confirming gas mixture equilibrium in the cell.

Another experimental procedure is described by Benedict et al.[11] Their mode of operation consisted of first heating the cell to 110 ^{o}C in order to avoid condensation, then filling it with steam by displacement. When recording spectra, a continuous stream of vapor from a gently boiling flask of distilled water entered at one end and escaped through the exit window. Even though the problem of the wall absorption was apparently diminished, the use of this system caused a serious restriction in the values for the parameters c, p, and T. Furthermore it is not clear what magnitude of concentration gradients may have existed along the infrared path.

When working with samples of pure water alone

it is possible to determine the absorber concentration, with reasonable good accuracy, from a measurement of the vapor pressure. However, after a gas such as nitrogen has been added to the water sample there arises serious doubts as to the actual concentration that exists in the optical path. These doubts arise not only because of the effect of nitrogen on the process of wall absorption-desorption of water molecules, but also because of the lack of certainty of proper N_2-H_2O mixing.

A serious attempt to overcome these experimental complications was made by Burch et al in 1962.[12] The concentration was determined by directly measuring the dew point of the sample in the absorption cell. This was accomplished by the use of a "well" made of a thin piece of inconel tubing, which was closed on one end and was soldered to the wall of the absorption cell, projecting into the interior. Ether was put into the tube and nitrogen was bubbled through in order to cool it until condensation formed on the outside wall of the tubing, which could be observed through a window in the absorption cell. A thermometer immersed in the ether was used to determine the temperature at which condensation started. Burch demonstrated the magnitude of the effect of wall contamination by injecting a small amount of water directly into an evacuated cell. By considering the volume of the absorption cell, it was possible to calculate the pressure that could be expected from a known quantity of liquid water if one assumed that all the water went into the vapor phase and none were absorbed on the cell walls. In most cases they found that the

gaseous pressures were only 40 to 60 percent as great as the calculated value. This result indicates that approximately one half of the water was absorbed on the cell walls since care was taken to avoid condensation. If the sample was left in the cell, the pressure was found to decrease gradually for a few hours, thus indicating that more absorption was occurring. Various coatings on the interior of the cell were tried in an attempt to diminish this problem. None seemed to change significantly the amount of water absorbed; however, more time was required to "out-gas" the system.

Another method of determining absorber mass was used by Izatt et al.[13] Subsequent to each spectral scan, the water which had been introduced into the cell for the scan was collected in a liquid N_2 cold trap and weighed. This method might have some advantages, however no mention was made concerning a comparison between the amount of sample injected and that recovered. This form of operation would not be advantageous in our experimental set-up.

With the operational difficulties of measuring water vapor clearly in mind, our method is now scrutinized. First of all, as much as possible the essential components of our system were constructed of stainless steel which has relatively low water absorption properties.

At the heart of the system is a dew point hygrometer with automatic read-out which provides continuous monitoring and does not perturb the vapor concentration in the optical path. This is because the hygrometer may sample the gas either at the cell entrance or exit. It judges condensation on a cooled mirror with a photo

electric device.

The concentration gradients at various positions in the infrared path were checked by means of a series of hygristors. This initial investigation established that errors introduced because of gradients had little consequence.

In the modes of operation in which a given amount of water is injected into the cell or the cell is connected directly to a bottle of water, one major disadvantage is the long lead time required for wall absorption-desorption equilibrium to be established. If one desires a large number of measurements, this time loss becomes a substantial hindrance. This plus the added burden of the long continuous operation of the equipment in order to stablize the other thermodynamic parameters rendered this solution impractical in our experiment. It was important that we cut all lead times for thermodynamic equilibria to a minimum. For concentration equilibrium this was accomplished by the vapor cross-flow system. The establishment of pressure and temperature equilibria are less complicated than that of the concentration. The details of the experiment are given in chapter III.

Chapter II Calculation

A. Introduction

We now consider a method of calculating the band absorptance of the 6.3 μm band of water vapor. The water molecule is a non linear triatomic molecule with three normal vibrations: ν_1, ν_2, and ν_3.[14] The 6.3 μm band corresponds to the ν_2 fundamental vibration.

Consider a parallel beam of radiation with intensity I_ν passing through a gaseous medium. I_ν is the intensity per unit frequency interval at wavenumber ν. If I_ν is the incident intensity then after passing through an absorber element du, the decrease in the intensity will be

$$dI_\nu = - k_\nu I_\nu du \tag{4}$$

where k_ν is the coefficient of absorption at wavemumber ν. Near a particular line, k_ν is not constant even over a small ran_ of ν. This occurs because the individual rotational lines can be rather sharp. Of course, pressure broadening, which is the most important broadening factor in our case, smoothes the lines.[15] If equation (4) is integrated over a single line, one obtains the total change dI in the energy of the beam,

$$dI = \int_{Line} dI_\nu d\nu = - I_\nu du \int_{-\infty}^{\infty} k_\nu d\nu \tag{5}$$

where I_ν may be considered constant over the frequency interval of that particular line.

Now we write

$$dI = -I_\nu du \int_{-\infty}^{\infty} k_\nu d\nu = -SI_\nu du \tag{6}$$

where

$$S = \int_{-\infty}^{\infty} k_\nu d\nu \tag{7}$$

and S is known as the strength of the line. If equation (6) is further integrated over all wavenumbers of the vibration-rotation band, the strength of the entire vibrational transition is obtained.

B. Calculation Method

A method of calculating the absorptance of various molecules is developed by reference 1. This method assumes that various parameters of the individual lines in the band are known. The parameters of importance are the line strength, half-width and line positions.

In the calculation, the lines are all assumed to have the Lorentzian line shape:

$$k_\nu = \frac{S}{\pi} \cdot \frac{\alpha}{(\nu - \nu_o)^2 + \alpha^2} \tag{8}$$

As a matter of fact the experimental results are analyzed on this basis and the S and α values derived with it. Here α depends on the mean collision time of the molecules; α is proportional to the number of molecules per unit volume as well as proportional to their mean speed. Therefore at a particular pressure (p) and temperature (T) we have

$$\alpha(p,T) = \alpha_o(p_o,T_o) \left(\frac{p}{p_o}\right) \left(\frac{T_o}{T}\right)^{\frac{1}{2}} \tag{9}$$

Since most infrared spectrometers do not have sufficient resolving power, the actual line shape cannot easily be determined. However, the integrated absorptance for a particular line is nearly independent of the shape of the band pass of the instrument. Therefore the strength and width of the line may be calculated from the observed values.

Returning to the method of the calculation, the following quantities and their thermodynamic dependencies occur:

$$S_i = \text{line strength} = C_s T^{-(3/2)} e^{-(E_i/kT)} \qquad (10)$$

$$\alpha = \text{half-width} = C_\alpha p T^{-\frac{1}{2}} \qquad (11)$$

$$u = \text{absorber mass} = C_u c p T^{-1} \qquad (12)$$

where c, p and T are concentration, total pressure and temperature respectively. E_i denotes the energy level of the lower state of the transition. C_s, C_α and C_u are proportionality constants. See Appendix I for a discussion of the units of S, α and u. Because equations (10), (11) and (12) represent simple power laws, the dependence upon c, p and T of absorptance and its derivatives can be indicated generally.

The calculation of the absorptance $A(\nu_j)$, i.e., the fractional absorption over a wavenumber interval $\Delta\nu$ at wavenumber ν_j, is given by

$$A(\nu_j) = \frac{\sum_i w_i \cdot (a - |\nu_i - \nu_j|)}{a^2} \qquad (13)$$

where w_i = equivalent line width and a = band pass. The sum is over all lines ν_i in the range ν_j - a to ν_j + a. The factor $(a - |\nu_i - \nu_j|)$ is the triangular band pass imposed upon the calculation.

A band pass of 25 cm^{-1} was used for the 6.3 μm H_2O band. With these values $A(\nu_j)$ becomes

$$A(\nu_j) = \frac{1}{625} \sum_i w_i \cdot (25 - |\nu_i - \nu_j|) \qquad (14)$$

The quantities S, u and α are all used in the calculation of the equivalent line width w_i. The functional relationships are rather long and will not be reproduced here. They may be found in reference 1.

Since the 6.3 μm water band consists of unevenly spaced lines, the calculation considers either that the lines are well separated, combining their contributions to the absorption and adding appropriate corrections, or that the lines are close enough to be merged into an equivalent line for which the appropriate parameters can be calculated.

At T = 287.7 ^{o}K and 1 atmosphere pressure, the line parameters are listed in reference 16. In the calculation, the 720 strongest of the 5000 lines were used. Lines with S-values from a maximum of 11,000 cm/gm down to 3 cm/gm (down to 1 cm/gm in the wings) were selected. Figure 1 shows the calculation of absorptance for this pressure and temperature. The values for the absorber masses are listed.

The derivatives of A are found from equation (13), hence involve the derivatives of w_i. Figures 2, 3 and 4 show the results of the calculated first derivatives $c \cdot \left(\frac{\partial A}{\partial c}\right)_{pT}$, $p \cdot \left(\frac{\partial A}{\partial p}\right)_{cT}$, and $T \cdot \left(\frac{\partial A}{\partial T}\right)_{cp}$. This form for the derivatives is useful in that $y\left(\frac{\partial A}{\partial y}\right)$ has the same units as A and all the magnitudes of the absorption fall here in the range - 0.7 to + 0.7.

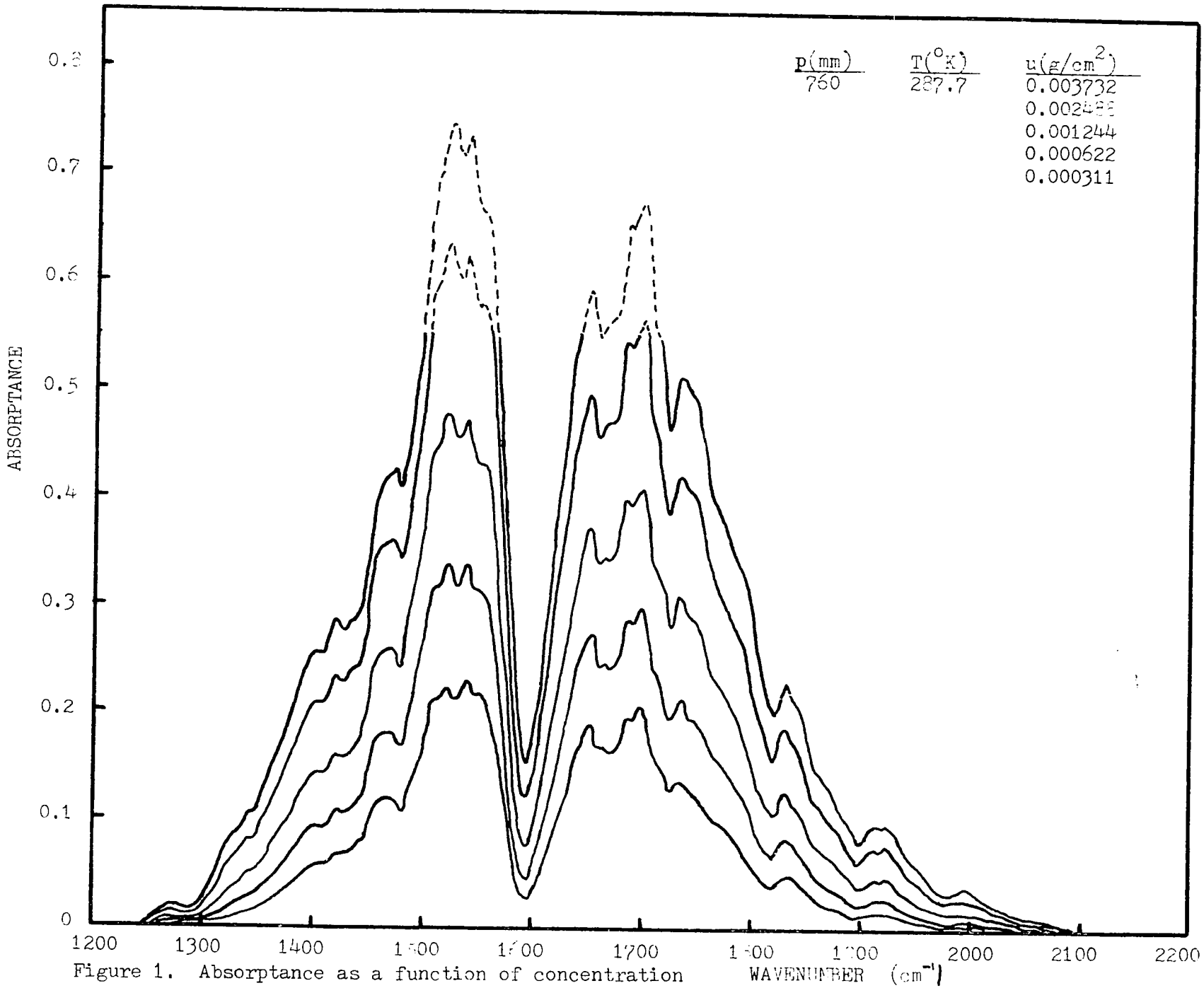


Figure 1. Absorptance as a function of concentration

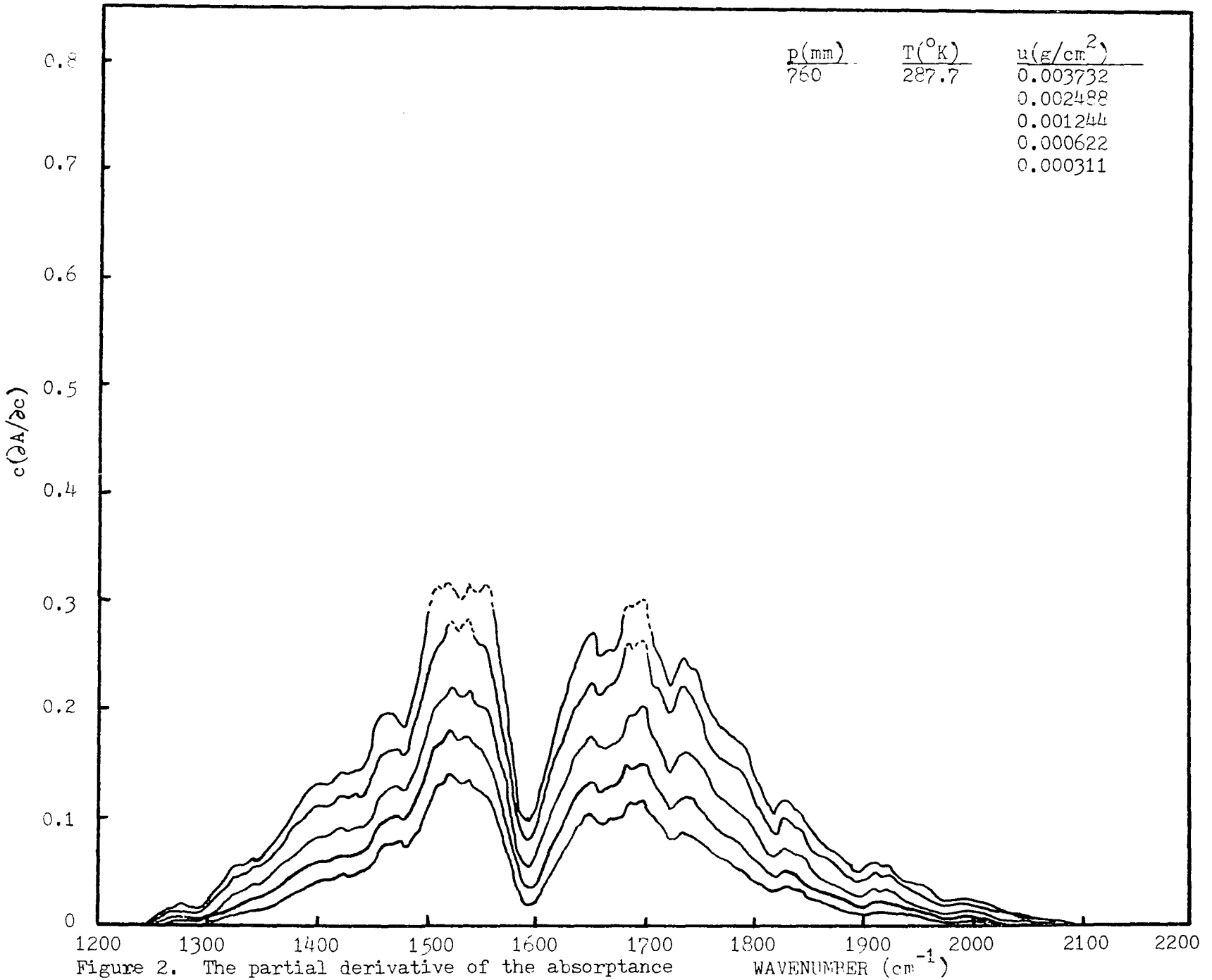


Figure 2. The partial derivative of the absorptance with respect to concentration

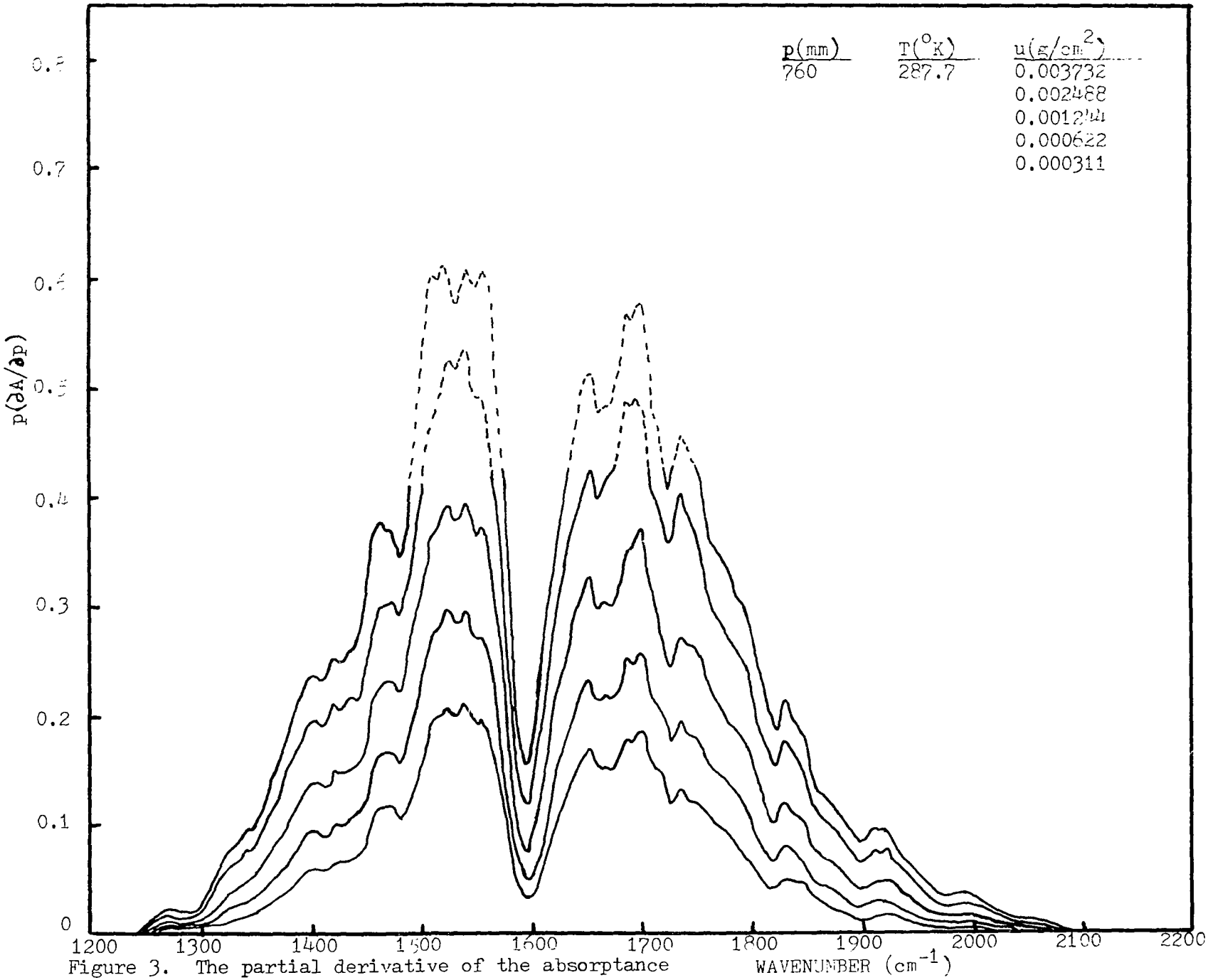


Figure 3. The partial derivative of the absorptance with respect to pressure

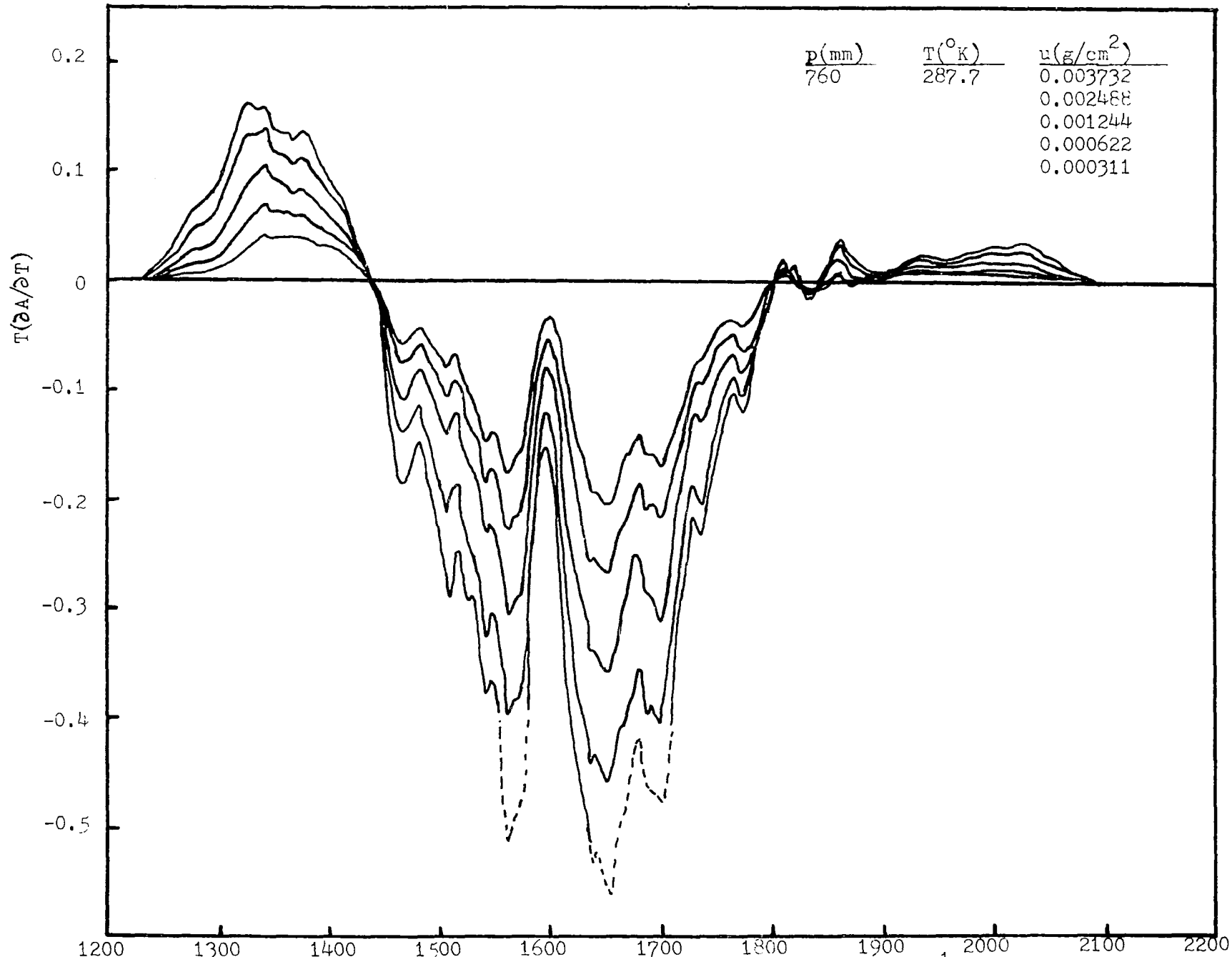


Figure 4. The partial derivative of the absorptance with respect to temperature

The second derivatives are then calculated. A convenient notation here is $xy \frac{\partial}{\partial y}\left(\frac{\partial A}{\partial x}\right) = xyA_{xy}$. Figures 5 through 10 show the calculated derivatives.

Upon inspection of a high resolution absorption curve, one finds that most, as well as the strongest, lines occur near the band maxima. Therefore as the absorber mass increases, tne absorption peaks will be the first location subject to computational uncertainty. This is because the uncertainty increases in the merged lines as the number of merged lines increases and also as they interact more strongly. In the wings this problem is not as serious when the concentration increases. The spectral regions where 7 or more rotational lines have been merged are denoted by dashed lines.

Of particular interest are the regions where the temperature derivative is small, i.e. the so called "cross-over" points. From figure 7 we see that this occurs near $1435\ cm^{-1}$ and $1800\ cm^{-1}$. In contrast to this, farther out in the wings there are regions where the temperature derivatives are relatively large compared with the concentration and pressure derivatives.

Chapter IV gives a comparison of these calculated results with those obtained from experiment.

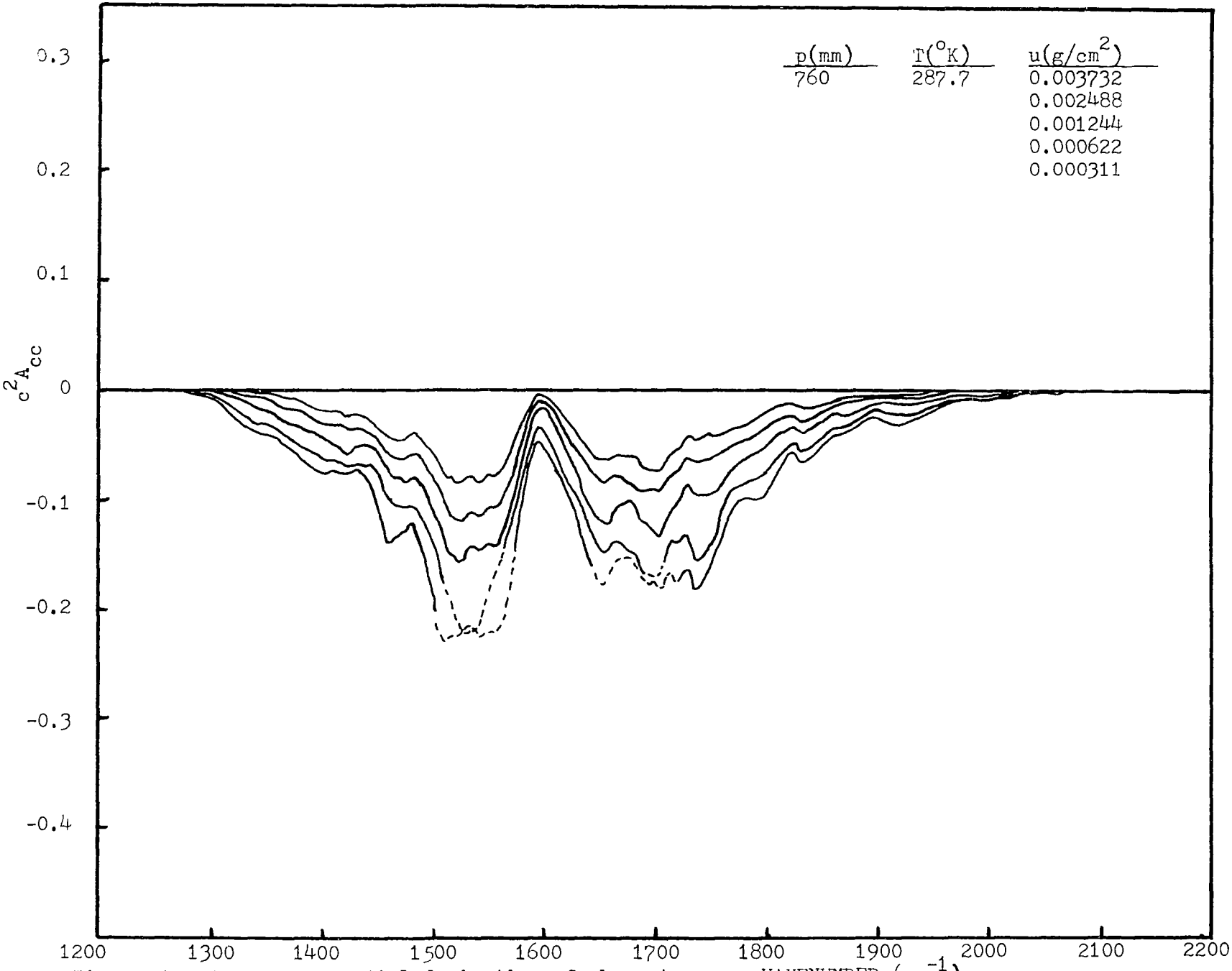


Figure 5. The second partial derivative of absorptance with respect to concentration

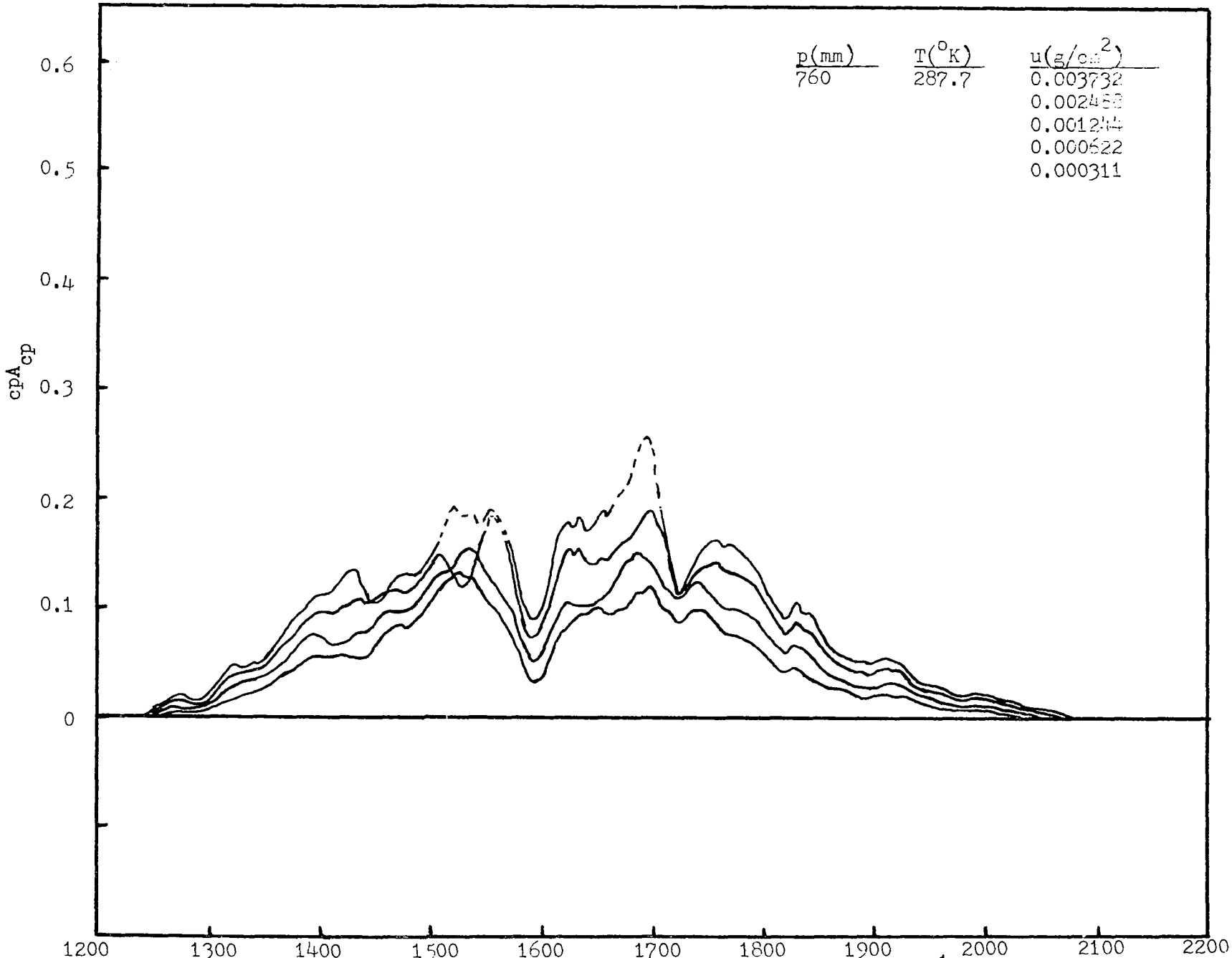


Figure 6. The second partial derivative of absorptance with respect to concentration and pressure

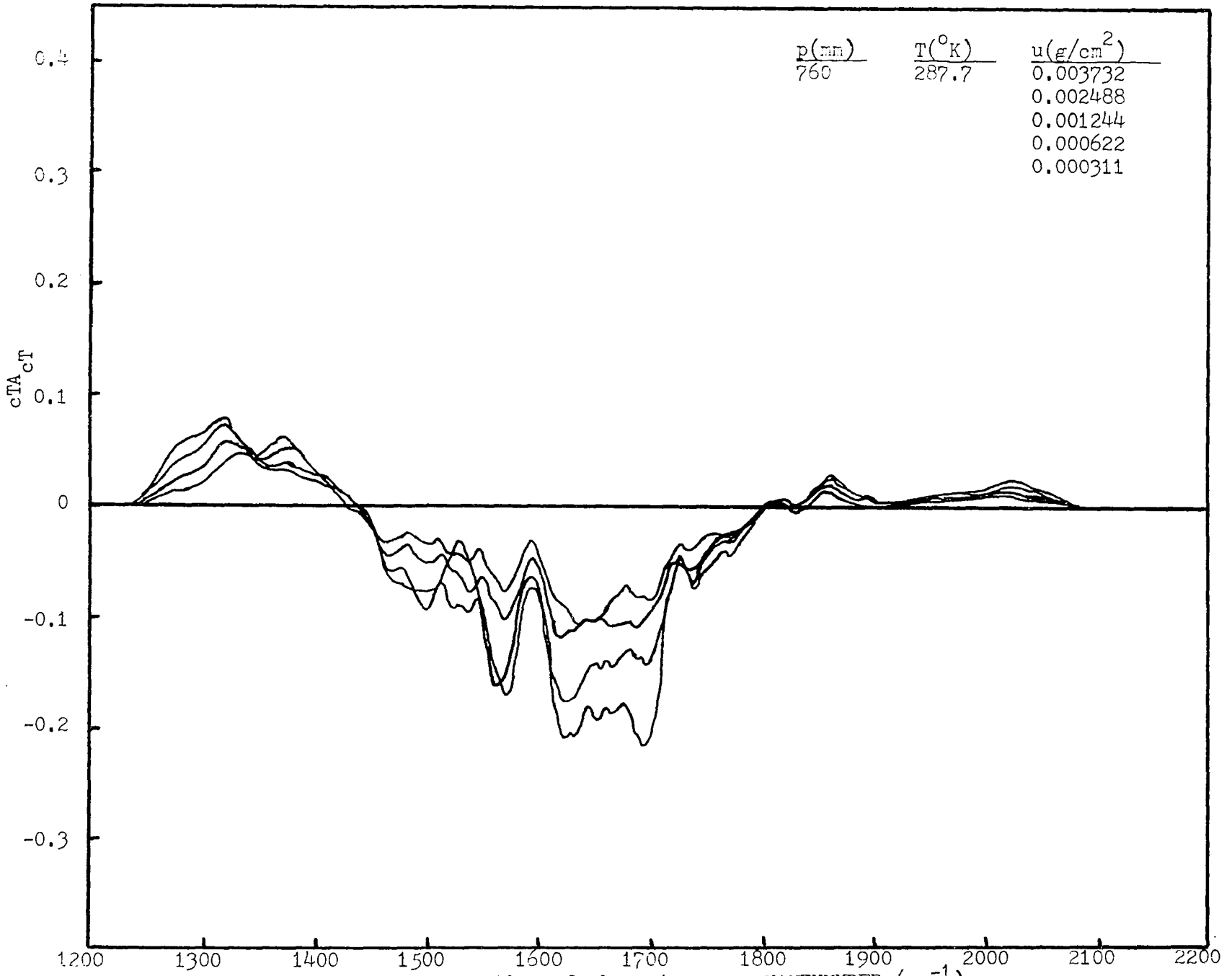


Figure 7. The second partial derivative of absorptance with respect to concentration and temperature

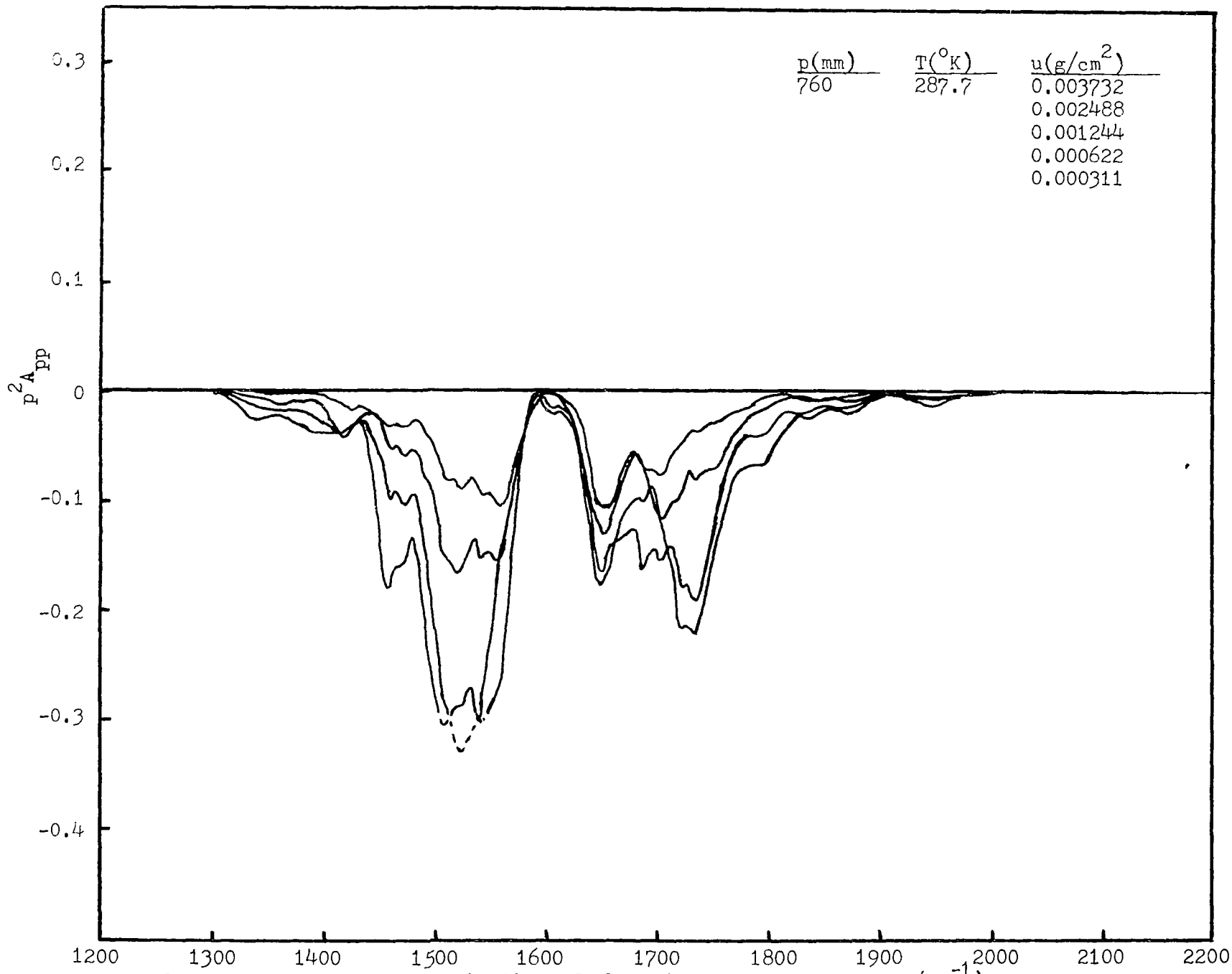


Figure 8. The second partial derivative of absorptance with respect to pressure

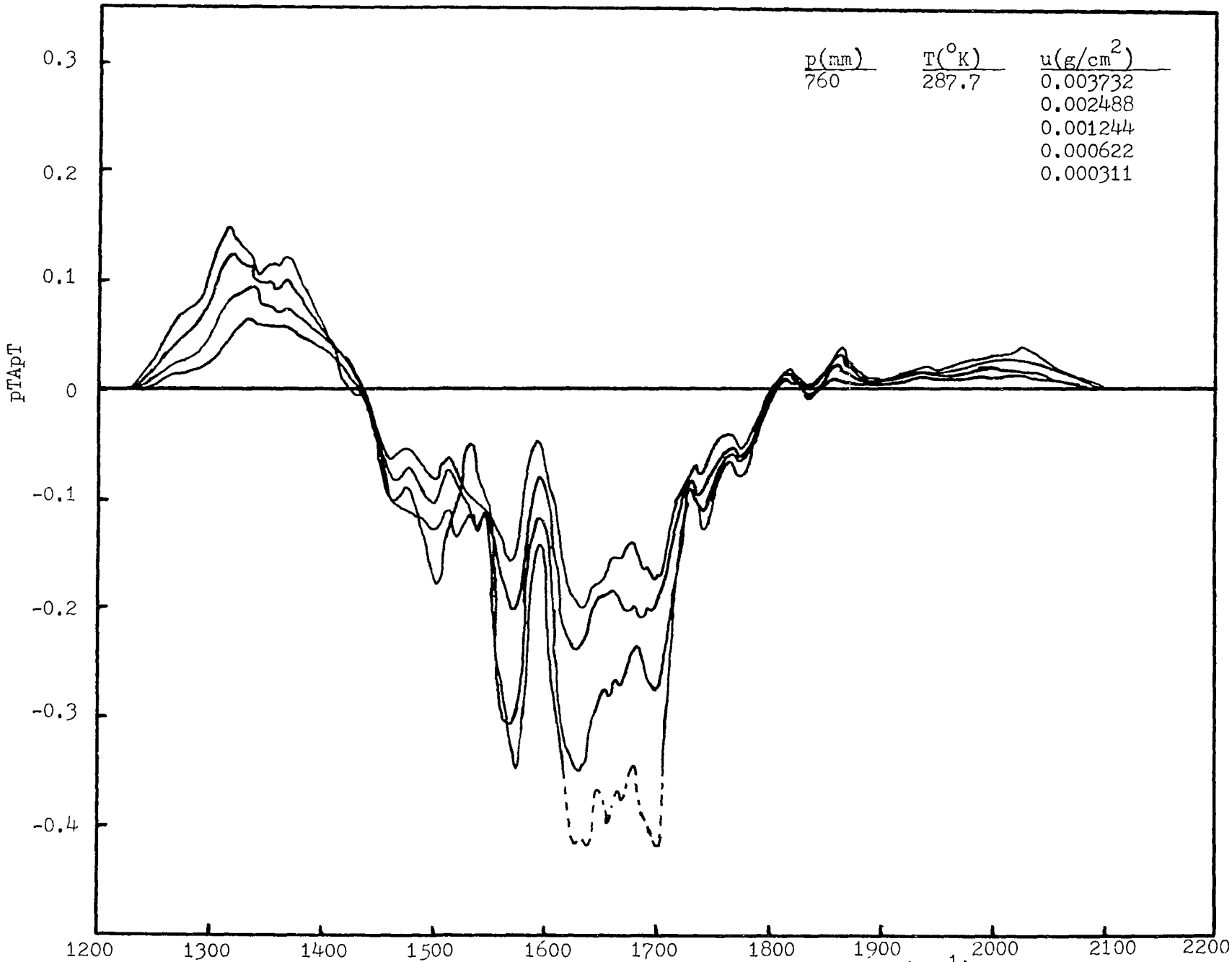


Figure 9. The second partial derivative of absorptance with respect pressure and temperature

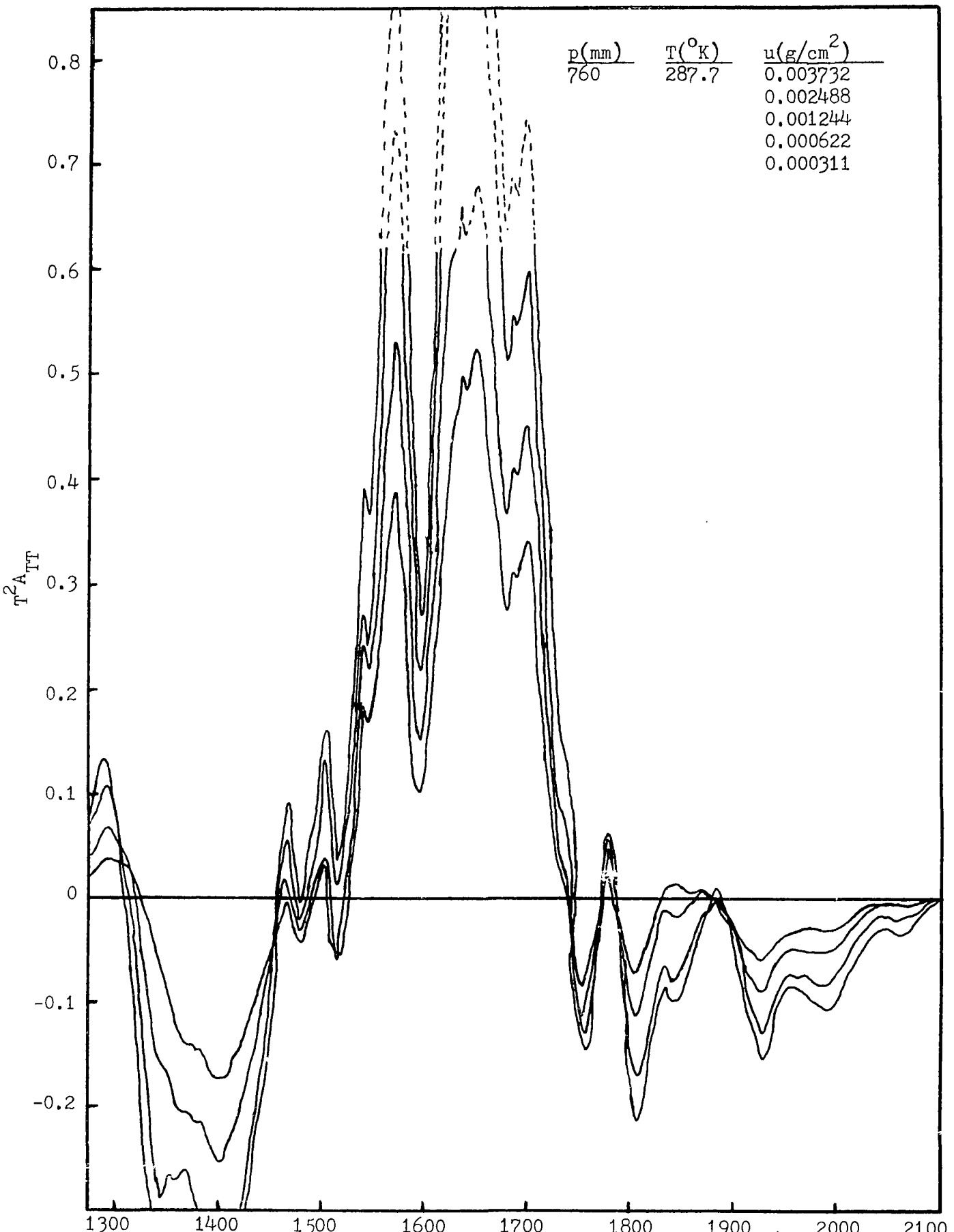


Figure 10. The second partial derivative of absorptance with respect to temperature

Chapter III Experiment

A. Basic Experimental Apparatus

The apparatus utilized in this experiment is an optical absorption cell described by Cann.[17] The cell was first designed and built for work in the Vacuum U.V. Later it was modified for infrared operation. A description of this instrument operation for CO_2 is given by Lysobey.[18]

In the basic mode the instrument analyzes the infrared spectral absorptance of the sample gas. This is accomplished by passing collimated light from a globar via a mirror through the gas. The light which is chopped at the source is sent to a McPherson model 218 scanning monochromator. From the exit slit of the monochromator the light is focused upon a HgCdTe detector which in turn sends an A.C. signal to the lock-in amplifier. A reference A.C. signal which is produced by the same wheel that chopped the globar light is also sent into the lock-in. The resulting D.C. output signal is then fed through a voltage divider into a strip chart recorder.

Although the instrument had the capability of operating in the "dynamic" mode (the gas sample is subjected to sinusoidal pressure fluctuations), this was not a concern in the present investigation.

Retaining optical and electrical parts of the instrument described above, the new design was centered around the investigation of the infrared absorption spectra of water vapor-nitrogen gas mixtures. It was necessary to eliminate the effect of wall contamination; the

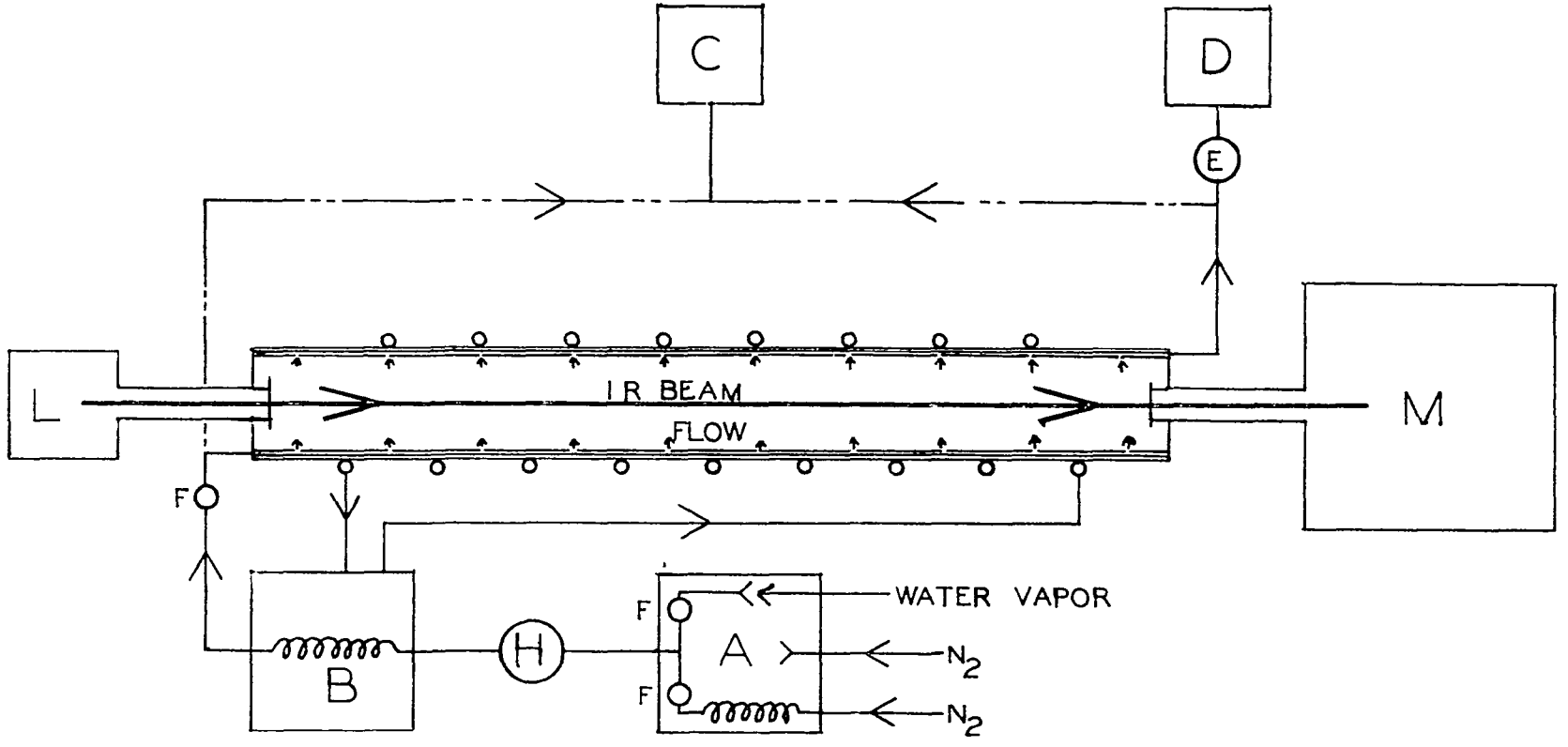
absorption-desorption of the vapor by the container walls and associated components. In order to diminish these troublesome problems a vapor-cross flow system was designed. Thus unbounded air with a wide variety of meteorological conditions could be simulated.

It is important to control the thermodynamic parameters pressure (p), temperature (T), and concentration (c), and to be able to change any one with relative ease. This control may be accomplished in a simple way in a closed system which contains a gas that does not contaminate easily. However, all these variables are not so easily regulated simultaneously when a gaseous flow system is to be employed.

Therefore in the design a prime concern was flexibility. Of course, water vapor is not the only molecule that offers handling difficulties.

Figure 11 shows the principle of the newly designed instrument. A water vapor-nitrogen mixture is first produced in a humidity chamber (A). The desired relative humidity is then obtained by mixing the prescribed ratio (as measured by flowmeters F) of the H_2O-N_2 from the humidity chamber with N_2. Subsequently the mixture is transported through a coil placed in bath (B). The fluid in this temperature bath is circulated through a 50 turn coil soldered around the stainless steel chamber walls. Thus thermal equilibrium between the gaseous mixture and the cell chamber is established.

The vapor enters into the light path through a stainless steel



A WATER VAPOR GENERATOR
B THERMAL BATH
C DEW POINT HYGROMETER
D VACUUM PUMP
E VACUUM-PRESSURE REGULATOR
F FLOW METERS
H COMPRESSOR
L INFRARED SOURCE-EVACUATED
M MONOCHROMATOR, DETECTOR-EVACUATED

Figure 11. ABSORPTION CELL
WATER VAPOR CROSS FLOW
IN CELL CHAMBER

tube of 1.2 cm diameter by 1 meter length. This tube which has 80 orifices, is aligned parallel to the absorption path and is matched by a similar parallel exit tube opposite the light path. Two additional holes were added near the end of each tube in order to reduce end effects. For uniformity it is necessary to have the vapor enter on the one side and exit on the other side of the optical path.

The concentration equilibrium in the cell chamber is influenced by the diffusion rate of the vapor, as well as by the overall convective exchange rate. As we will see, these two rates are comparable. In the case of diffusion, Fick's law may be considered to determine the diffusion of a particular molecule as a function of time. The solution to the one-dimensional diffusion equation yields

$$\overline{z^2} = 2D \cdot t \qquad (15)$$

where the z-axis represents the direction of diffusion, D is the diffusion constant and t is time.

The derivation of the above equation applies to the simple case of self-diffusion; i.e, all molecules are identical. For the more general case of mutual diffusion where the molecules are unlike, the diffusion coefficients found are of the same order of magnitude.

We use the experimental value (Guglielmo[19]) of D = 0.239 cm^2/sec for water vapor diffusing into air at 8 ^{o}C and 1 atmosphere. For our cell with a diameter of 12 cm, we find that

$$t = \frac{z^2}{2D} = \frac{12^2 cm^2}{2 \cdot 0.239\ cm^2/sec} = 300 \text{ sec} = 5 \text{ min.}$$

Hence it takes an interval of the order of 5 minutes for the water vapor to diffuse across the cell once it is introduced.

Taking a typical operating vapor flow of 2 liter/min. one finds that the gaseous mixture is convectively exchanged in time

$$t = \frac{\text{Vol of cell}}{\text{flow rate}} = \frac{10 \text{ liter}}{2 \text{ liter/min.}} = 5 \text{ min.}$$

On the basis of these estimates for the diffusion and convective exchange rates it is possible to indicate the time required for the water vapor equilibrium to be established in the cell chamber with the accuracy required. For example, one would like to know the time needed for the cell concentration to be within 1% of the originally produced mixture. We consider the convective exchange momentarily.

Let the concentration of the incoming mixture be designated by $n_o \cdot H_2O$ molecules/liter of nitrogen, while in the 10 liter cell chamber there are $n \cdot H_2O$ molecules/ liter. Defining the exit flow which equals the entrance flow, by Q liter/sec, we have

$$\frac{dn}{dt} \cdot \text{Cell Volume} = Q(n_o - n) \tag{16}$$

$$\frac{dn}{n - n_o} = \frac{-Q}{\text{Cell Volume}} \tag{17}$$

This equation assumes mixing. This can be considered to be satisfied by the diffusion which has the same rate as the convective exchange.

Using the typical value of Q = 2 liter/min., a solution to equation 17 is readily obtained to be

$$n = n_o(1 - e^{(2/10)t}) \tag{18}$$

where t is measured in minutes. This solution assumes the boundary condition of zero vapor concentration in the cell at t = 0. This is more severe than the actual case where a H_2O-N_2 mixture is allowed to fill an evacuated cell.

For $n/n_o = 0.99$ one finds from (18) that $t = 5 \cdot \ln 100 \approx 23$ min. Therefore concentration equilibrium will be established to within 1% of its final value within a time of 23 minutes while diffuse mixing aids in the process. A conservative estimate would be approximately 30 minutes.

Experimental checks of concentration equilibria as well as of concentration gradients were made with a series of hygristors (humidity sensitive resistive elements) placed at strategic locations inside the cell chamber. It was indeed found that 30 minutes was sufficient to obtain equilibrium and that along the absorption path uniform unbounded space was quite well imitated.

Care was taken to keep the temperature of all the critical components of the instrument above the dew point. Of particular importance were the windows, which defines the cell path, since any condensation there would introduce a serious error in the data. Therefore heating tapes were wound around each end of the cell and thermocouple probes were placed strategically along the light path. The thermocouples were useful not only in checking the temperature near the windows but also in determining any thermal gradients. Figure 12 shows the location of the thermocouples for the optical path length of 100.5 cm. In order to obtain a reasonable absorption

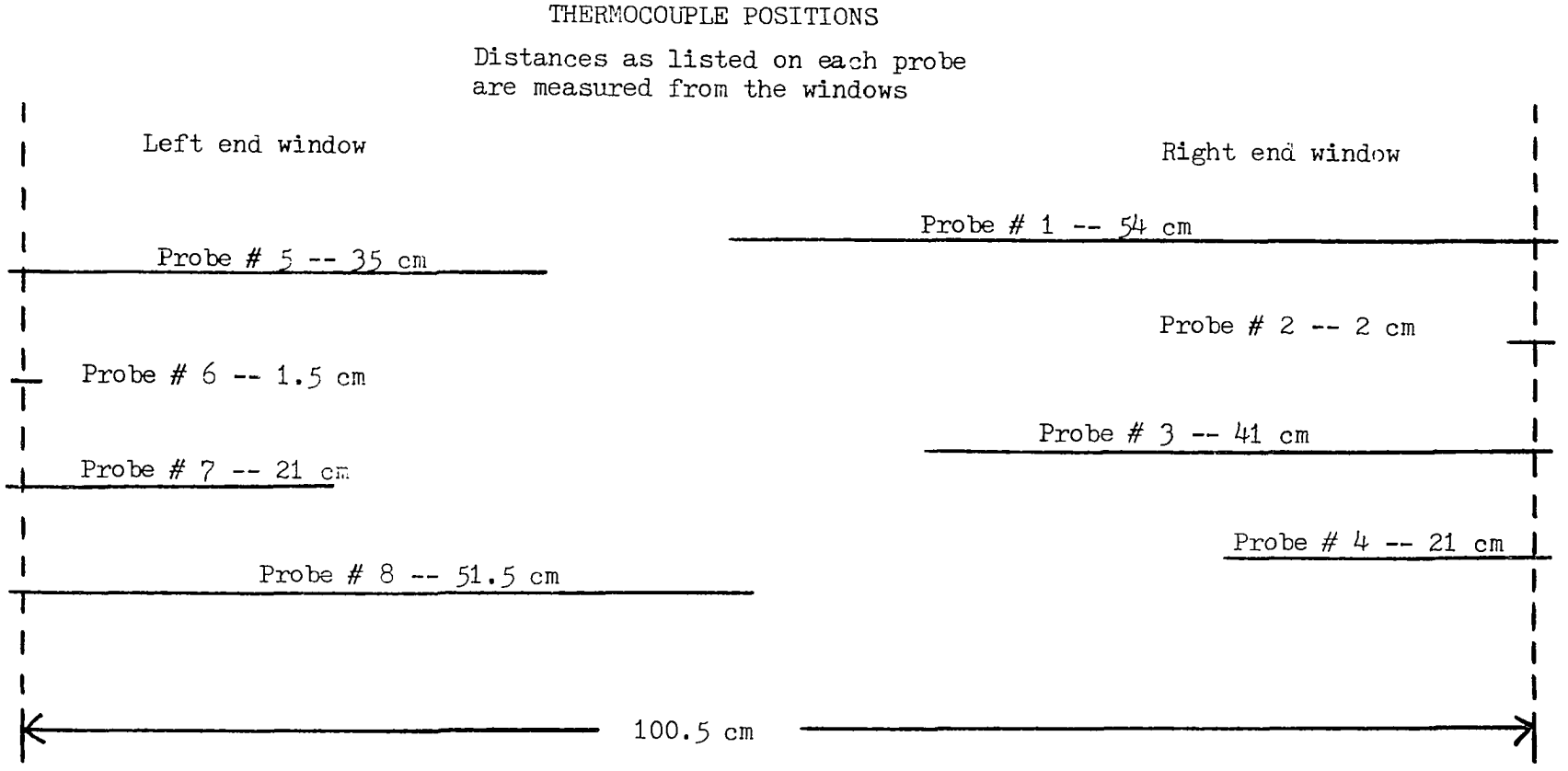


Figure 12. Thermocouple positions within the absorption cell

the longest optical path, compatible with the cell, was chosen.

A calibration in situ was performed to minimize any temperature errors. First the thermocouples were compared to a thermistor probe(which itself had been calibrated) with the reference thermocouple junction at 77 ^{o}K. Taking 33 measurements over a temperature range of approximately 20 ^{o}C to 50 ^{o}C, the thermocouples read high as compared with the official calibration with an average difference of 1.90 ^{o}C and a standard deviation of 0.31 ^{o}C.

Thereafter 39 temperature readings were taken over a range of approximately 10 ^{o}C to 50 ^{o}C with the reference thermocouple at 273 ^{o}K. These measurements along with the previous 33 gave a comparison of the reference thermocouple at the temperatures of 77 ^{o}K and 273 ^{o}K. Here the 273 ^{o}K junction yielded values with an average difference of 0.13 ^{o}C and a standard deviation of 0.53 ^{o}C. We concluded that the 0 ^{o}C reference should be used since the values agreed with the correct temperature to within less than one standard deviation.

A vital component of the system is the dew point hygrometer (C in figure 11) which is capable of continuously monitoring the vapor concentration either at the cell entrance or exit. The details of the hygrometer are given in section B of this chapter.

Referring again to figure 11, the desired operating cell pressure was regulated by a vacuum-pressure regulator (E). The vapor is ejected from the system by the pump (D).

The above description gives an overview of the gaseous flow system. It was very important to maintain control of and periodically

monitor the various parameters during the instrument operation. Further details of this operation which pertain specifically to the components added by us are given in section B.

In addition to the major additions there were also some minor changes made that contributed to an improved overall stability of the instrument operation. Two of these may be mentioned here.

First of all, serious instabilities were observed in the output of the globar light source when powered by the set-up previously used. This power supply was adequate for relatively short (in time) data scans. However, scans of the 6.3 micron water band took much longer. Therefore a Hewlett Packard model 6434B low voltage regulated power supply was used. One had the option of either current regulation or voltage regulation. Since the light output of the globar depends on I^2R and R was fairly independent of temperature, the current regulation mode was chosen. Thus the effect of changes in contact resistance of the globar mount was small. Current regulation was found to be $\pm$ 0.002 amp over a time interval of 4 hours with a globar current of approximately 3.5 amp. Overall light stability was improved vastly with the only remaining unavoidable problem of globar aging or deterioration. Generally however, once a globar is properly installed, its operating lifetime surpasses the time required for many data scans; indeed all the data in this thesis was taken with one globar.

In order to stabilize the mechanical chopper frequency, a hysteresis synchronous motor was installed. Many minor annoyances

such as motor alignment and belt tension had to be overcome in order to produce optimum chopper performance. A secondary benefit of the synchronous motor installation was the elimination of electrical noise which was generated by the old type universal motor. Thus the new motor did not have to be electrically shielded in order to avoid interference with the electronics.

B. Major Components of the Water Vapor Apparatus

1. Infrared Absorption Cell

Figure 13 gives a cross-sectional view of the chamber showing the 3" tube, the 5" tube, and the union via the flanges. The end sections are made of type 304 stainless steel tubing with 0.120" wall thickness. This wall thickness permitted some machining on the outer ends so that sufficient clearance was obtained when inserting the unit into the instrument assembly. Furthermore the thick wall aided in the mechanical stability of the cell chamber. The center section is constructed from type 304 stainless steel tubing with 0.067" wall thickness. A thinner wall here meant a considerable saving in the cell chamber weight. The cell chamber is pictured in figure 14. The flanges C and D were heliarc welded to their respective cell chamber tubes. The ports for gas transport as well as electrical feed-through provide easy access to the cell chamber. Figure 15 shows an expanded view of the flange union area. Here the gas entrance and exit ports are shown in greater detail. The center section is enlarged to provide adequate space for the gas transport tubing along each

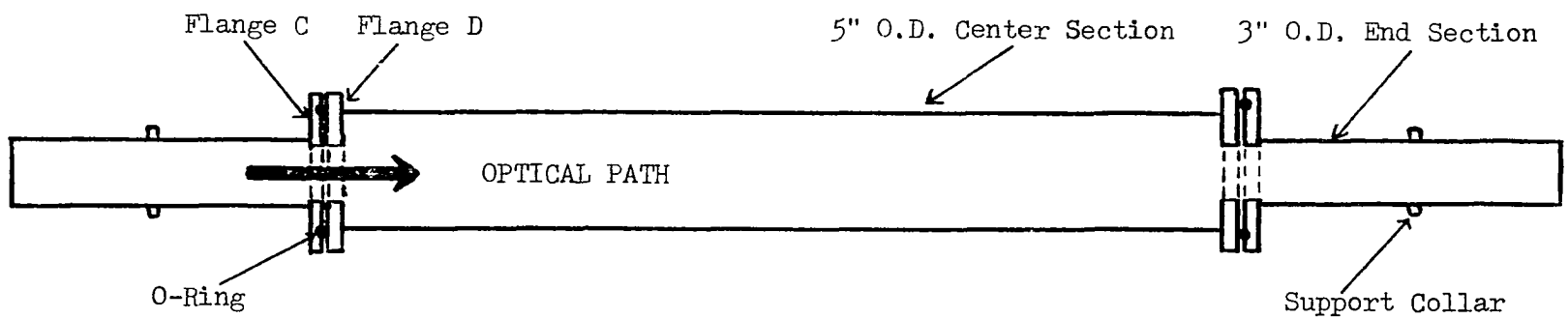


Figure 13. Absorption cell - cross sectional view
Material - Type 304 S/Steel
Overall length - 66.0"

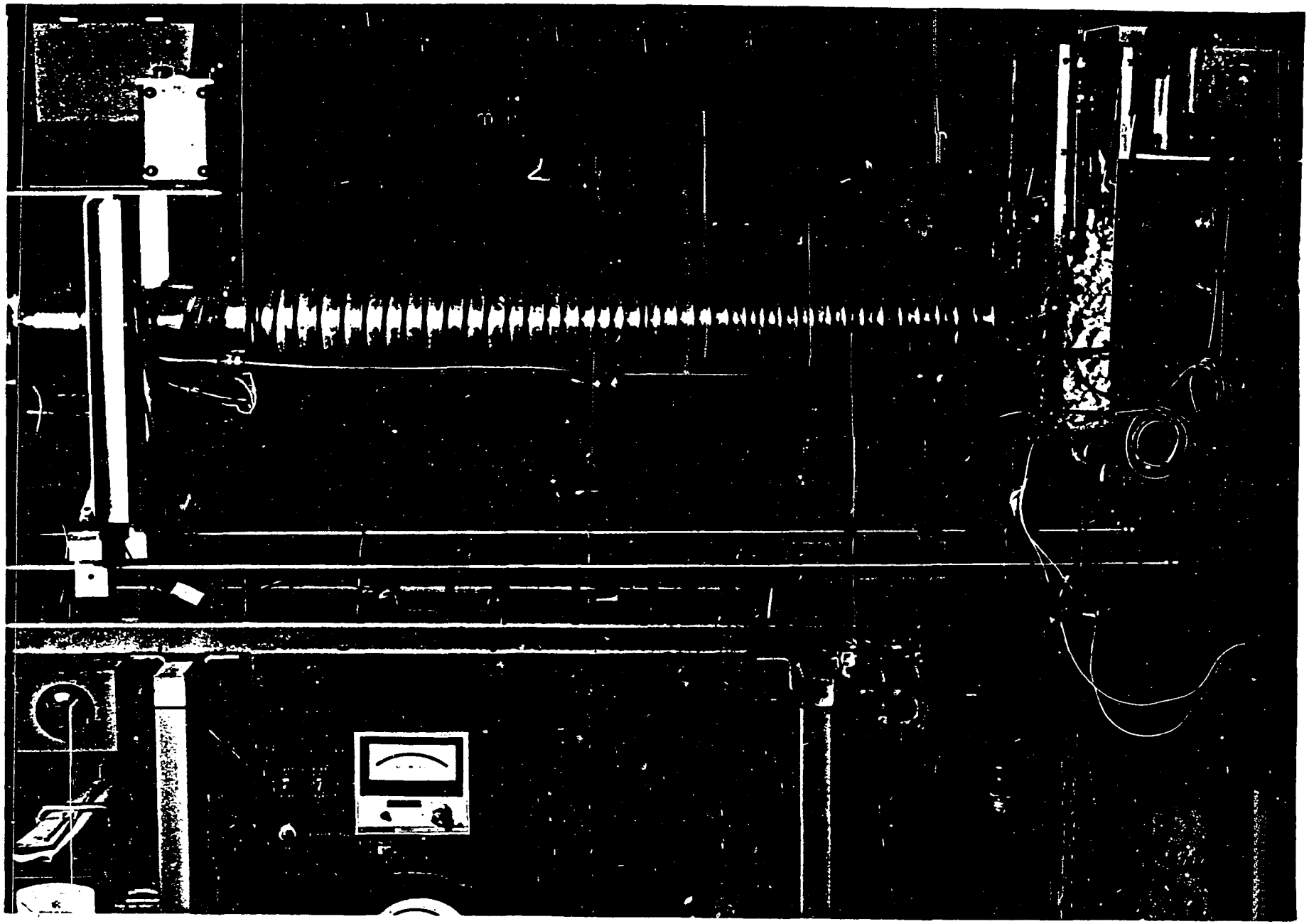


Figure 14. Absorption cell

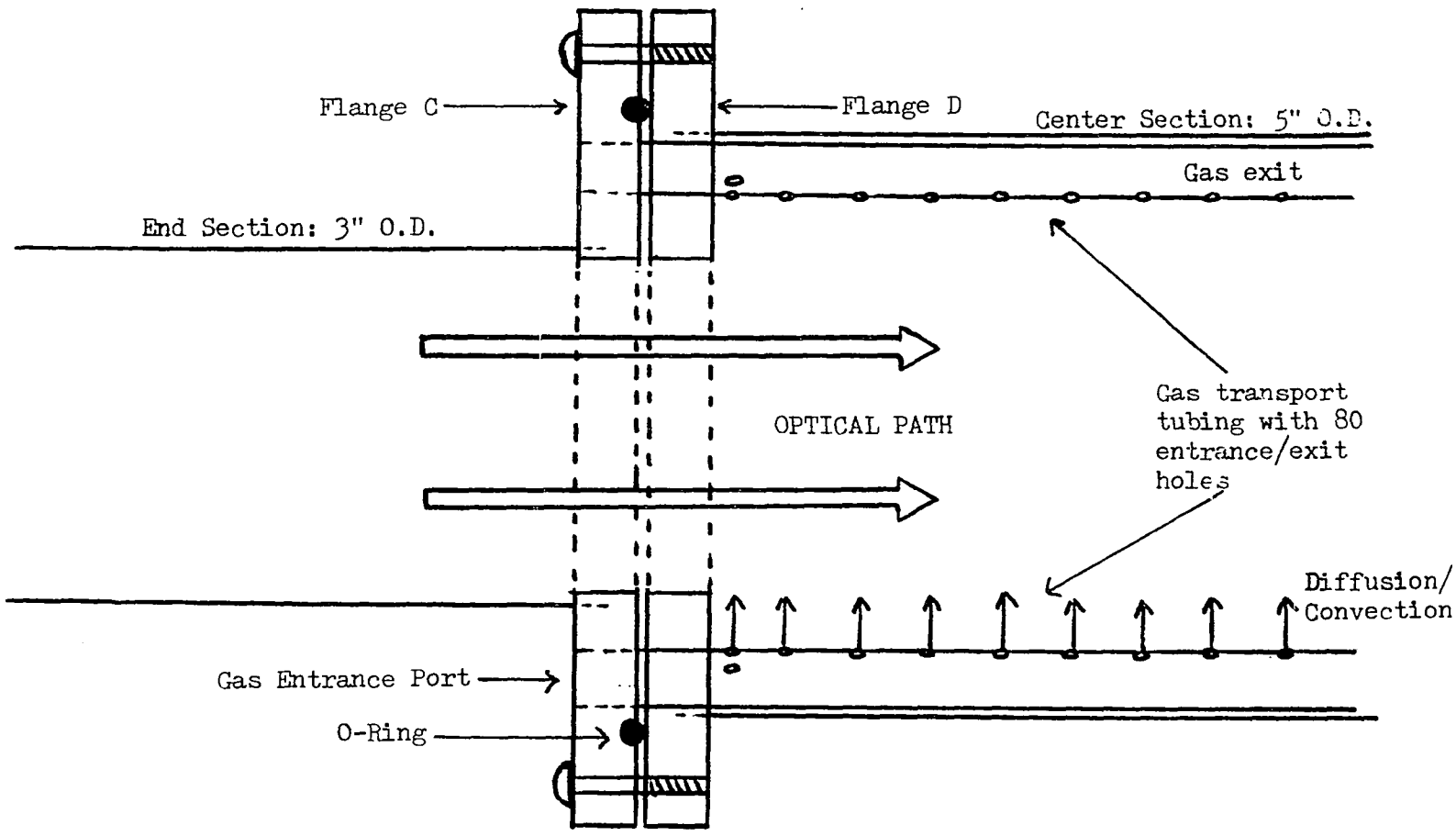


Figure 15. Absorption cell - flange union area

side of the optical path. This tubing provides for concentration establishment by diffusion and convection. The O-ring between the flanges provide a vacuum seal. All components were thoroughly cleaned before installation in order to minimize outgassing by contaminants.

2. Production of Water Vapor

Of vital importance in the system is a source of constant humidity from which the vapor flow system may continuously draw. The continuous withdrawal of vapor from the source meant that a dynamic rather than a static humidity generating device must be employed. Furthermore the capacity of the source must be large enough so that for example replacing humid nitrogen with dry nitrogen will have an insignificant effect on its relative humidity.

The operating range of humidities must be compatible with the desired concentrations in the experiment. Also the precision of the device must be sufficient to produce a constant humidity over time intervals of the order of hours. This aids in the instrument operation even though an independent humidity monitoring device is employed (dew point hygrometer).

Based upon the above criteria, a Blue M model VP - 100AT - 1 constant temperature and humidity chamber (see equipment list(2)) was used to establish the dew point and the initial temperature of the gas samples. Figure 16 shows the humidity chamber.

Figure 17 shows the basic principle of operation. Distilled water from an inverted reservoir bottle furnishes the supply container.

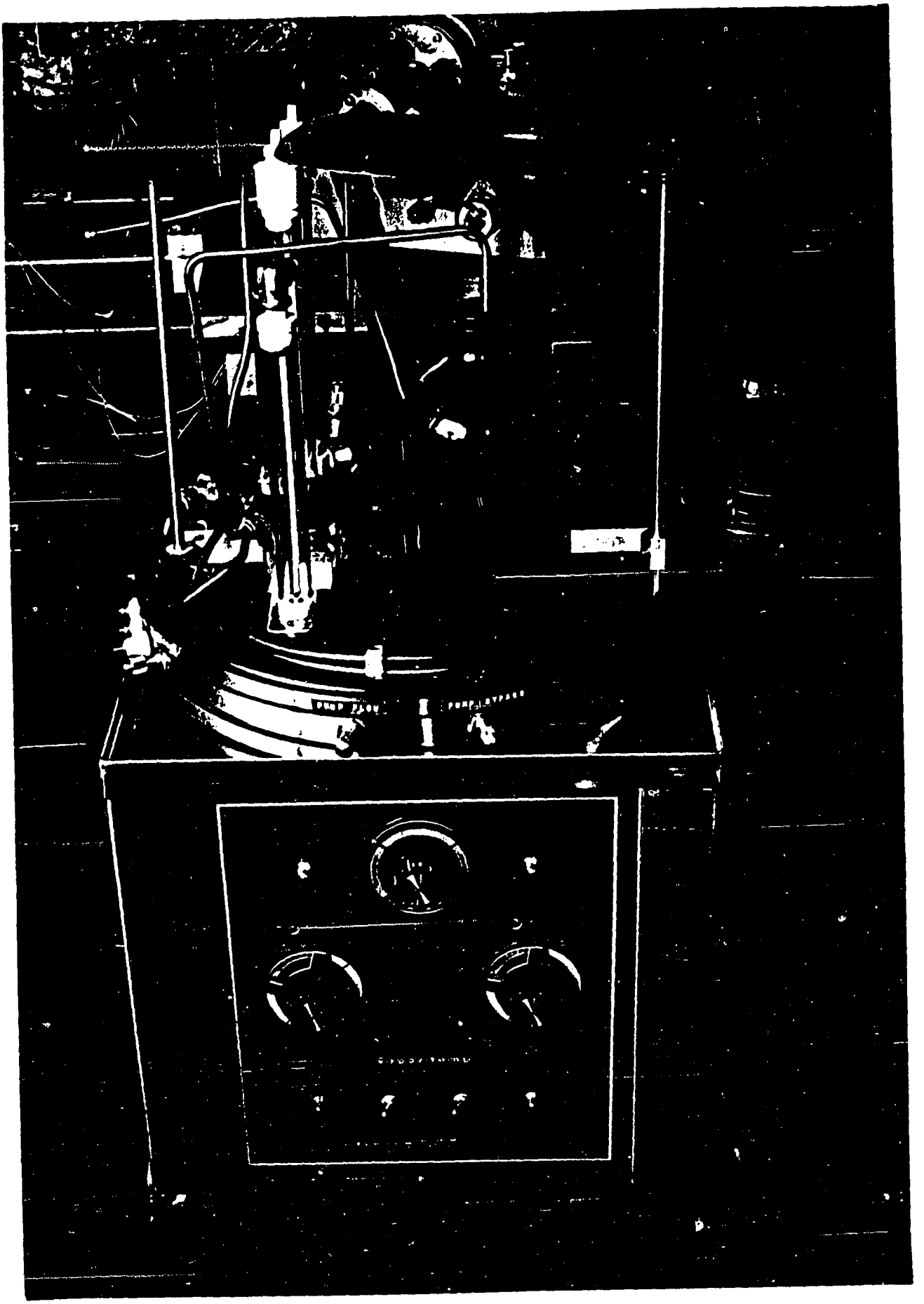


Figure 16. Humidity chamber

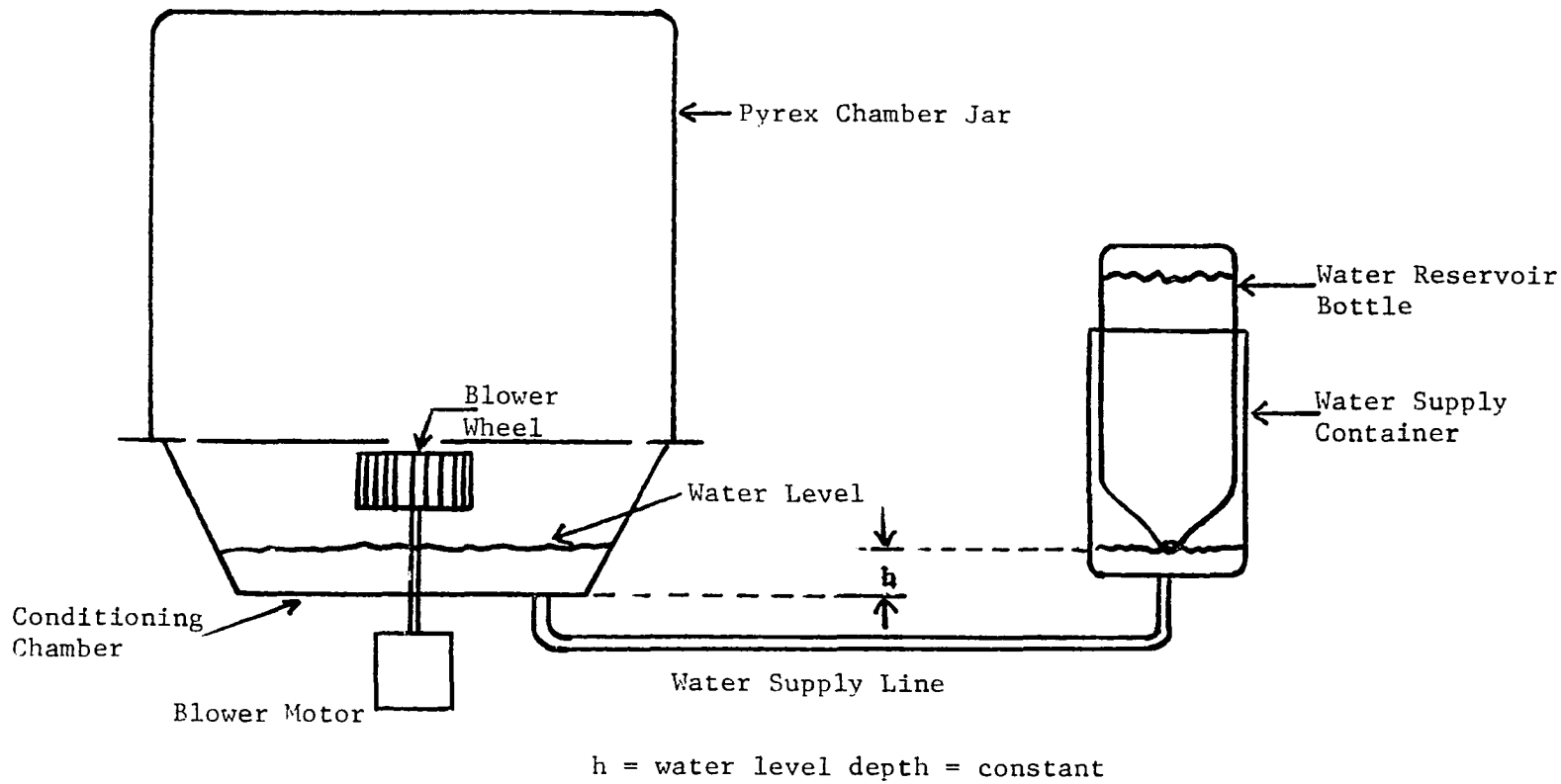


Figure 17. Humidity chamber - principle of operation

The vertical position of the reservoir bottle is fixed so that the level of the water in the bottom of the container is always maintained. The water is then transported to the conditioning chamber where the value of h determines the constant water depth. The blower wheel circulates the humid nitrogen of the conditioning chamber into the working area defined by the pyrex chamber jar. Wet and dry bulb thermometers are kept in this area to aid in setting the nominal values of relative humidity as determined from a psychrometric table.

This model humidity chamber has a stated ability to regulate the relative humidity to $\pm 1\%$ and the dry bulb temperature to $\pm$ 0.5 ^{o}C. Figure 18 is the range chart for relative humidities attainable at various dry bulb temperatures. The stated area is obtainable using +21 ^{o}C water as a cooling medium and operating over the range of ambient temperatures of + 21 ^{o}C to + 27 ^{o}C.

An optimum regulation is obtained when the device is operated within the stated area that is not too close to the outer limits. The values of wet and dry bulb temperatures were thus chosen to achieve this regulation.

The method of regulation employed by the device involves the direct control of the wet and dry bulb temperatures. There are two such sensing elements which depend upon the thermal sensitivity of certain fluids. These elements control the power to the wet and dry bulb heaters through the use of silicon controlled rectifiers. To obtain the full relative humidity range of figure 18, tap

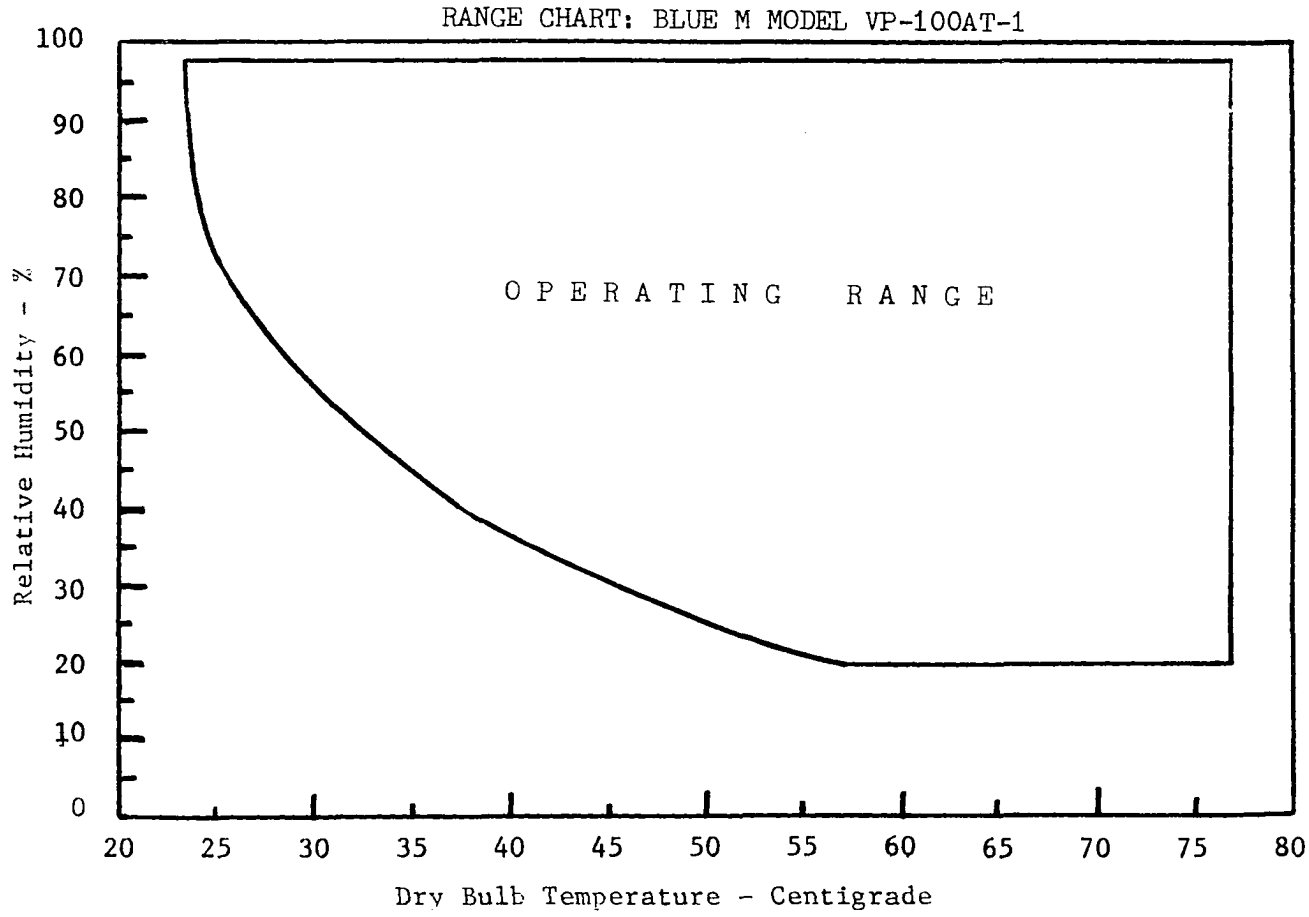


Figure 18. Humidity chamber - range of operation

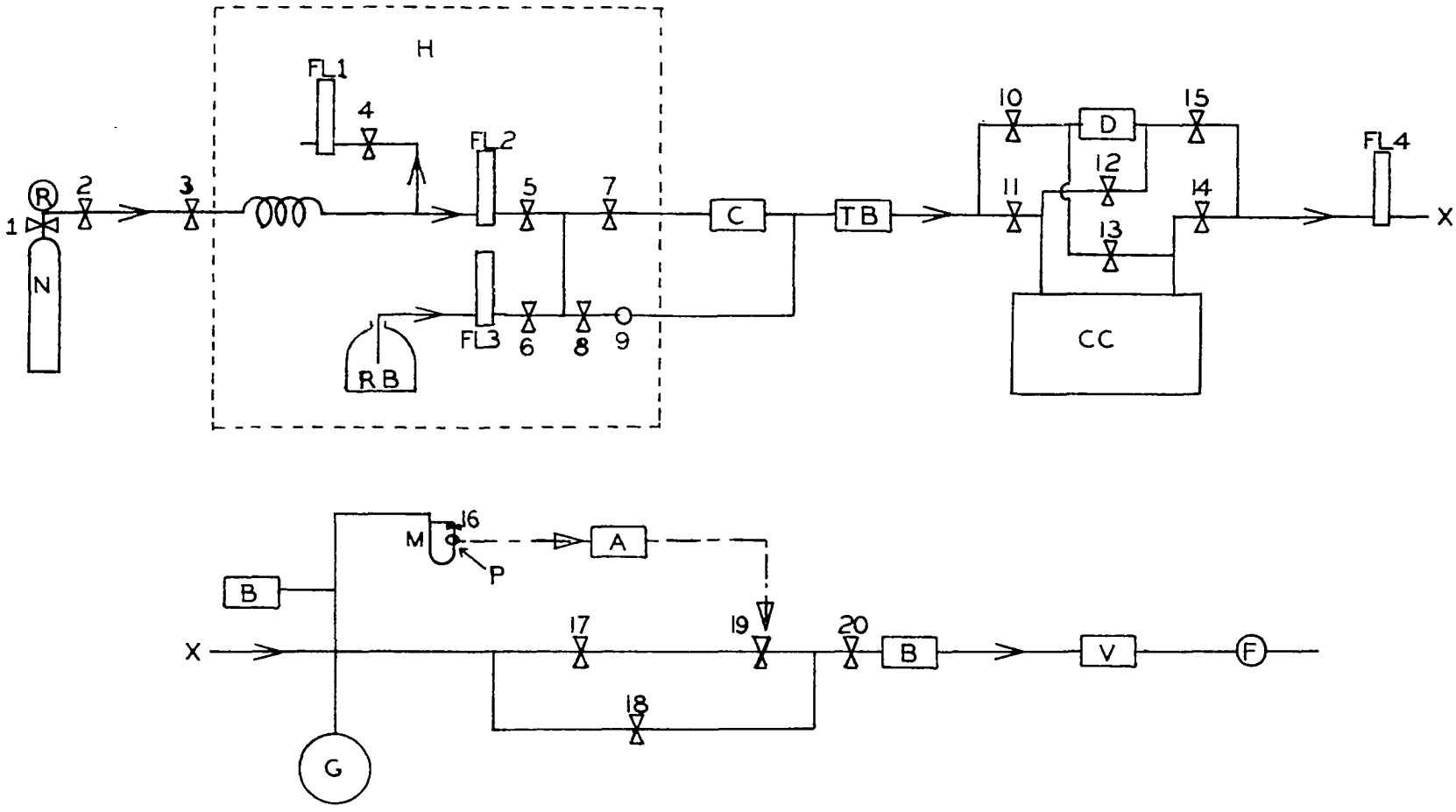
water may be necessary as a cooling agent to lower the partial pressure of the water in the conditioning chamber. The wet bulb circuit has the dual function of controlling heating as well as cooling. Both the wet and dry bulb sensing elements are located in the chamber working area where the vapor is to be withdrawn. Short term variations of the humidity, caused by the cycling of the chamber heaters and cooler, is effectively damped by withdrawing the gas sample from the bottom of a 2 liter bottle (RB in figure 19) before it is transported to the cell chamber. Long term drifts of the humidity in the chamber are diminished by controlling the room temperature to within 1 ^{o}C and by circulating room air through the electronic components of the chamber.

Dry nitrogen is fed from a cylinder into the humidity chamber through flow meter FL1 (see figure 19) (see equipment list (3)). Since the chamber gaskets, which are around the bottom of the pyrex chamber jar, do not completely seal the working area, slightly more dry nitrogen is fed into the chamber than is withdrawn for gas samples. This insures that room contaminants are not introduced into the vapor flow system.

3. Determination of Humidity

The desired vapor concentration for the absorption measurement is determined by proportioning the flow rates in FL2 and FL3 respectively (see figure 19).

At the heart of the instrument is the device which determines and continuously monitors the vapor concentration. The criteria for



N - Dry nitrogen
R - Pressure regulator
H - Humidity chamber
RB- Reservoir bottle
C - Compressor
TB- Temperature bath
D - Dew point hygrometer
CC- Cell chamber
G - Pressure gauge
B - Ballast
M - Manometer
A - Pressure regulation amplifier
V - Vacuum pump
F - Exhaust fan

Figure 19. WATER VAPOR FLOW SYSTEM

choosing such a device were:

1. Continuous monitoring with a minimum perturbing effect on sample.
2. Operation at pressures other than atmospheric.
3. Reproducibility with negligible hysteresis.

The EG&G dew point hygrometer model 880 met these criteria adequately (see equipment list (5)).

The operating range as stated by the manufacturer provides for a dew point depression of 44 ^{o}C if the ambient temperature is 27 ^{o}C. The dew point is insensitive to the sample flow rate over the range of 0.25 liter/min. to 2.5 liter/min. The instrument will operate over the pressure range of 2 psia to 60 psia.

The basic design principle is shown in figure 20. Here the gas sample is transported through the sensor where it passes over a cooled metal surface (a highly polished gold plated copper disc) so that the gas at the metal surface and the metal have the same temperature. As the metal is chilled below the dew point by a thermoelectric "Peltier" cooler, condensation will form on the mirror. Water droplets or ice crystals will continue to accrete as long as the surface is below the dew point. Just the opposite results for temperatures above the dew point. When the surface is at the dew point temperature the rate of condensation will be equal to the rate of evaporation. This temperature is measured by a precision thermistor which is embedded just under the mirror surface. Good thermal contact between the thermistor and the surface is insured by solidly embedding it into a high thermal

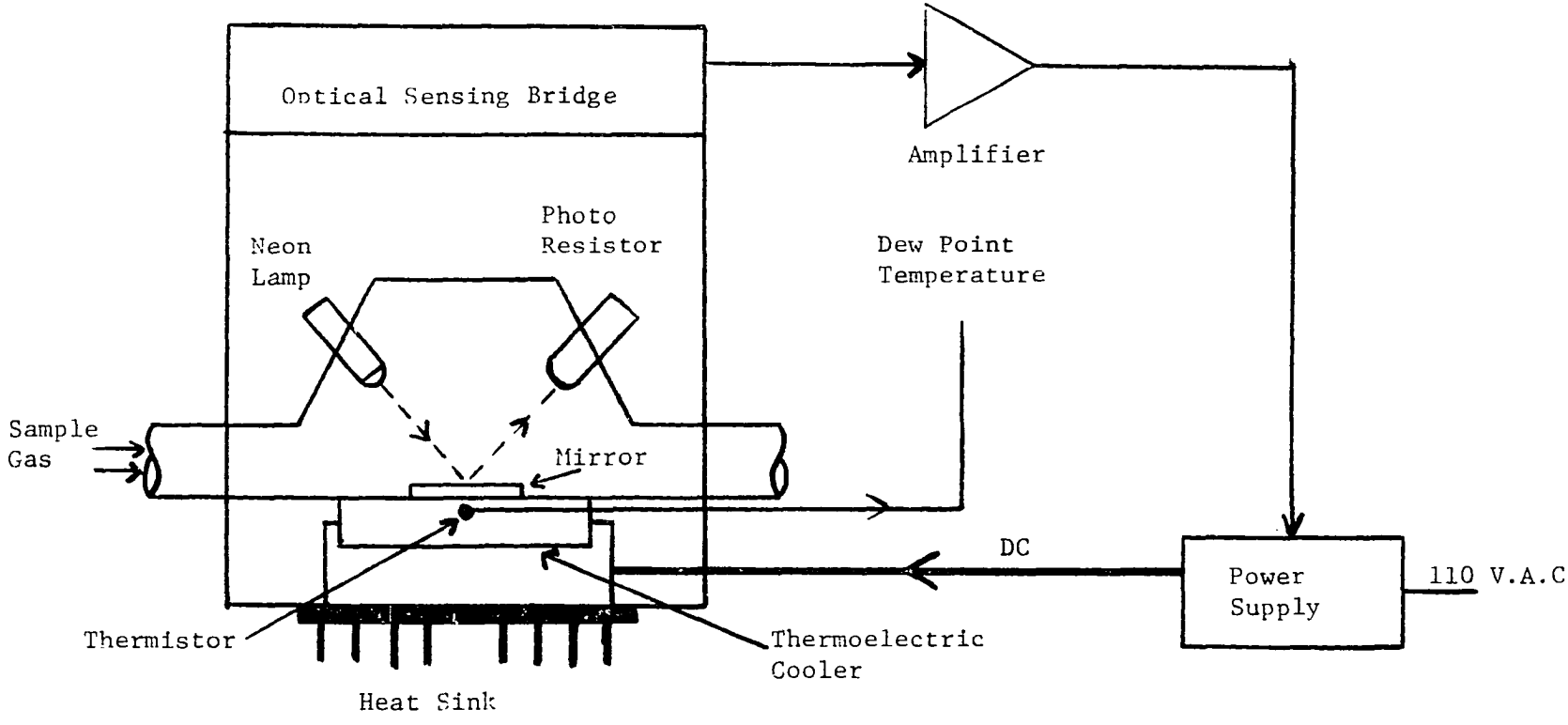


Figure 20. Dew point hygrometer - principle of operation

conductivity holder. The entire assembly is adequately insulated from its surroundings so that heat losses do not produce a significant error in the temperature reading. The temperature output of the hygrometer was displayed on a digital voltmeter, the actual temperature being determined from a calibration curve supplied from the manufacturer. The temperature output voltage ranged from 0 - 50 mv.

Light from a source is directed toward the mirror and reflected to the photoresistor. The intensity of the reflected light will be diminished by scattering as water droplets are formed. The photoresistor forms a branch of the optical sensing bridge so that the reflectance of the mirror is sensed. A signal from the bridge circuit is amplified and sent to the power supply where the power delivered to the thermoelectric cooler is controlled. This optical-thermal feedback system maintains the temperature of the mirror surface for a given value of light reflectance. The amount of cooling is proportionally controlled depending upon the amount of condensate on the mirror. This allows the mirror to continuously track the dew point temperature and detect changes of less than 0.05 ^{o}C.

The response time of the cooling system, which is 2 ^{o}C/sec maximum, is fast enough to detect short term variations in the concentration.

Contaminants as well as water droplets may produce a change in the instrument output by changing the mirror reflectance. Thus contaminants which collect on the mirror surface could be interpreted as water. However since the variation in the reflectance due to

contaminants does not change with temperature, they may be compensated for by properly balancing the bridge circuit. This procedure will suffice as long as the amount of the contamination is not excessive, otherwise the surface must be cleaned. Such contamination did not present a serious problem during all our data scans.

The position of the hygrometer is shown as C in figure 11 and D in figure 19. The manifold permits sampling the vapor either before or after passage through the cell. The former aids in making adjustments in the humidity chamber. The latter indicates whether vapor loss takes place in the cell. This loss sets an upper limit on the concentration at the particular temperature used.

It is essential that all the components associated with the sampling manifold be kept above the dew point temperature of the sample. This will avoid an erroneous dew point reading. Therefore all gas supply lines were either adequately insulated or housed where the temperature environment could be controlled. In particular the hygrometer sampling manifold and the hygrometer sensor were placed in a plexiglas box. Sufficient heating tape was placed within to control the temperature with the power to the tape being controlled by a variac. See figure 21.

This model hygrometer makes a primary humidity measurement since it determines the dew point temperature directly. The error of such a device is relatively small. The actual errors in the dew point are important since this has a direct bearing on the accuracy of our sample concentration. The errors may be

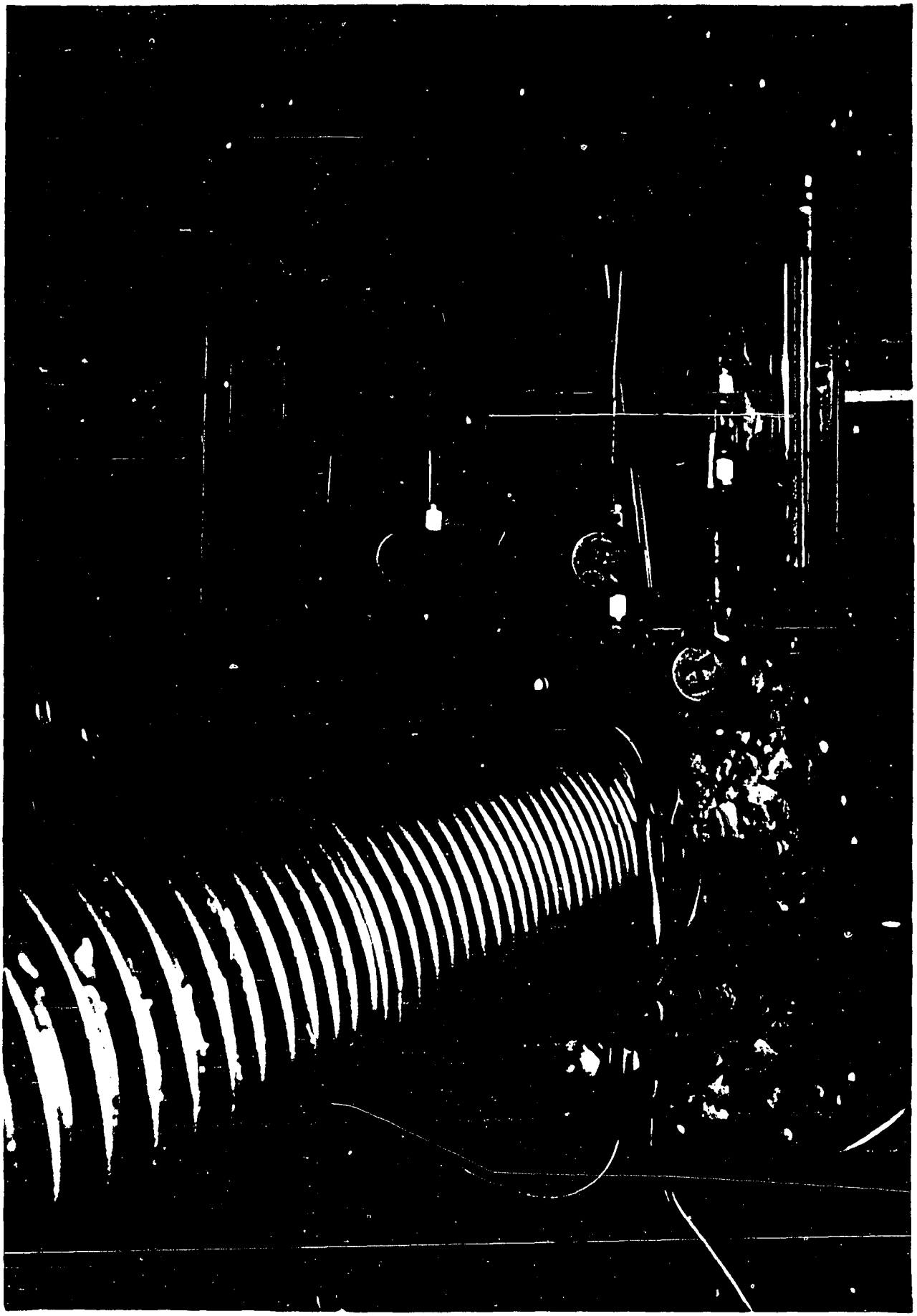


Figure 21. Dew Point hygrometer - gas sampling manifold

separated into two categories: those which occur at the surface and those which involve the measurement and display of the temperature. Some sources of error may be listed here with their errors.

Two surface errors, the Kelvin effect and the Raoult effect, are of the same order of magnitude (0.05 ^{o}C). They are opposite in sign but may not occur simultaneously.

The error caused by a temperature gradient existing between the water droplet surface and the mirror surface is approximately +0.002 ^{o}C. This value is about twice that expected from the temperature gradient between the mirror surface and the thermistor. The thermistor itself introduces an error from self-heating of about + 0.07 ^{o}C. As mentioned previously the copper disc is quite well insulated from its surroundings. Nevertheless, the thermometer leads cause an error of + 0.001 ^{o}C by thermal conduction. All these errors are fairly small in comparison to the next three. The error due to the thermistor calibration limitations is about + 0.2 ^{o}C. The readout calibration limitation error is stated as $\pm$ 0.28 ^{o}C while that from the readout calibration linearity is $\pm$ 0.67 ^{o}C.

The extreme error expected may be determined from the root mean square of the individual errors. This value is $\pm$ 0.78 ^{o}C.

4. Thermal Control

The sample gas from the humidity chamber flows through a coil of tubing placed in the liquid temperature bath (B in figure 11, TB in figure 19) before entering the sample cell space. Liquid from the bath is also circulated through copper tubing soldered to the outside of the center section of the cell chamber wall. All parts of the thermal equipment are carefully insulated.

Typically temperature equilibrium was established within 2 hours. Figure 22 demonstrates the rate of establishing temperature equilibrium along the optical path. Refer to figure 12 for the various positions of the thermocouple probes. As was expected the probe near the window lagged behind the others due to the thermal mass of the ceramic tube and other nearby components. Point A in the figure shows the effect of evacuation on the temperature. This drop in temperature near the window was of little consequence since reference spectral scans were taken under evacuated conditions.

The cell temperature could be established below ambient as well as above. This requires two temperature baths.

Since a series of spectral scans at a given temperature requires several hours it was imperative that the temperature controller had both long and short term stabilities. This demanded that each bath had a sufficient thermal inertia to smooth out any short term variation and also control sensors with ample sensitivity to provide

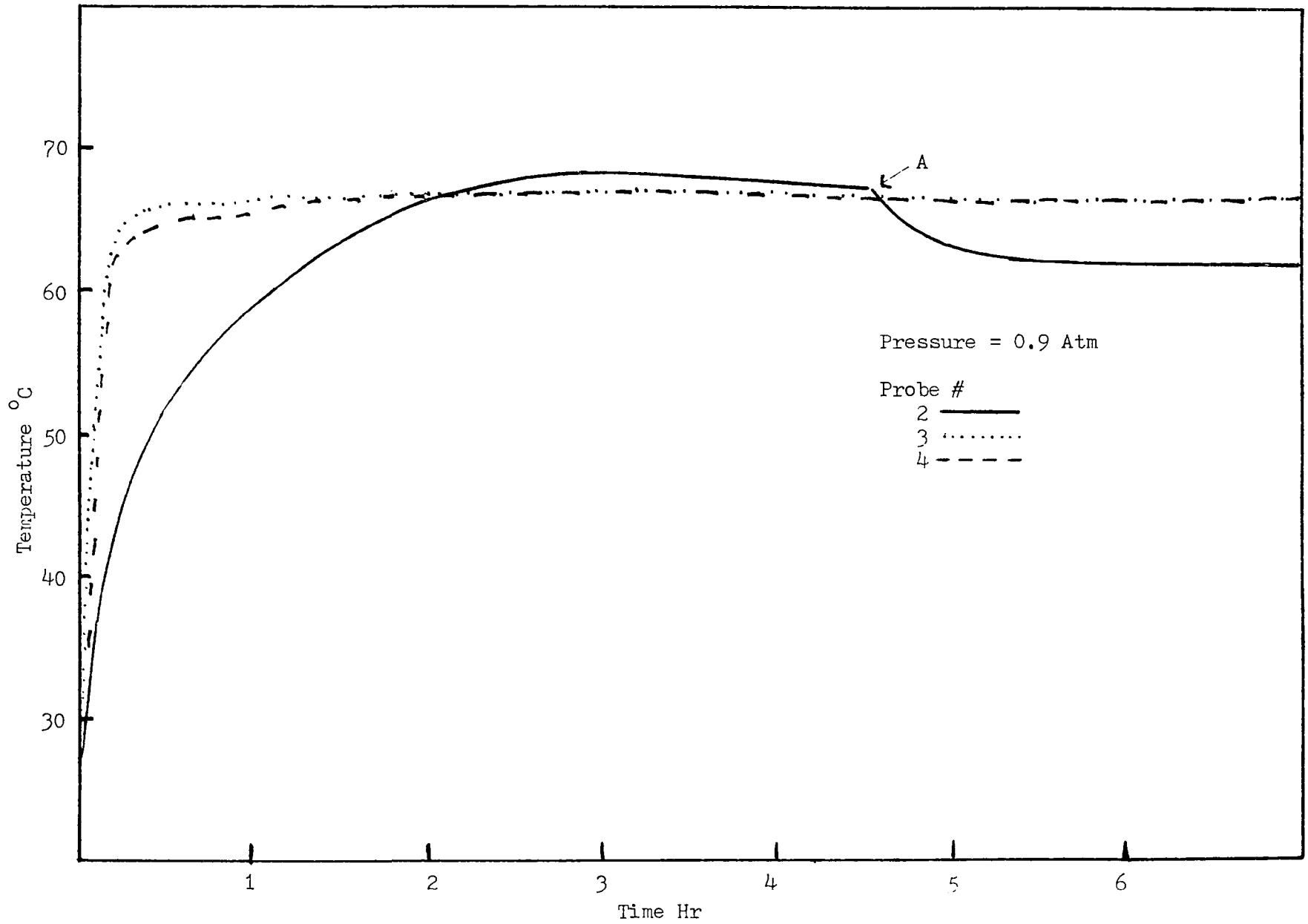


Figure 22. Absorption cell - temperature equilibrium

for long term stability. Temperature gradients within each bath were reduced by mechanical stirring.

For temperatures above ambient the bath is operated with heating coils which are regulated by a proportional temperature controller. The resulting regulated temperature was better than 0.1 °C. For temperatures below ambient a Blue M Cooling Unit model PCC-13A-3 (see equipment list (7)) is used. By adding a heat load, it is possible to obtain an appropriate duty cycle and produce a temperature regulation in the cold bath to better than 0.2 °C.

The cell temperature is checked with six thermocouples spaced along its length. The temperature variation along the cell is about 1 °C, while fluctuations in time at a given point are 0.1 °C.

5. Pressure Regulation

The compressor (H in figure 11, C in figure 19) is used for operations above 13 psi and is bypassed otherwise. The bellows type compressor (see equipment list (4)) is constructed entirely of stainless steel to eliminate contamination of the sample gas. A pressure relief valve is set to release at 7 psig for protection of the cell windows.

The cell pressure is measured with a Bourdon tube type gauge (see equipment list (8)). The pressure is regulated with a photoelectric manometer controller (see equipment list (6)) with a precision of 0.2 mm Hg. The controller (E in figure 11 and A in figure 19) actuates a solenoid valve regulating the rate at which the gas is exhausted through a vacuum pump.

6. HgCdTe Detector

A HgCdTe detector with a sensitive surface area of approximately 4 mm^2 was used to record the light intensity which exited from the monochromator. Figure 23 shows its spectral response as measured by the Santa Barbara Research Center.

The HgCdTe detector (see equipment list (9)) is photoconductive and thus a bias voltage is required to generate the output signal (see figure 24). Because of the low impedance of the detector, a transformer with a ratio of about 50 was used to match it to the high impedance input of the Princeton Applied Research preamplifier (see equipment list (10)). The electrical phase shift caused by the transformer is compensated by a readjustment of the reference lamp position.

A voltage divider circuit is used between the lock-in amplifier and the strip chart recorder input.

The detector is designed for operation at 77 ^{o}K and is housed in a type 520S dewar; thus its spatial orientation was prescribed. This style dewar requires that the light beam enter the detector window vertically. Two detector housing plates were fabricated to accomodate this orientation. Figure 25 shows the elliptical mirror mounting plate which was set vertically inside the detector housing. The top plate of the housing, figure 26, is constructed so that the detector can be positioned in the path of the exit beam. Since the detector's sensitive area is fairly small careful horizontal and vertical positioning is needed to optimize its output signal.

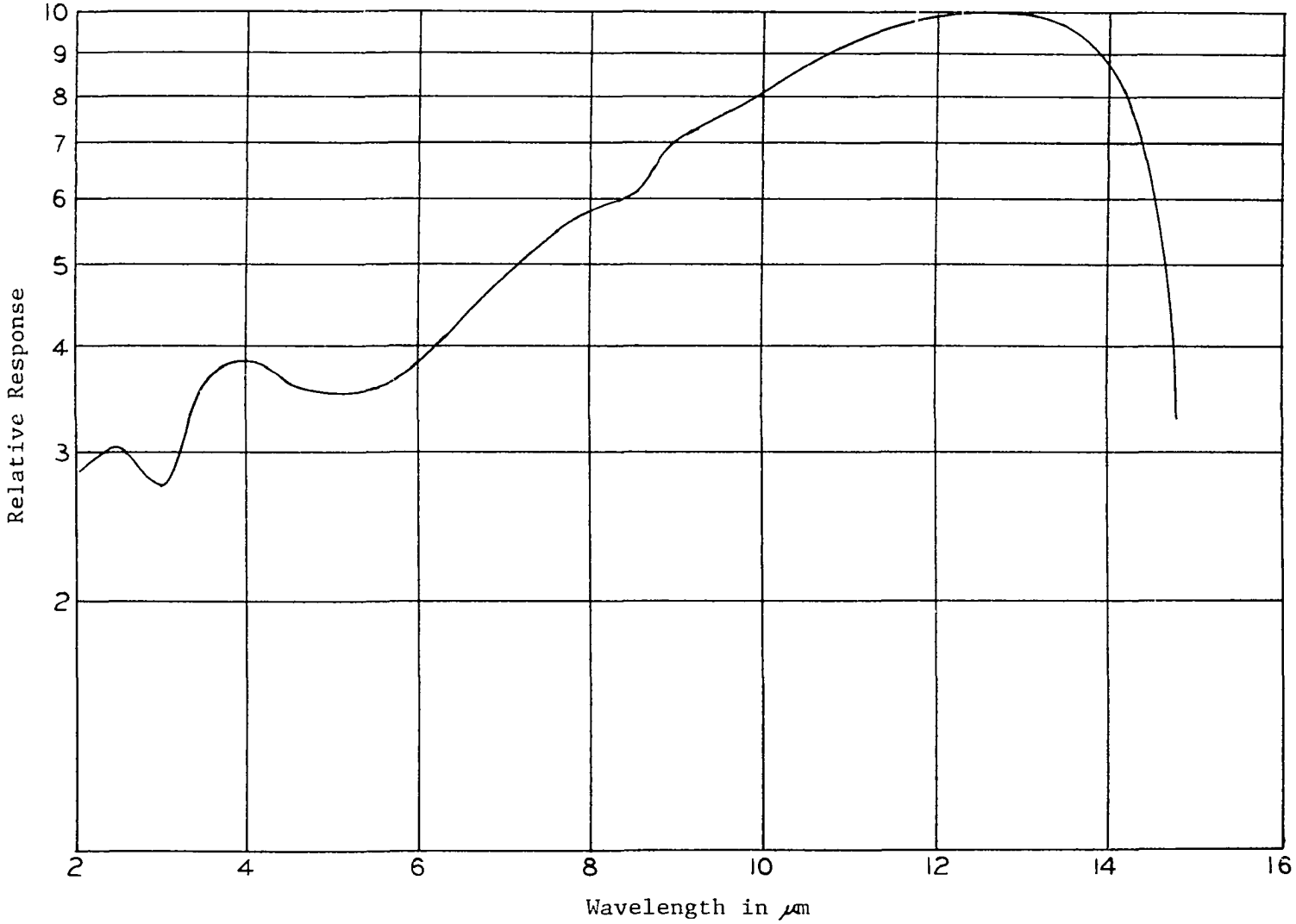
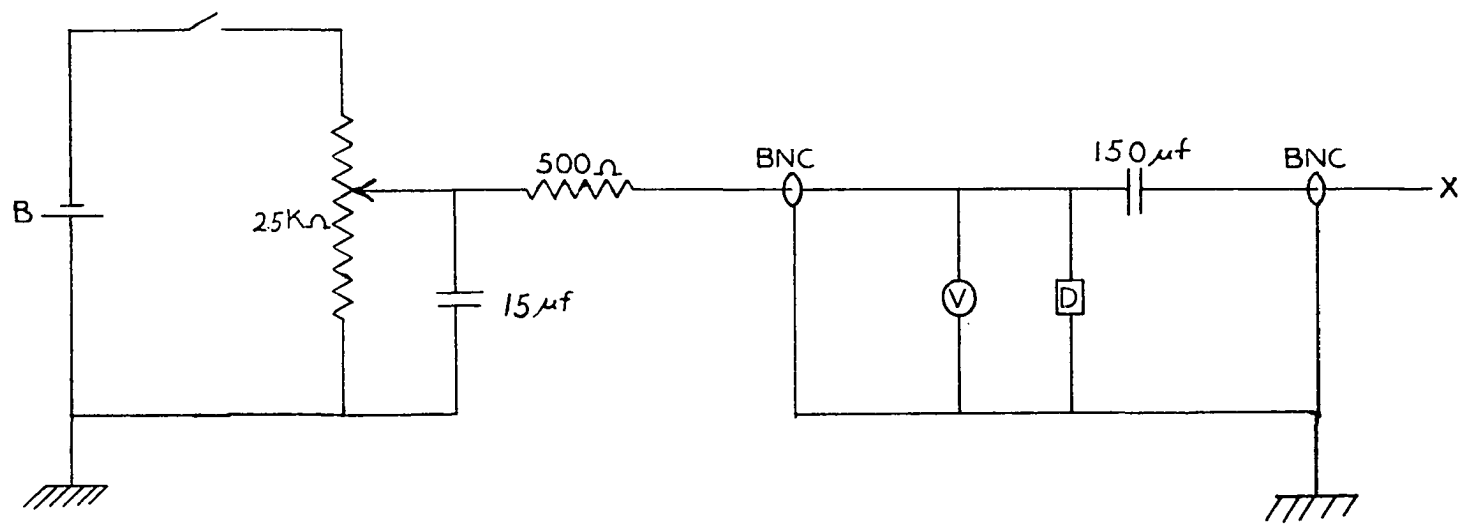


Figure 23. HgCdTe detector relative spectral response
Detector No. 86262, Temperature = 77 °K, IRtran II windows



B 4.2 V MERCURY CELL
D DETECTOR, 167Ω AT 77°K
V VOLTMETER
X TO TRANSFORMER INPUT OF PREAMP

Figure 24. HgCdTe DETECTOR BIAS CIRCUIT

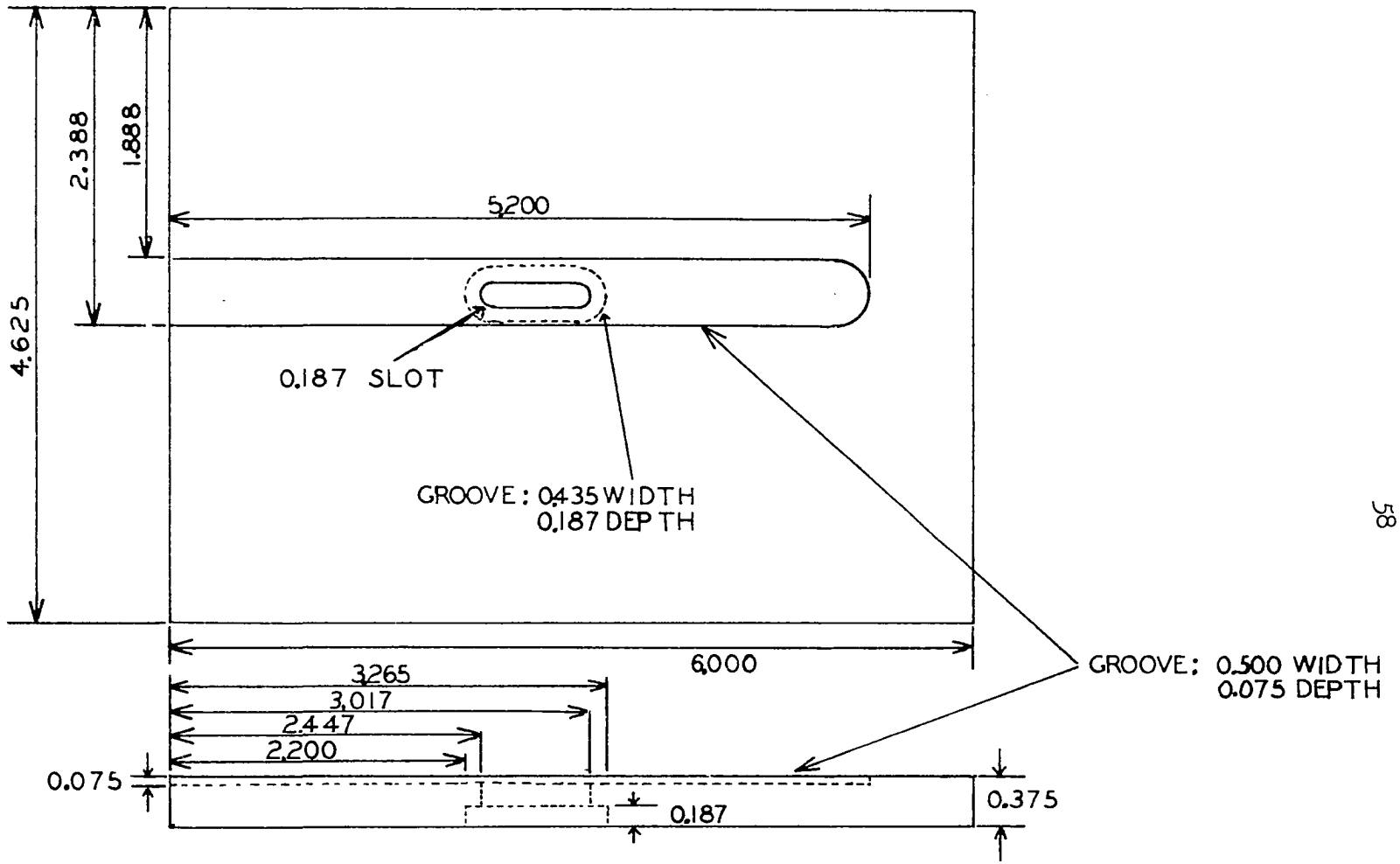


Figure 25. ABSORPTION CELL — DETECTOR HOUSING
BASE PLATE FOR ELLIPTICAL MIRROR MOUNT
MATERIAL —— ALUMINUM — BLACK ANODIZED

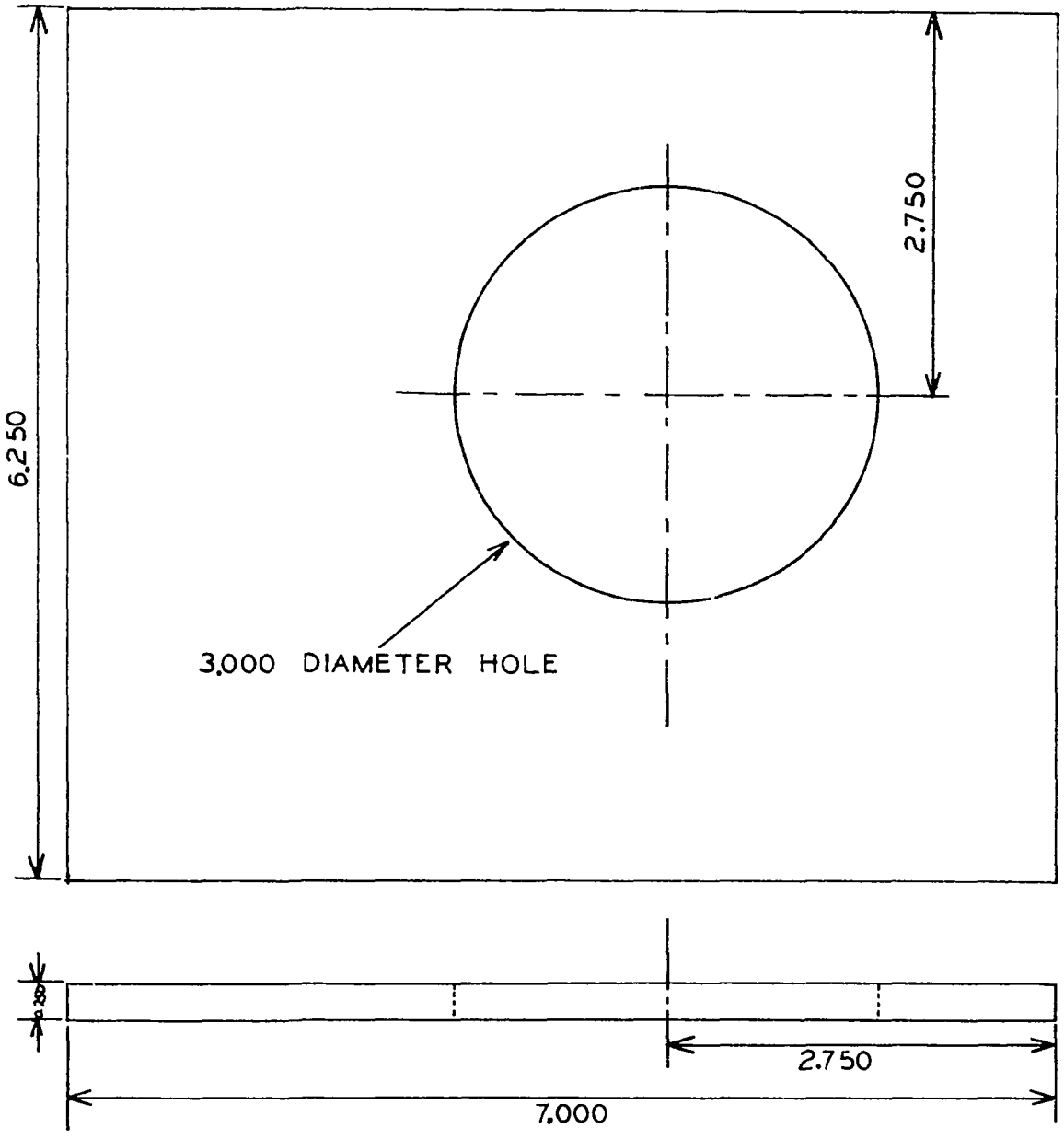


Figure 26. ABSORPTION CELL — DETECTOR HOUSING
TOP PLATE
MATERIAL —— ALUMINUM - BLACK ANODIZED

All housing components, most of which were constructed from aluminum, were black anodized. This was preferred over a chemical coating on account of possible chemical vapor contamination. Furthermore the housing was continuously flushed with dry nitrogen during all data acquisition. The detector housing was light tight. Also in order to prevent any extraneous light, which traveled along the optical path, from striking the detector, a long wave pass filter was installed at the exit slit of the monochromator. The filter which has a germanium substrate has a transmission of $< 0.1\%$ below $4\ \mu m$ and $> 75\%$ in the range of $4.16\ \mu m$ to $8\ \mu m$. Figure 27 shows the filter holder.

7. Detector Extension Dewar

The infrared detector was mounted in a type 520S dewar which has a very short liquid nitrogen hold time of only about 10 minutes. This meant adding liquid N_2 approximately every 5 minutes. An instrument operation with this constant annoyance would have seriously impaired data acquisition.

Two solutions were readily available. One was the installation of a liquid nitrogen level control. This was undesirable partly because of the large expense involved. Secondly a miniature Joule-Thomson cryostat was considered. This device would have been rather cumbersome because of the large amounts of compressed N_2 required.

Therefore we designed an extension dewar. Figure 28 shows a cross-sectional view. To minimize heat losses, the inner dewar wall

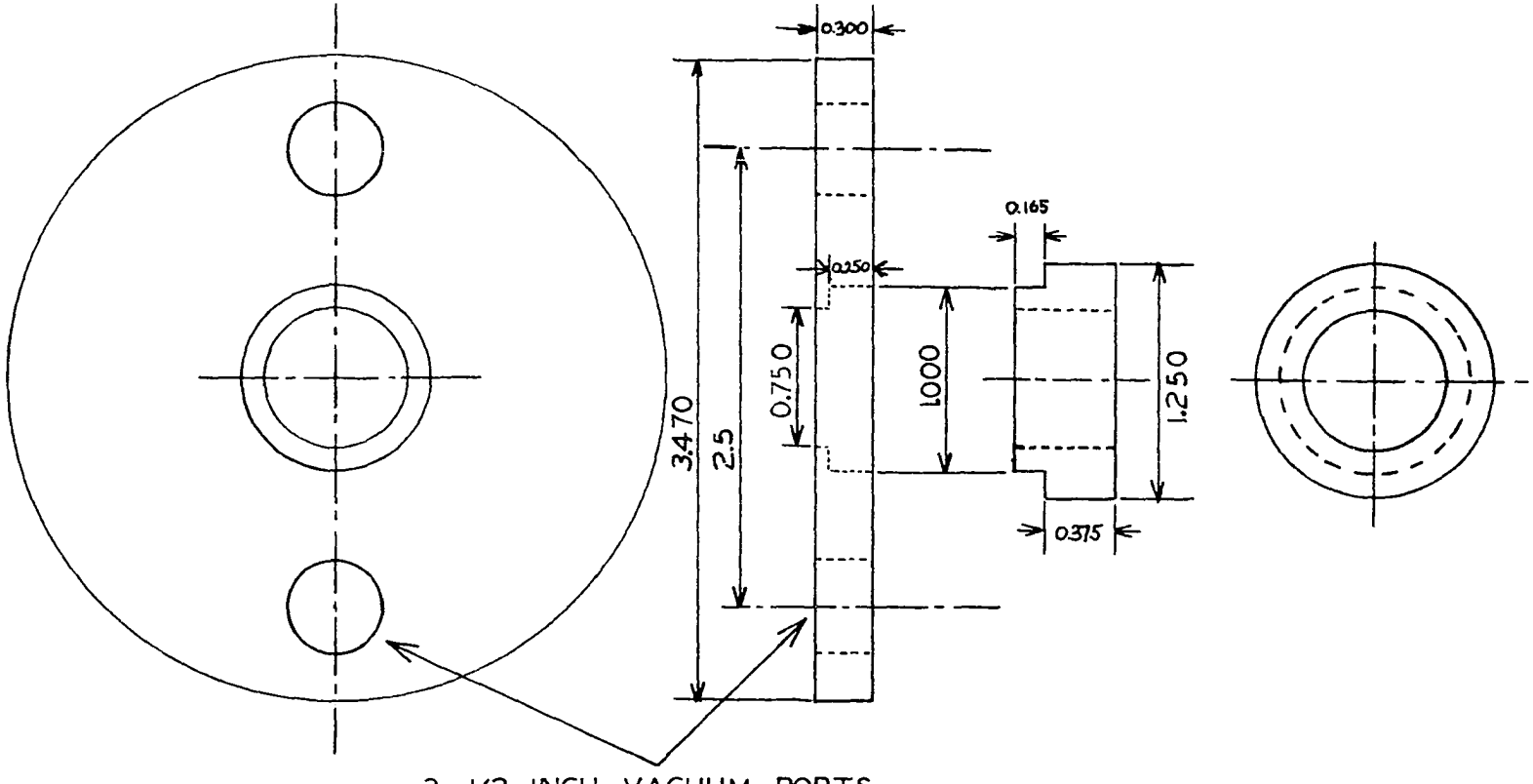


Figure 27. LWP FILTER HOLDER
MATERIAL —— PLEXIGLAS

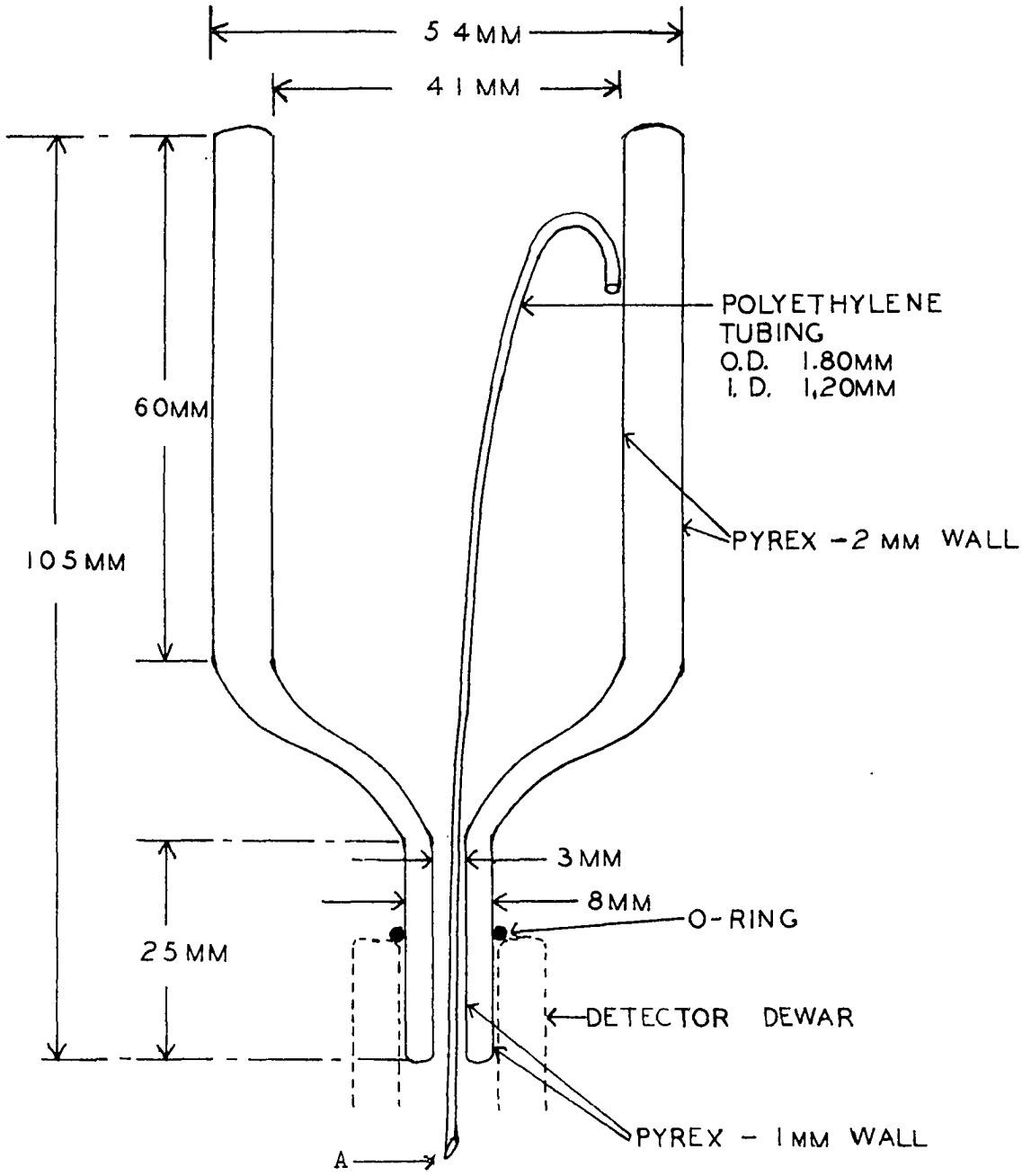


Figure 28. LIQUID NITROGEN EXTENSION DEWAR

Liquid nitrogen from the detector dewar is ejected through the polyethylene tubing into the extension dewar when the liquid level in the detector dewar reaches point A.

were silvered before evacuation. With the extension dewar operating in conjunction with the detector dewar, the liquid nitrogen hold time was increased to approximately 100 minutes. See figures 29 and 30.

In its operating position a snug O-ring, placed around the lower neck of the extension dewar, makes a seal against the detector dewar. A small amount of stop-cock grease was used to maintain this seal.

When filled with liquid nitrogen the extension dewar provides a slow flow into the detector dewar below. The gaseous nitrogen produced in the lower dewar can at first escape through the polyethylene tubing. When the liquid level in the detector dewar, as it is being filled up, reaches the lower end of the polyethylene tubing, excess liquid nitrogen is ejected through this tubing into the extension dewar. The operating level of liquid nitrogen in the detector dewar is thus automatically maintained at this constant value. The vertical position of the polyethylene tubing and the O-ring was reproduced for all data runs.

8. Vapor Flow Operating Procedure

The following discussion gives a detailed description of the procedure used in operating the flow system manifold and is therefore written step by step. Refer to figure 19.

For protection of the mercury U-tube manometer in the pressure cell regulator, stopcock (16) should remain open until the desired cell pressure is nearly attained.

Starting with all valves closed, open valve (1) and set the pressure regulator on the N_2 cylinder to 20 psig. Subsequently open

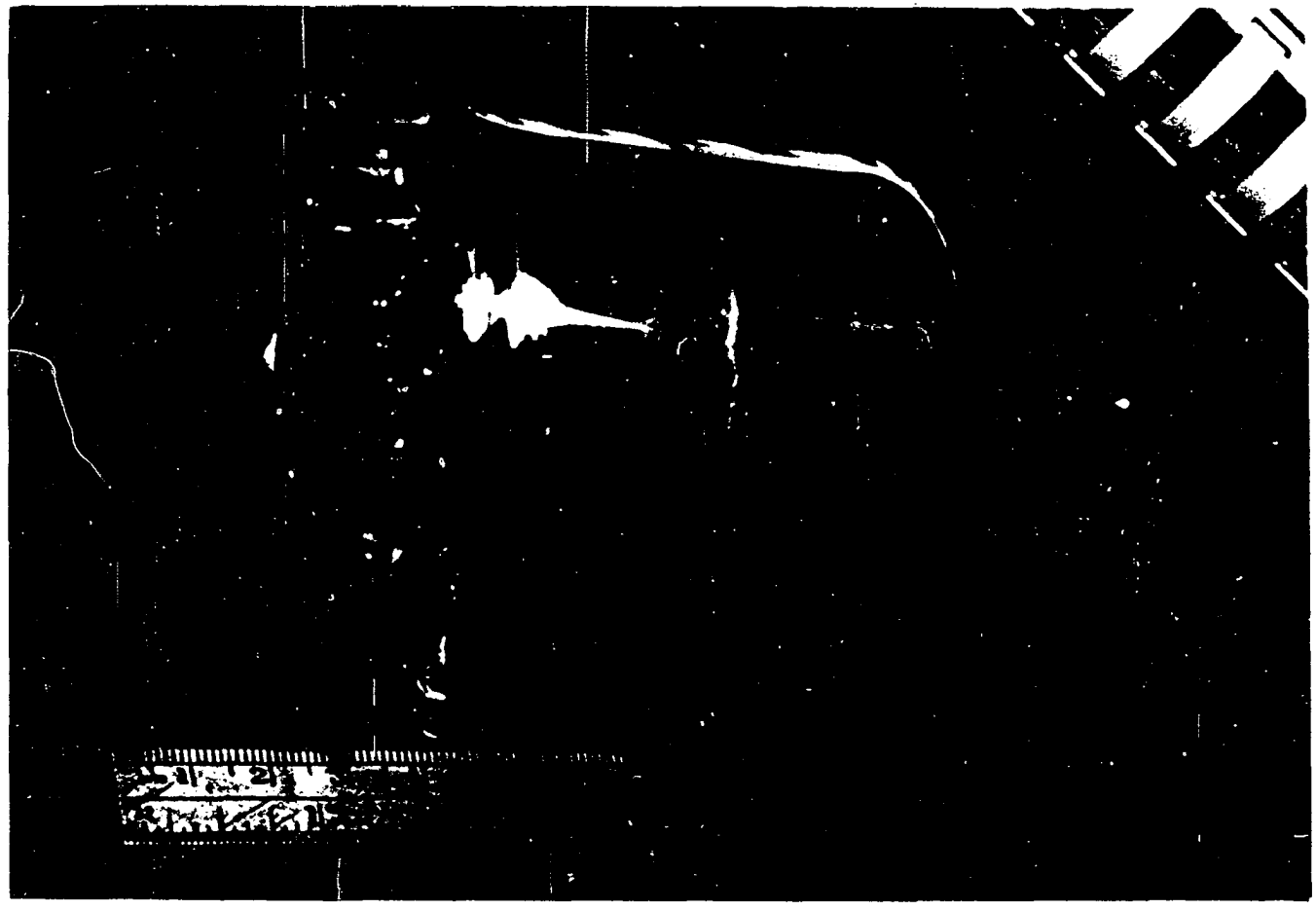


Figure 29. Liquid nitrogen extension dewar

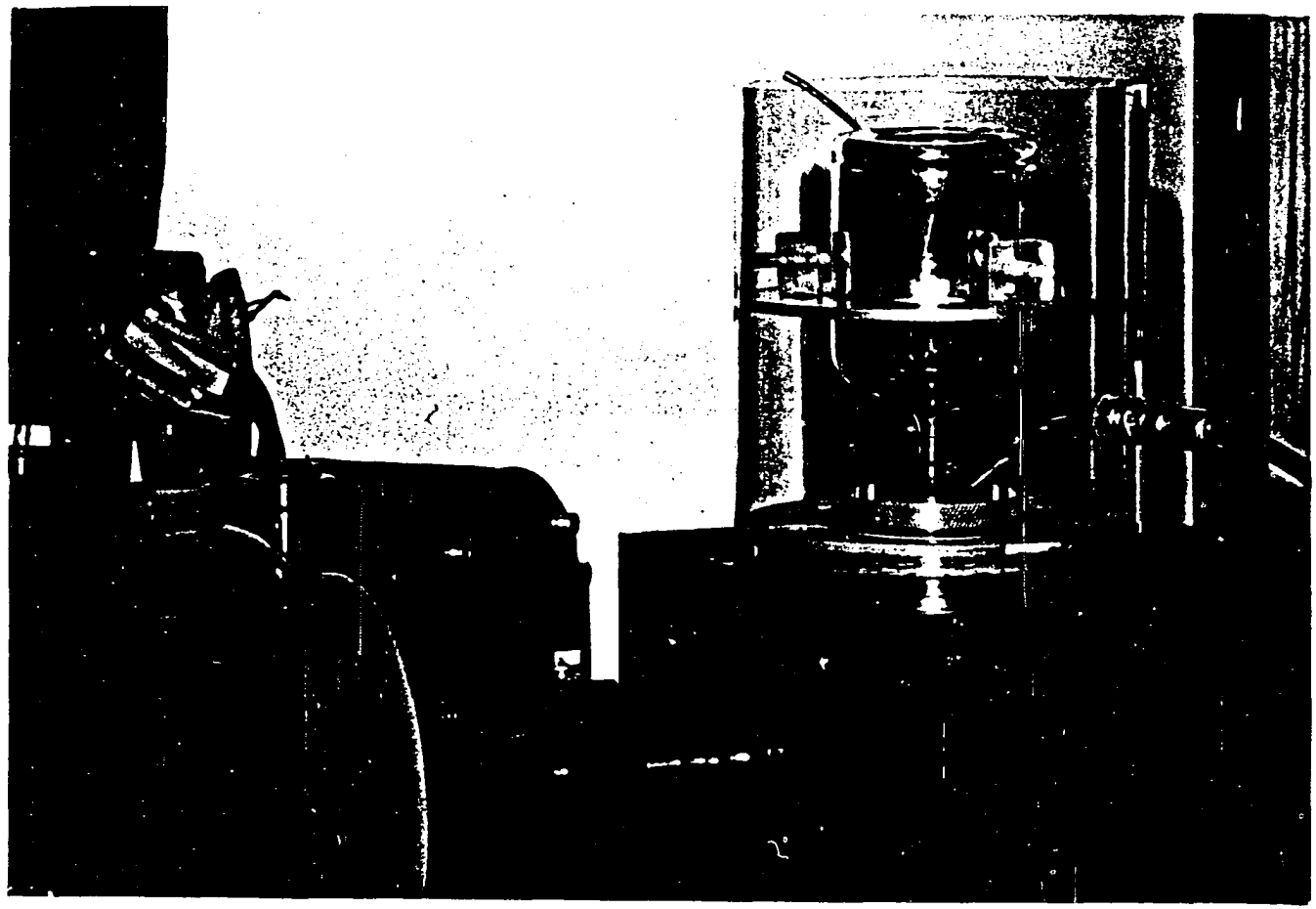


Figure 30. Liquid nitrogen extension dewar in its operating position

needle valve (4) completely and then open valve (2). Adjust needle valve (3) for the desired total flow of nitrogen as measured by the flowmeter FL1. Turn on the exhaust fan (F) which exhausts the cell to outside the building. Next turn on the vacuum pump (V). Open exhaust valve (20); allow the cell to be pumped down and then close this valve. Open valves (11), (5), (6), and either (7) or (8) depending on whether or not the compressor (C) is being used. The compressor is used if the cell pressure is to be greater than 13 psi. Adjust needle valves (5) and (6) to give the desired mixture of dry and humid nitrogen. The cell is now being filled with approximately the proper water vapor concentration. A fine readjustment of the humidity will be made later. When the desired cell pressure is obtained, close stopcock (16), open exhaust valve (20), and adjust needle valves (17) and (18) so that this pressure is maintained. About 5% of the gas should go through valve (17) when the solenoid valve controlled by the cell pressure regulator is open. The solenoid will then switch with about a two second cycle.

The humidity may now be readjusted by using valves (5) and (6) with little disturbing effects of the total flow. Also the total flow rate through the cell may be adjusted with valves (18) and either (7) or (8) with little effect on the humidity.

Now turning our attention to the function of the hygrometer manifold we see that valves (10) through (15) provide four possible modes of operation. First the hygrometer may be bypassed completely with only valves (11) and (14) open. Secondly the hygrometer may

monitor the vapor before entrance into the cell. This is fulfilled by opening valves (10), (12), and (14). Next the exit vapor may be monitored by opening (11), (13), and (15). Finally the vapor may be monitored while bypassing the cell chamber completely. This is done by opening (10) and (15). This is useful for adjusting the concentration before injection into the cell.

C. Data Acquisition

The data recorded was the transmitted light intensity as a function of wavelength over the range of 4.6 μm to slightly above 8 μm.

It was desirable to utilize those procedures that produced the best accuracy and most reproduceable results. Therefore all conditions that might have any influence upon the results were recorded. Various environmental conditions were noted and controlled as much as possible for it was necessary to make comparisons of any one data scan with another. Periodic checks of critical parameters were made during data acquisition. This aided in the prevention of any otherwise unaccounted for errors or drifts in the instrument function. This became an important ritual since much of the data was taken over periods of continuous operation for as long as 30 - 35 hours. These long times of continuous operation permitted more measurement time, since the start up time (time for all equilibria to be established; about 3 hours) and shut down time (about 1 hour) was a significant portion of a day.

Getting ready for a particular data scan meant turning the instrument on in a systematic way. This included starting the left and right fore-pumps to evacuate the ends of the cell; turning on all electronics to allow time for sufficient warm-up; starting and setting the temperature bath; turning on the humidity chamber and allowing time for its operation to stabilize; checking and resetting (when necessary) all conditions of the cell.

Once the cell was in full operation it would run almost automatically; especially the aid of the detector extension dewar permitted a steady measurement.

Since establishment of thermal equilibrium of the system required a much longer time than that of either pressure or concentration, temperature was given priority in the operating procedure. For any given temperature, all necessary data scans were obtained by going through the prescribed series of pressures (starting at the lowest value) at a given concentration, then changing the concentration to the next higher value and repeating the series of pressures. I_o scans were taken before the introduction of water vapor into the cell as well as between changes of concentration and at the end of the particular temperature series.

Cell history was an important factor as is reflected in the discussion of the reference scans (I_o) in the next chapter. After each series of scans was completed, the same procedure was followed in terminating the operation of the instrument. After evacuating the cell chamber it was always filled with dry N_2 for the periods of

inoperation. This reduced the pump down time when used again and diminished any long term corrosive effects that the water may have on the internal components such as windows. For similar reasons, in general, room air was not allowed inside the cell.

Chapter IV Analysis of Results

A. General Procedure

As mentioned previously our instrument recorded the transmitted infrared light intensity as a function of wavelength λ. In all data scans the abscissa was linear in wavelength. Each spectrum was digitized by reading the infrared transmission at 435 equally spaced values of the wavelength. This wavelength spacing (0.008 μm) was necessary to give an accurate representation of the spectra in all wavelength regions of the spectra. The data was converted to absorptance according to

$$A_i = 1 - I(\lambda_i)/I_o(\lambda_i) \tag{19}$$

where $I(\lambda_i)$ and $I_o(\lambda_i)$ are the transmission of the sample and reference at a given λ_i. The values of A_i are, of course, the averages as weighted by the monochromator spectral distribution function.

The monochromator entrance and exit slits were set at 2 mm width for all data scans. The spectral distribution function is assumed to be a triangle with a half-intensity band pass $(\Delta\lambda)_{\frac{1}{2}}$, given by the product of the slit width and the reciprocal linear dispersion, i.e.

$$(\Delta\lambda)_{\frac{1}{2}} = (2 \text{ mm})(0.0212 \ \mu\text{m/mm}) = 0.04 \ \mu\text{m}$$

The half- intensity band pass in terms of wavenumber is given by

$$(\Delta\nu)_{\frac{1}{2}} = (\Delta\lambda)_{\frac{1}{2}}/\lambda^2 = (400/\lambda^2), \quad (\lambda \text{ in } \mu\text{m})$$

For the wavelength range of 4.6 μm to 8.0 μm the half-intensity

band pass varies from 18.9 cm^{-1} to 6.25 cm^{-1}.

The most widely accepted spectral format is to let the abscissa be linear in wavenumber. We chose to do this. We also chose to further degrade the data by computer to a constant half-intensity band pass of 25 cm^{-1} using a triangular slit function. The 25 cm^{-1} band pass was also useful for a comparison with theoretical calculations of the absorptance.

The slit function $\rho(\nu)$ chosen for the computer degrading is

$$\begin{aligned} \rho(\nu) &= a - |\nu_i - \nu_j|, \quad \nu_j - a \le \nu \le \nu_j + a \\ \rho(\nu) &= 0 \qquad\qquad\qquad \text{otherwise} \end{aligned} \tag{20}$$

where $a = 25\ cm^{-1}$. Each of the original data points represents the mean fraction absorption in a small wavenumber region $\Delta\nu$.

$$A_i \approx \frac{1}{\Delta\nu_i}\int_{\Delta\nu_i} A(\nu)\,d\nu \tag{21}$$

Thus $A_i \Delta\nu_i = A_i(\Delta\lambda/\lambda_i^2)$ represents the total absorption in each region $\Delta\nu_i$ (here $\Delta\lambda = 0.008\ \mu m$ is the data point spacing taken in the digitizing process). Now we have the absorptance as a function of wavenumber, $A(\nu_j)$, given in terms of the original digitized data points (A_i, λ_i) as

$$A(\nu_j) = \frac{\int A(\nu)\,\rho(\nu)\,d\nu}{\int \rho(\nu)\,d\nu} \approx \frac{1}{a^2}\sum_i (A_i \cdot \Delta\lambda/\lambda^2)(a - |\nu_i - \nu_j|) \tag{22}$$

Here the sum is over all i such that $\nu_j - a \le \nu_i \le \nu_j + a$. We chose ν_j at 5 cm^{-1} intervals. Thus the 435 points read from each spectra over the range 4.6 μm to 8 μm became 185 points equally spaced from 1225 cm^{-1} to 2150 cm^{-1}.

The total number of data points read from the original charts for all scans approached 20,000. All of these three digit values were entered into the computer via a time-sharing terminal.

Figure 31 displays the effect of degrading the data by computer. Curve A shows a typical scan of absorptance vs wavenumber with a band pass of 0.04 micron. It is obvious that extreme care had to be exercised in the reading of the original curves since a small shift in the abscissa may result in a large error in the ordinate, especially in the steep regions of the curve. For the same reason careful attention was always given to accurately synchronizing the monochromator and the chart recorder. The B curve is the result of the data after having been degraded by computer to a band pass of 25 cm^{-1}. The main thrust of this investigation was directed toward examining the effect of the band absorption as a function of c, p, and T; thus this choice for the band pass supressed all fine rotational structure in the band. All the results are degraded to 25 cm^{-1} unless stated otherwise.

B. Reference Spectra

Several reference spectra (I_o) were obtained throughout each series of data scans. This sequence is shown in table I , column 3. The absorption data scan ratio I/I_o was used to plot the sample absorptance.

It was found that during the course of taking a data series the reference curves had certain "background water" absorption trends.

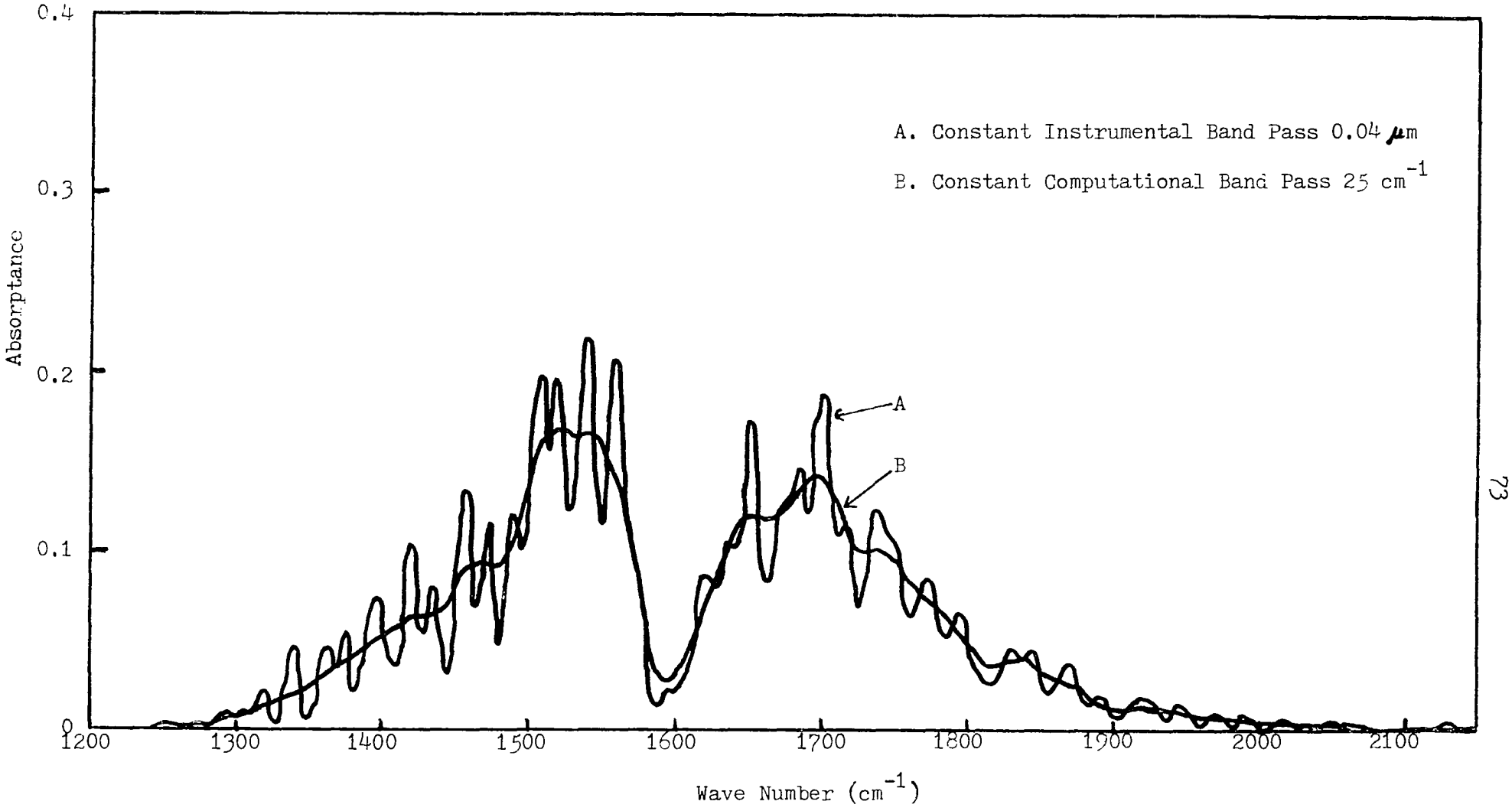


Figure 31. Absorptance as a function of band pass

TABLE I Data Sequence

Data Series	Scan no.	Reference I_o	T(^oC)	C(%)	P(atm)	Interpolated I_o
I	1	x	15			
	2		15	0.4	1	$1.5I_o$(I-3) - $0.5I_o$(I-5)
	3	x	15			
	4		15	0.8	1	$0.5I_o$(I-3) + $0.5I_o$(I-5)
	5	x	15			
II	1	x	15			
	2	x	15			
	3		15	1.6	1/3	$2I_o$(II-6) - I_o(II-9)
	4		15	1.6	1/2	$1.67I_o$(II-6) - $0.67I_o$(II-9)
	5		15	1.6	2/3	$1.33I_o$(II-6) - $0.33I_o$(II-9)
	6	x	15			
	7		15	1.6	5/6	$0.67I_o$(II-6) + $0.33I_o$(II-9)
	8		15	1.6	1	$0.33I_o$(II-6) + $0.67I_o$(II-9)
	9	x	15			
	10	x	15			
	11	x	15			
III	1	x	40			
	2	x	40			
	3	x	40			
	4	x	40	1.6	1/3	$2I_o$(III-8) - I_o(III-11)
	5	x	40	1.6	1/3	$2I_o$(III-8) - I_o(III-11)
	6		40	1.6	2/3	$1.67I_o$(III-8) - $0.67I_o$(III-11)
	7		40	1.6	1	$1.33I_o$(III-8) - $0.33I_o$(III-11)
	8	x	40			
	9		40	3.2	1/3	$0.67I_o$(III-8) + $0.33I_o$(III-11)
	10		40	3.2	1	$0.33I_o$(III-8) + $0.67I_o$(III-11)
	11	x	40			
IV	1	x	40			
	2		40	4.8	1/3	I_o(IV-4)
	3		40	4.8	1	I_o(IV-4)
	4	x	40			
	5	x	40			
V	1	x	65			
	2		65	1.6	1/3	$1.67I_o$(V-4) - $0.67I_o$(V-7)
	3		65	1.6	1	$1.33I_o$(V-4) - $0.33I_o$(V-7)
	4	x	65			
	5		65	4.8	1/3	$0.67I_o$(V-4) + $0.33I_o$(V-7)
	6		65	4.8	2/3	$0.33I_o$(V-4) + $0.67I_o$(V-7)
	7	x	65			
	8	x	65			
	9		65	4.8	1	$0.67I_o$(V-7) + $0.33I_o$(V-12)
	10		65	4.8	1	$0.67I_o$(V-7) + $0.33I_o$(V-12)
	11		65	4.8	5/4	$0.33I_o$(V-7) + $0.67I_o$(V-12)
	12	x	65			
	13	x	65			

In the worst cases errors in excess of 10% could easily be introduced by ignoring these trends. This indicated that a careful use of the I_o scans was critical.

It is apparent from figures 32 to 34 that the I_o curves display some random instrument instabilities but also may have maxima in the same regions where water vapor has its maximum absorption. Whatever the reasons for this variation in the "background water", the importance of taking sufficient reference data is demonstrated.

With reference to table I , the scans which were taken at the beginning of each data series were obtained after the cell had been unused for several hours. During these periods of nonuse, the cell first had been evacuated and then filled with dry nitrogen for storage. This ritual was adhered to since we desired to minimize any discrepancies in the absorption data arising from variations in the cell history.

The extent of the instrument instabilities may readily be extracted from the reference data. Figure 32 is a comparison of one vacuum scan with another taken in sequence. Here the nature and the magnitude of the instabilities are shown. The ordinate is greatly expanded to show detail. The instabilities are primarily due to variations in the globar output. One should note the absence of any "absorption" in the core of the water band.

Another aspect of the instrument operation concerns the effect of pressure; for comparison one curve (I) is taken at or near atmospheric pressure while the other (I_o) is recorded under evacuated conditions.

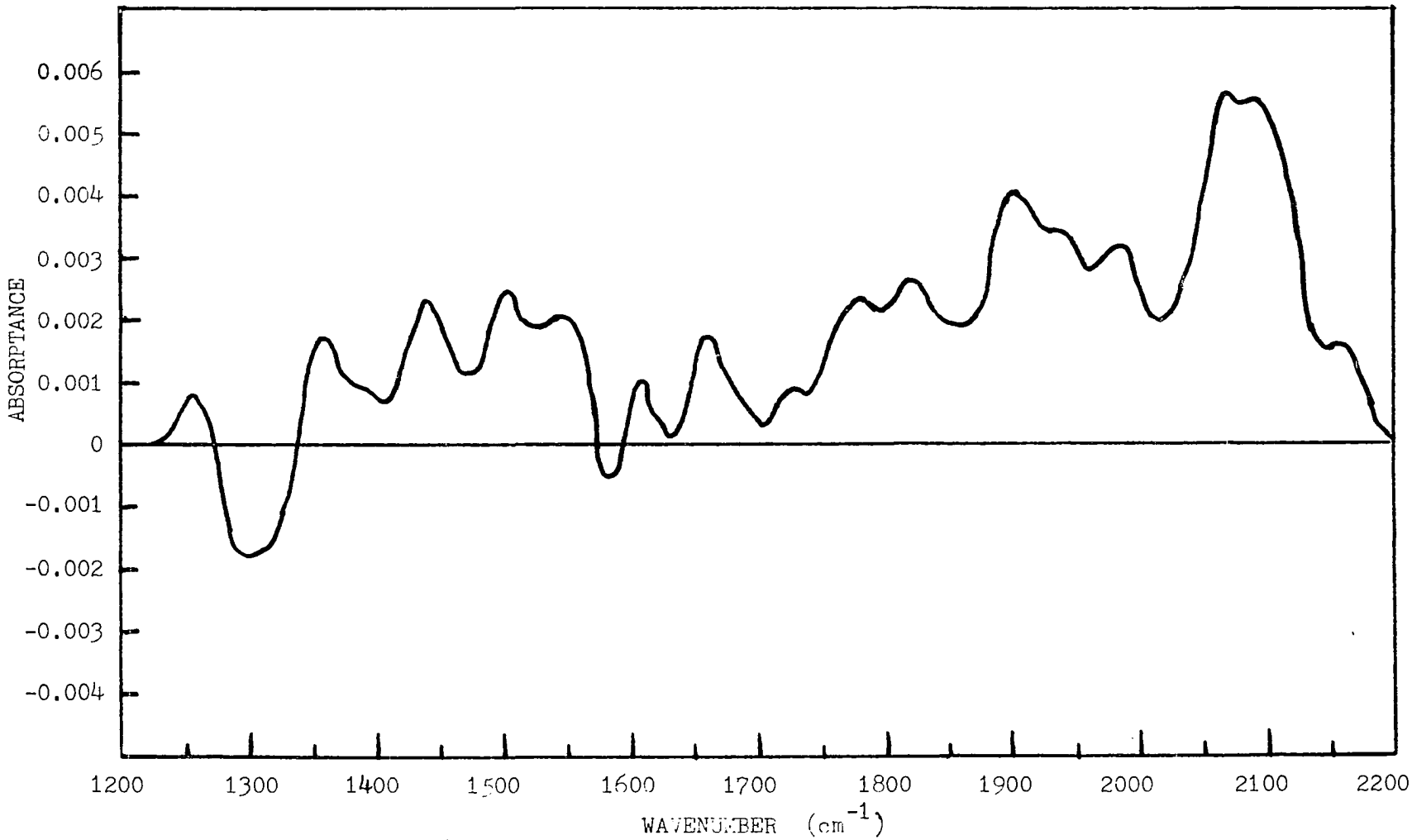


Figure 32. Apparent absorptance of vacuum vs vacuum reference scans

Could it be that the system optics were altered significantly in the process of cell evacuation? Or; might it be that a larger thermal nonuniformities in the instrument caused a discrepancy? This prompted a comparison of vacuum scans to those with dry nitrogen flow at atmospheric pressure. The results are shown in figure 33. Again the ordinate is expanded. The essential character of this graph does not differ from that of figure 32 where once again the dominant factor is the variation in the globar light flux.

The previous inquiry was logical considering the fact that in the process of evacuating the cell a change of 1% in the HgCdTe detector output was noted. However, inasmuchas this 1% change was not a function of wavelength, it was easily compensated for by a slight adjustment in the recorder gain. Thus for all I_o as well as I data scans, the gain was properly set at the starting point of λ = 4.6 micron. Ultimately this procedure reduced the amount of work necessary in handling the data by eliminating a scaling factor.

Now we turn our attention to the long range trends in I_o as illustrated in figures 34 and 35. Figure 34A shows little effect other than the random instabilities discussed previously. Evidently there were insignificant "background water" trends in the reference data for series II. This contained the bulk of the 15 ^oC work. Figure 34B shows a definite effect in the water band core. Note: the ordinate in (B) is contracted by a factor of 10 as compared to (A). These I_o scans correspond to the lower values of concentration at 15 ^oC. The difference in the two curves, (A) and (B), may be

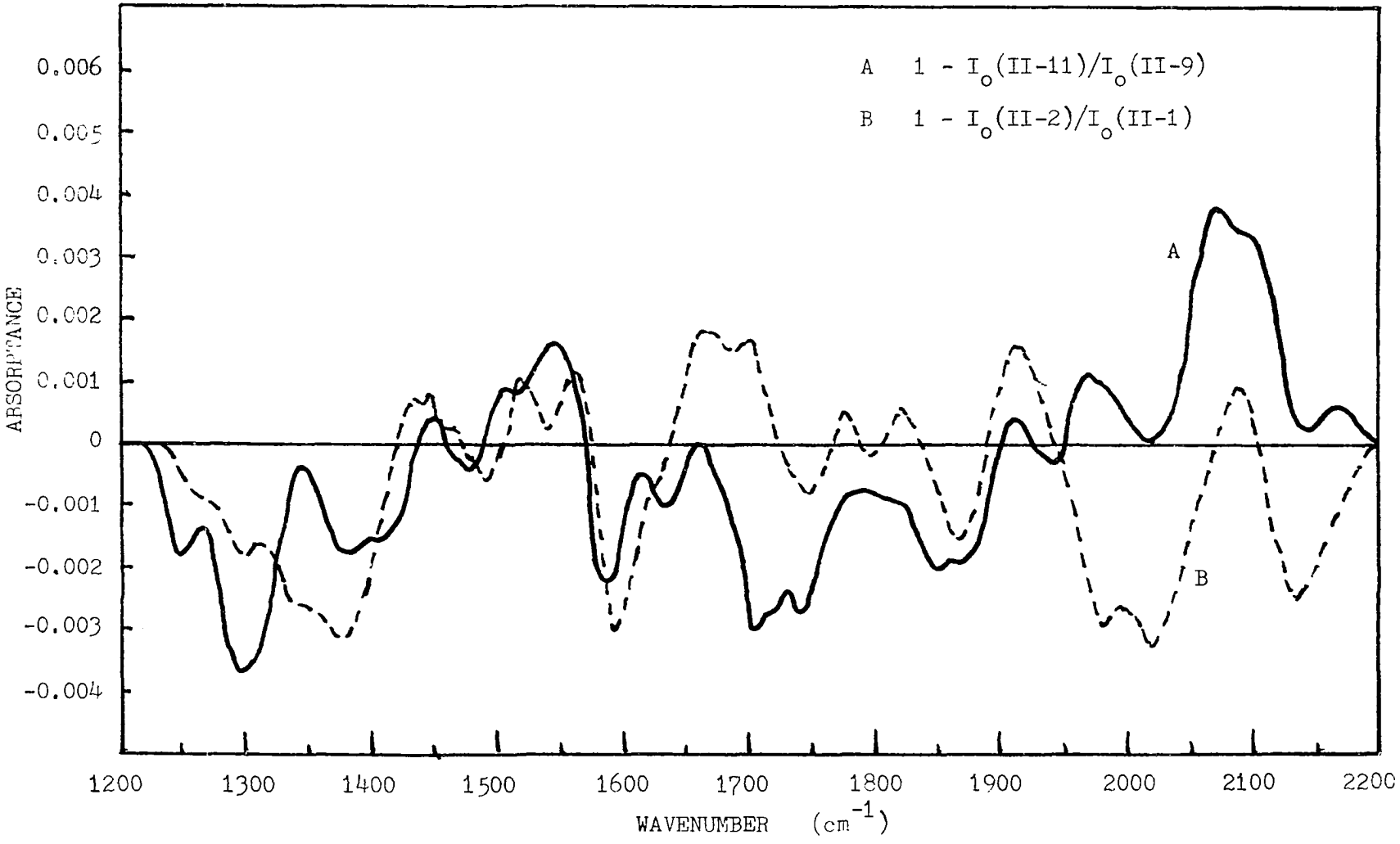


Figure 33. Apparent absorptance of dry nitrogen vs vacuum reference scans

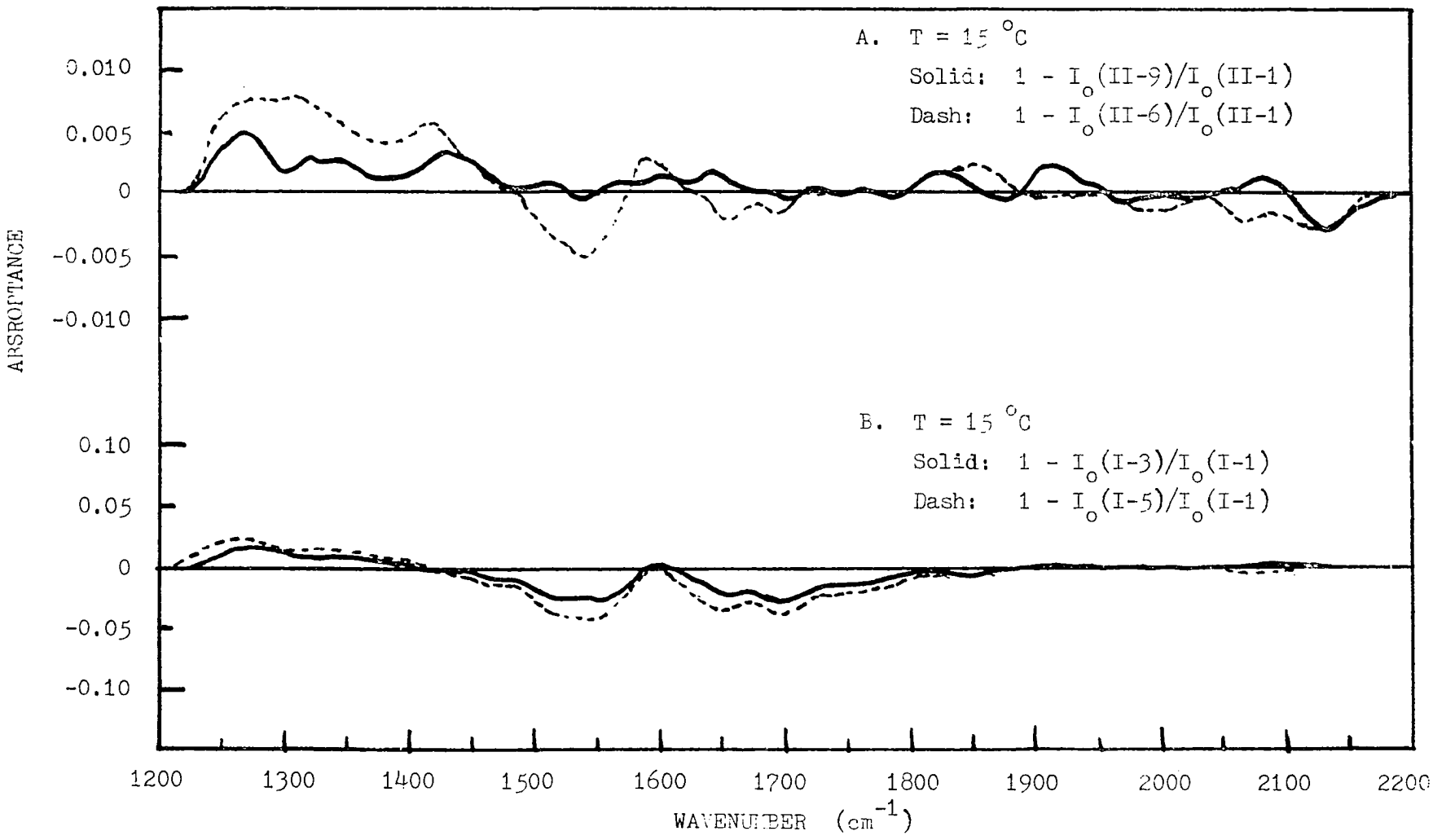


Figure 34. Trends in the 15 °C reference scans

related to the cell storage intervals. Whereas most data series were separated by storage times of only a few days, series I was taken after the instrument had not been used for several weeks. During this longer period of time the various optical surfaces were exposed to water vapor in the room. From this it seems that a more complete isolation of the instrument from the room would have been desirable.

Figure 35 reveals trends similar to the 15 ^{o}C graph. The effect is more pronounced for the higher temperature.

Obviously under optimum operating conditions one would attempt to eliminate all such trends in the reference data. Because these trends gradually developed over the total time needed for acquisition of a data series--typically 30-35 hours of continuous operation, the time demanded for their total elimination would have been excessive.

The proper question is how to eliminate the trend by using various I_o data scans. The solution finally judged best involved interpolating the I_o scans of any given data series to make one correspond with each I curve of that series.

Typically it was found that the rate of change in the I_o trends decreased as we progressed through a particular series. This indicated that the importance of the very first I_o taken in each series should be diminished. The interpolated I_o scans finally used are listed in the last column of table I.

Finally it should be noted that even though the background water effect is not fully understood, a sufficient number of I_o scans were

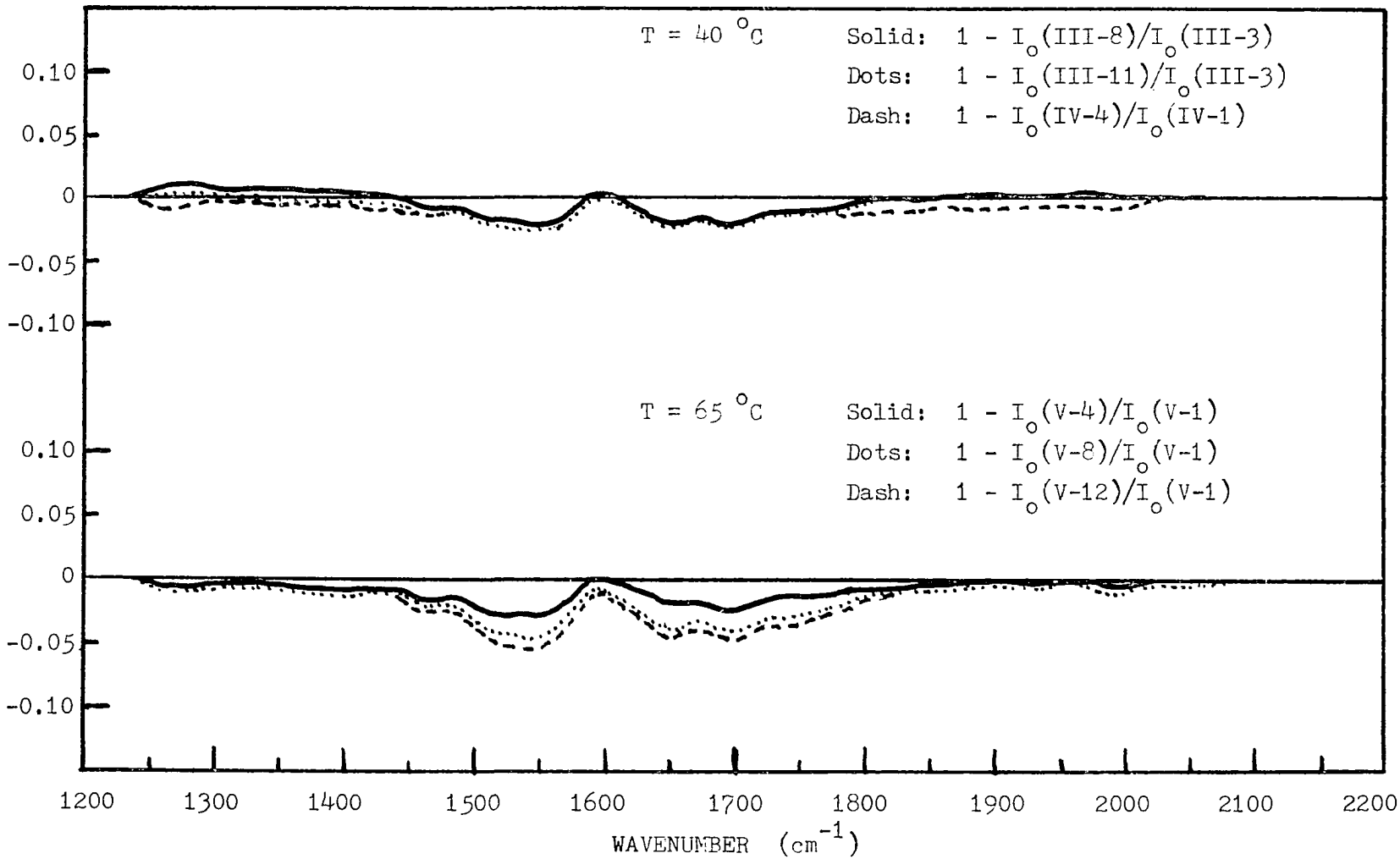


Figure 35. Trends in the 40 °C and the 65 °C reference scans

taken to permit a comparison between every sample measurement and a reference measurement obtained under similar conditions. We believe that in general the results for I/I_o(interpolated) can be relied upon to within 3% as far as variations in I_o are concerened.

C. Absorption Spectra

Figures 36 to 40 show the experimental absorption spectra curves. The solid lines represent the experimental values while the dot and circles indicate calculated spectra (Chapter II) for various values of concentration at 1 atmosphere and at 14.55 ^{o}C . Use was made of the line parameters of the individual lines for the calculation.[16]

The values of the band integrated absorptance for all the experimental curves are displayed in table II. The absorber mass in the column of 1.005 m length at 1 atmosphere and 14.55 ^{o}C for the five concentrations listed is 0.31, 0.62, 1.25, 2.49, and 3.74 in units of 10^{-3} gm/cm^2 respectively. The first integrated absorption column is taken from reference (20). The calculated values (at T = 14.55 ^{o}C) are listed in the 15 ^{o}C column at 1 atmosphere. The calculated values at 0.83 atm and 0.67 atm were obtained by using the calculated first and second order pressure derivatives. The values at higher temperatures were obtained by using the calculated first and second order temperature derivatives. The one value at 0.67 atm and 40 ^{o}C required the use of a calculated pT derivative.

The major experimental error in the integrated values (5%) is the accuracy of the concentration. In the calculations the ESSA

TABLE II

Integrated Absorptance for 1.005 m Column

c	p	Integrated Absorptance (cm^{-1})						
%	atm	15 °C			40 °C		65 °C	
	Total	Ref 20	exp	calc	exp	calc	exp	calc
0.405	1.00		53.4	60.6				
0.81	1.00		87	92				
1.62	0.33		47		41		42	
	0.50		69					
	0.67		92	91	84	88		
	0.83		115	113				
	1.00		137	133	128	129	128	125
3.25	0.33				66			
	1.00	180		187	188	181		
4.87	0.33				94		84	
	0.67						165	
	1.00	227		225	239	219	229	212
	1.25						260	

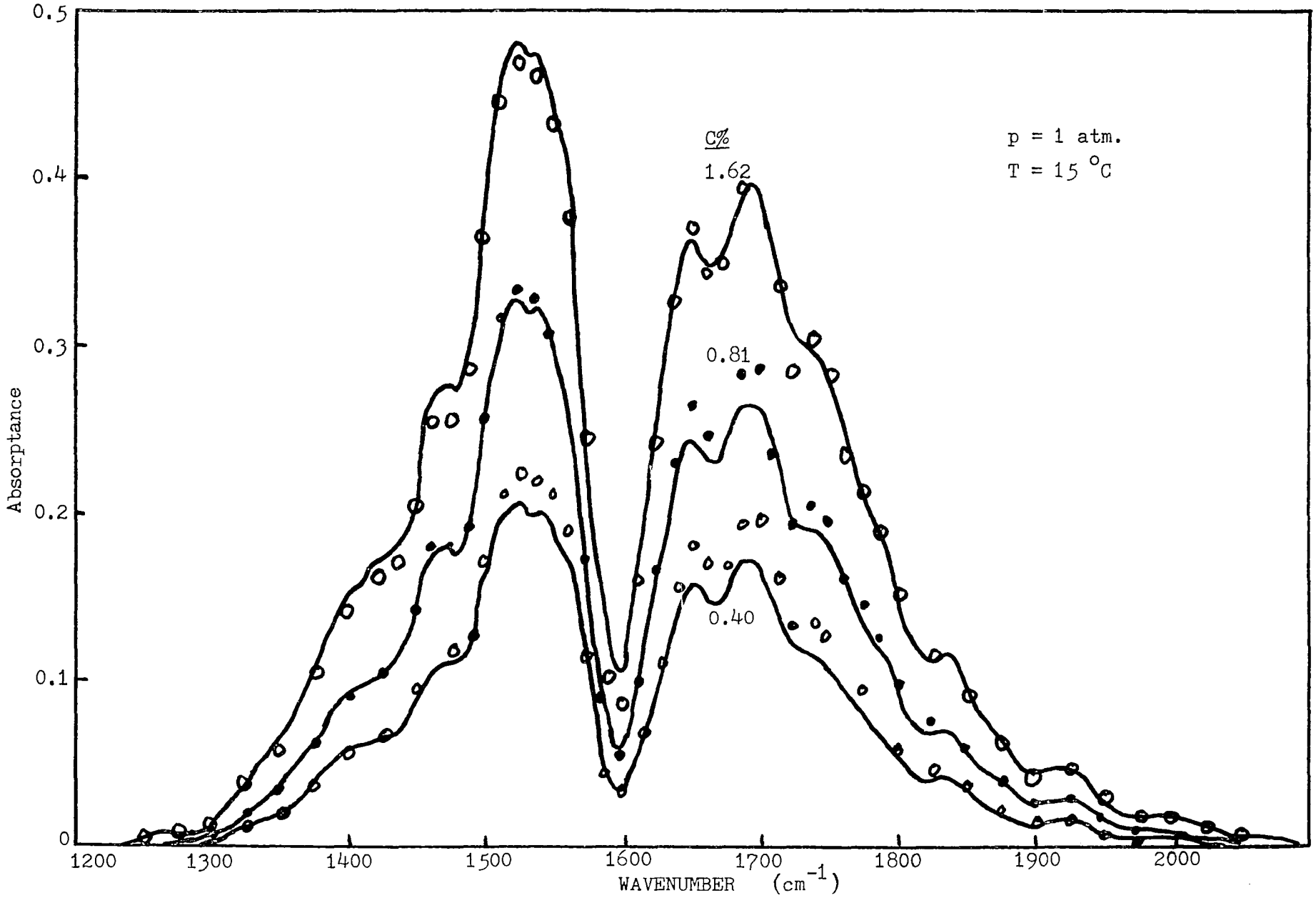


Figure 36. Absorptance as a function of concentration. The solid lines represent experimental values, while circles represent calculated values.

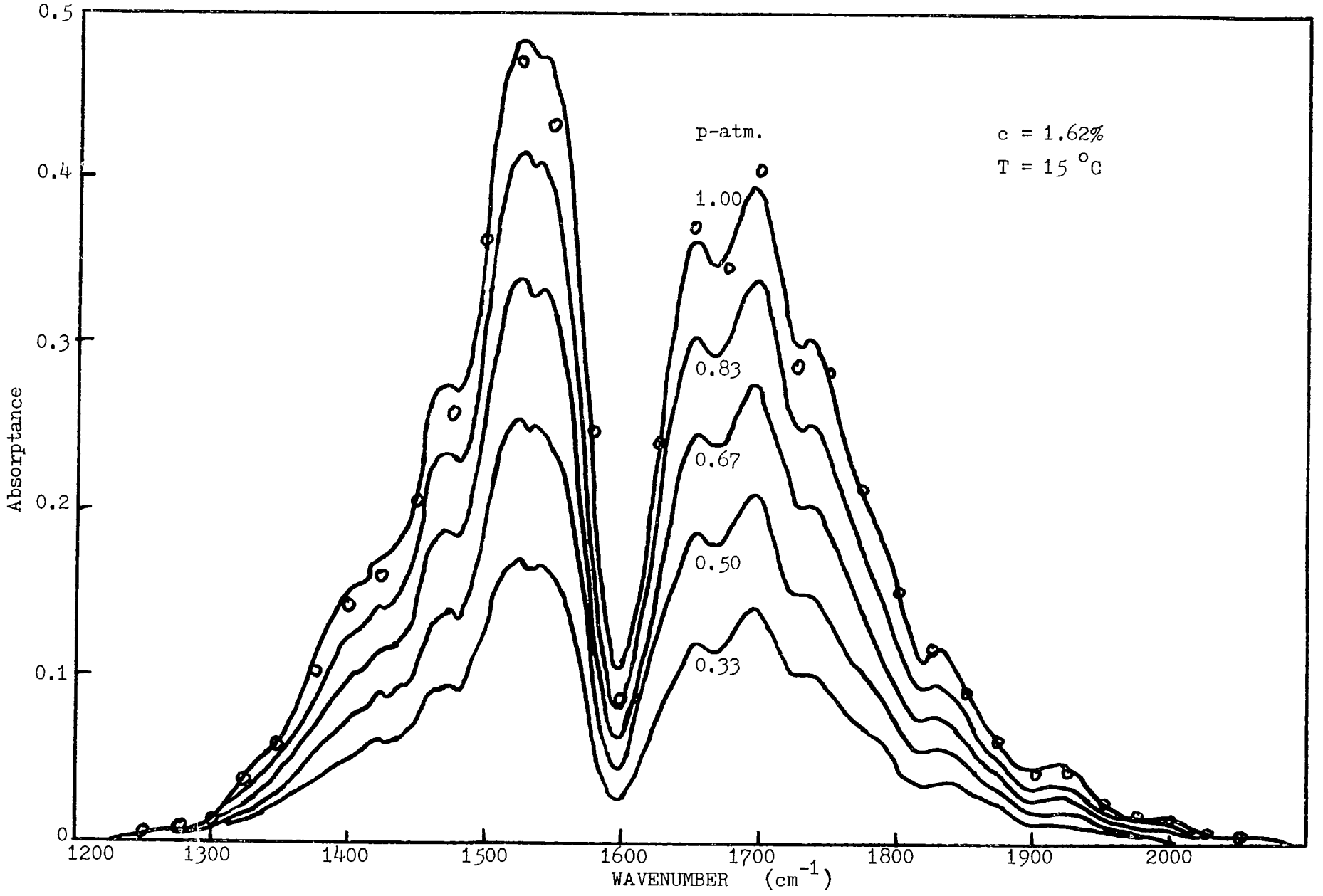


Figure 37. Absorptance as a function of pressure

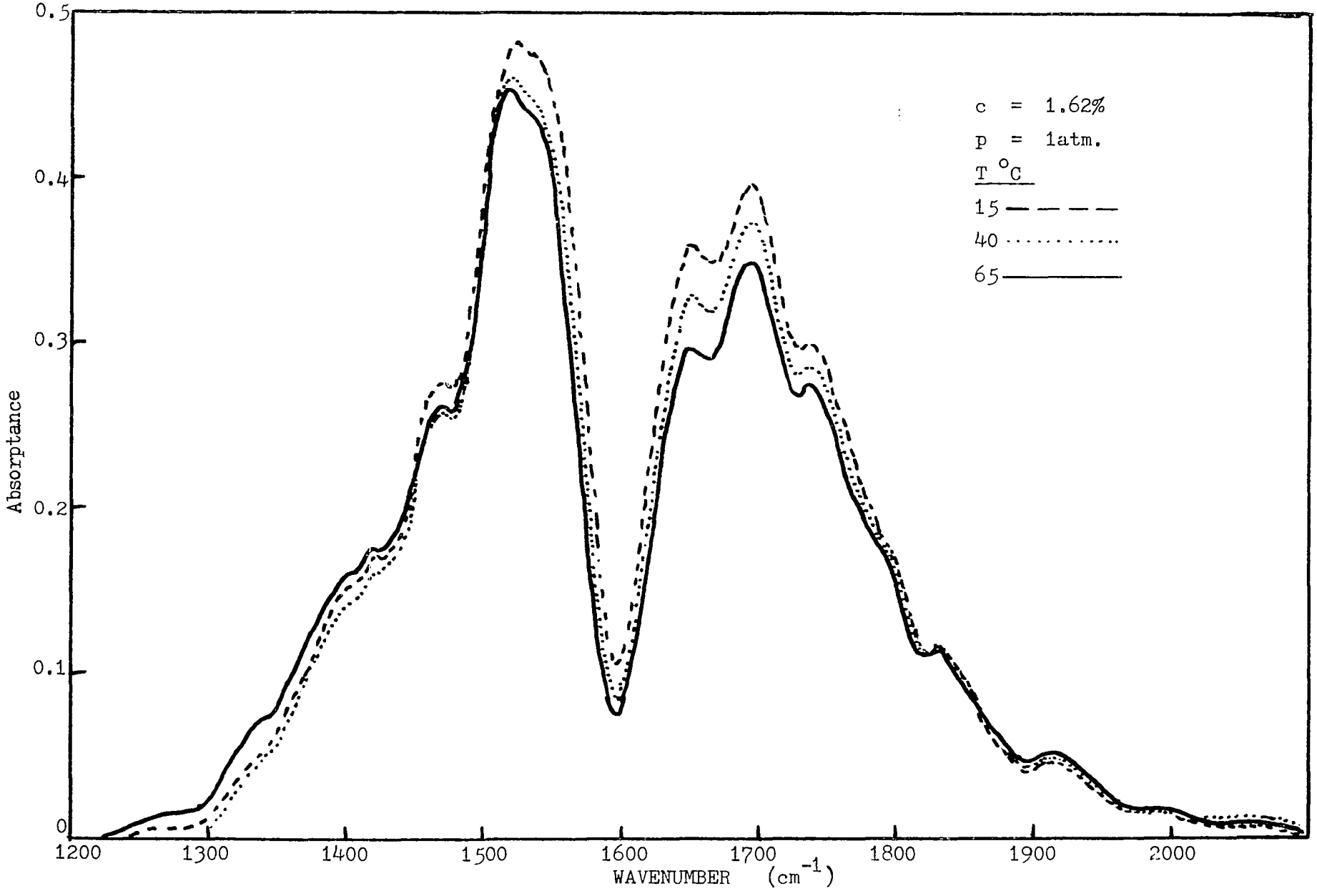


Figure 38. Absorptance as a function of temperature

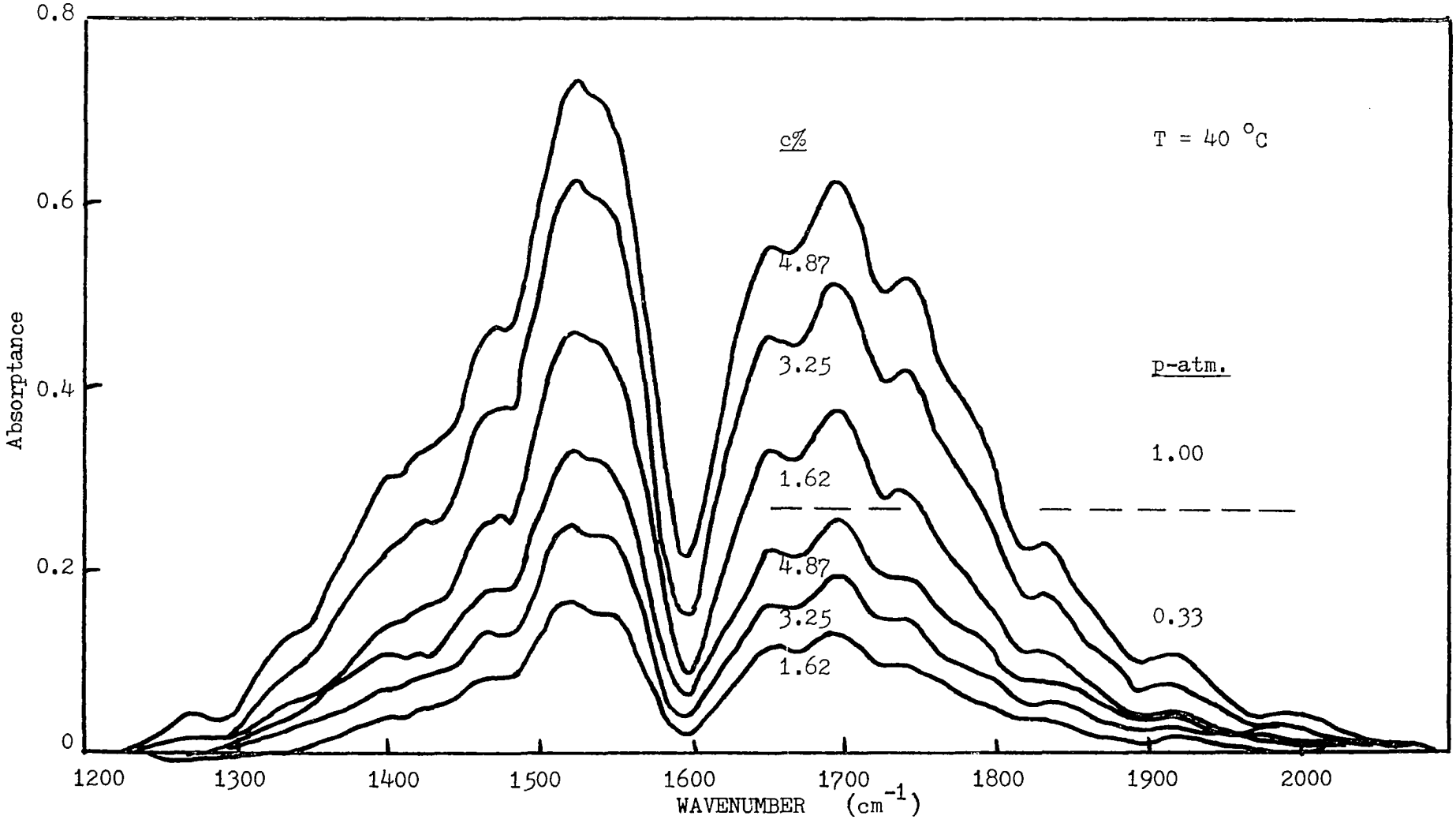


Figure 39. Absorptance as a function of concentration and pressure

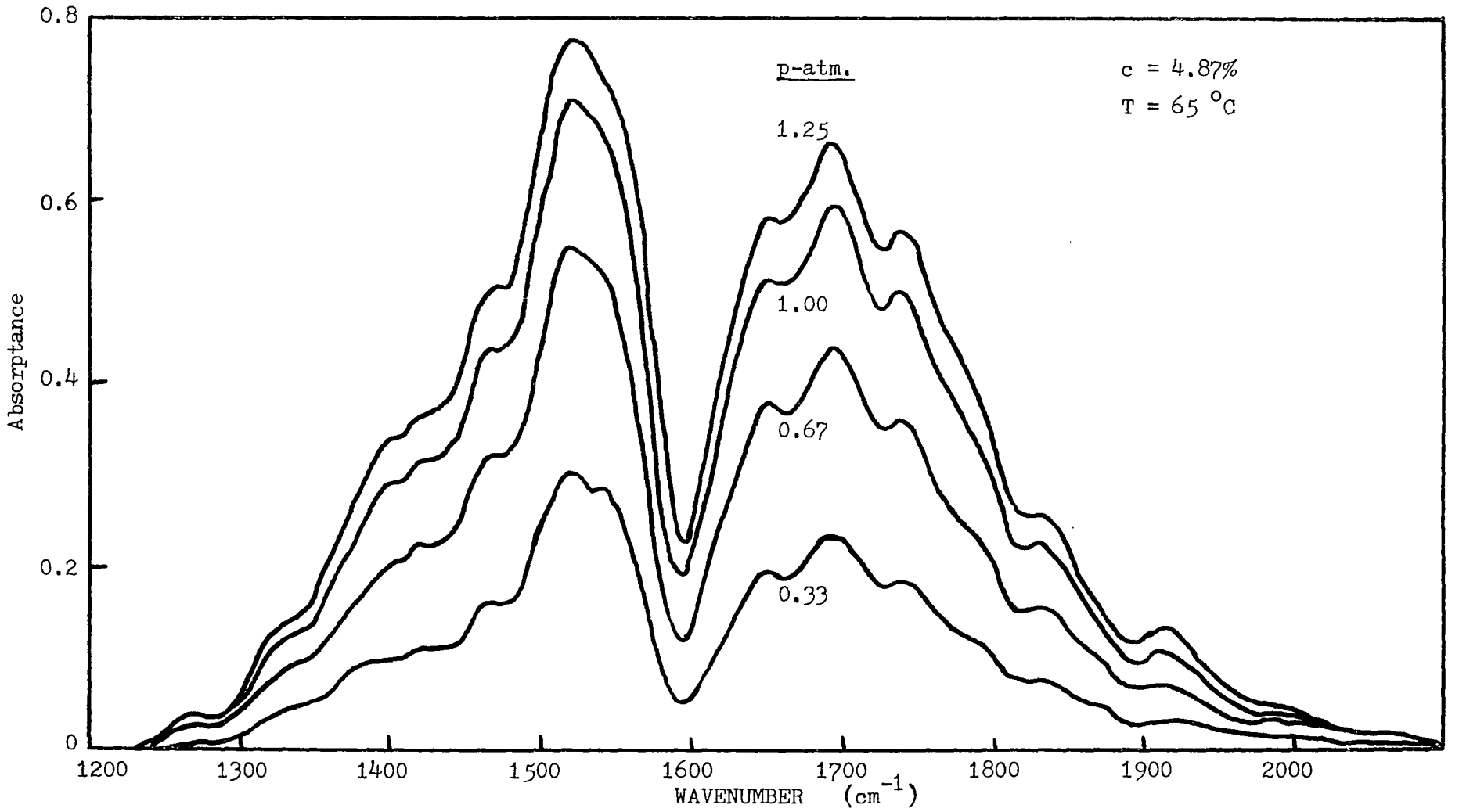


Figure 40. Absorptance as a function of pressure

compilations of line strengths were used , for which the uncertainty in the vibrational intensity is listed to be at least 5 per cent. The computational error is also about 5 per cent.[1] These three errors can account for the discrepancies observed. At low concentration the experimental error predominates, while at high concentration the error in the calculation becomes large. For these extreme cases table II indicates a discrepancy of the order of 10 per cent. At a medium concentration the discrepancy between calculation and experiment drops to as low as 5 per cent.

The precision of the experimental spectral values depends mostly upon the short term fluctuations in concentration and globar intensity (again see figure 32). Each is of the order of 0.3 percent, hence in a single reading the error does not exceed 0.5 per cent. The transmittance of the vapor, i.e. the ratio of the intensity through the vapor filled and the empty cell, carefully correcting for background water absorption, thus has a precision of about 1 per cent. For an absorptance A of 0.5, there is an absolute error in A of 5×10^{-3}. Then the absolute error in the first order difference dA is 10^{-2}, and in the second order difference d^2A is 2×10^{-2}. The relative range over which the thermodynamic parameters are varied in the evaluation of the derivatives is $\Delta c/c \approx \frac{1}{2}$, $\Delta p/p \approx \frac{1}{2}$, and $\Delta T/T \approx 1/6$. This means that the absolute precision in the first derivative, $y\partial A/\partial y$, varies from 0.02 to 0.06. Likewise the absolute precision in the various second derivatives, $xy\partial^2 A/\partial x \partial y$, can vary from 0.05 to 0.15. Use is made of the derivative times their

respective variables in the form as given since these have the same units and order of magnitude as A.

At low concentration the experimental error and the error estimate of the calculated spectral values can account for the difference between the experimental and calculated spectra. However, near the absorption peaks for high concentration larger discrepancies occur. A closer inspection reveals that under those conditions more than 5 rotational lines strongly interact. Hence, this is the limit of applicability of this calculation.

D. Derivative Spectra

The data sequence as displayed in table III was constructed as an aid in determining the c, p, and T values needed for obtaining first and second order derivatives. At any reference point determined by the average of the c, p, or T values, the experimental first order derivatives may be obtained from two absorption spectra. Using three absorption spectra one can interpolate and find the spectrum at a different c, p, or T point. This is convenient in the case of pressure, since most of the data is at or below 1 atmosphere.

In figures 41 to 43 the calculated first derivatives are computed for the experimental c and T conditions listed by using calculated first and second derivatives at 1 atm and 14.55 ^{o}C (dots and circles). These derivatives may be compared with the experimental derivatives (solid lines).

Experimental second derivatives and mixed derivatives are

TABLE III

Values of c, p and T for derivative spectra

c(%) \ P(atm)		1/3	1/2	2/3	5/6	1	5/4
0.4	15°C					x	
	40°C						
	65°C						
0.8	15°C					x	
	40°C						
	65°C						
1.6	15°C	x	x	x	x	x	
	40°C	x		x		x	
	65°C	x				x	
3.2	15°C						
	40°C	x				x	
	65°C						
4.8	15°C						
	40°C	x				x	
	65°C	x		x		x	x

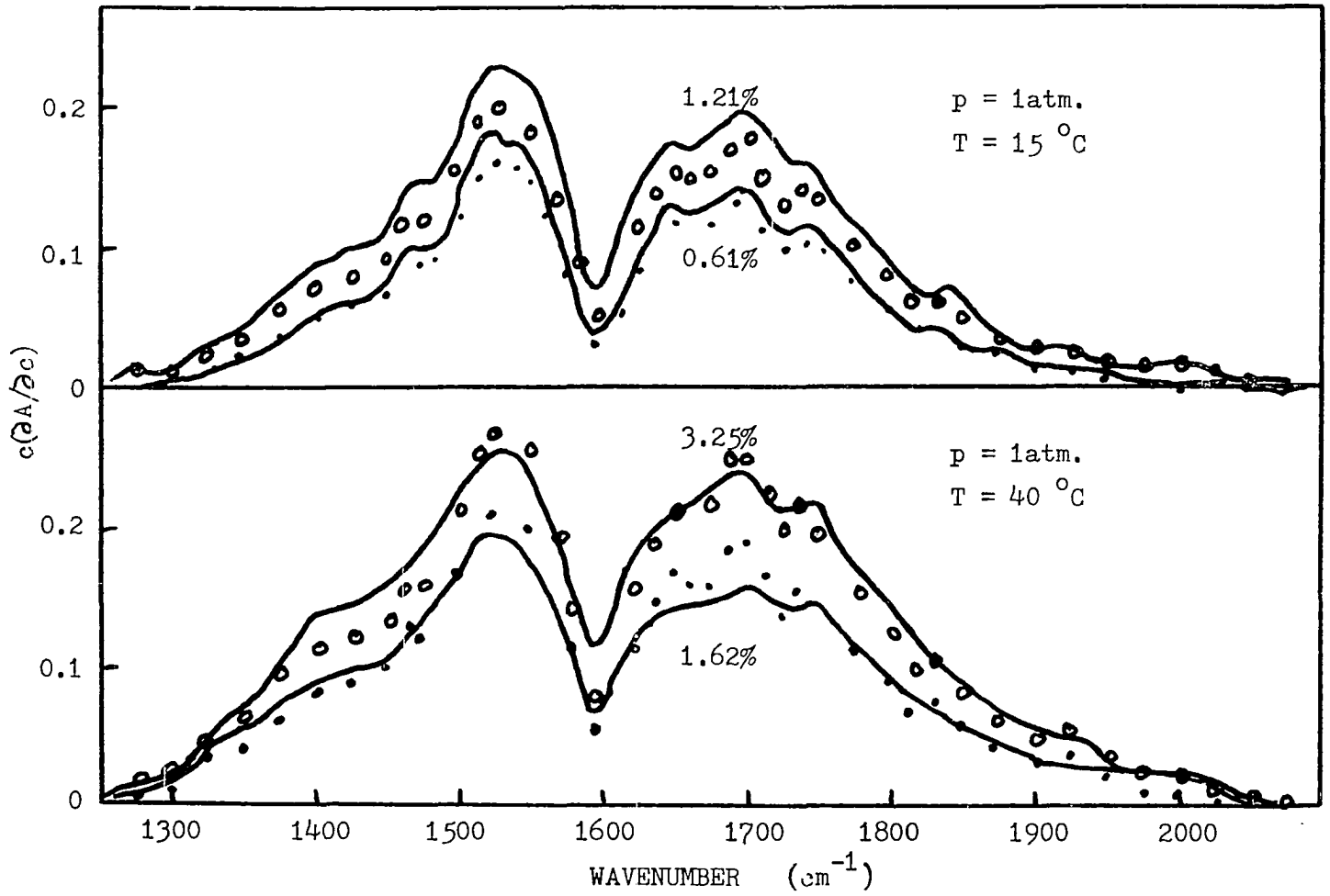


Figure 41. The partial derivative of the absorptance with respect to the concentration at constant pressure and temperature. The calculated values indicated by the circles and dots refer to the higher and lower concentrations, respectively. There is agreement within the estimates of error.

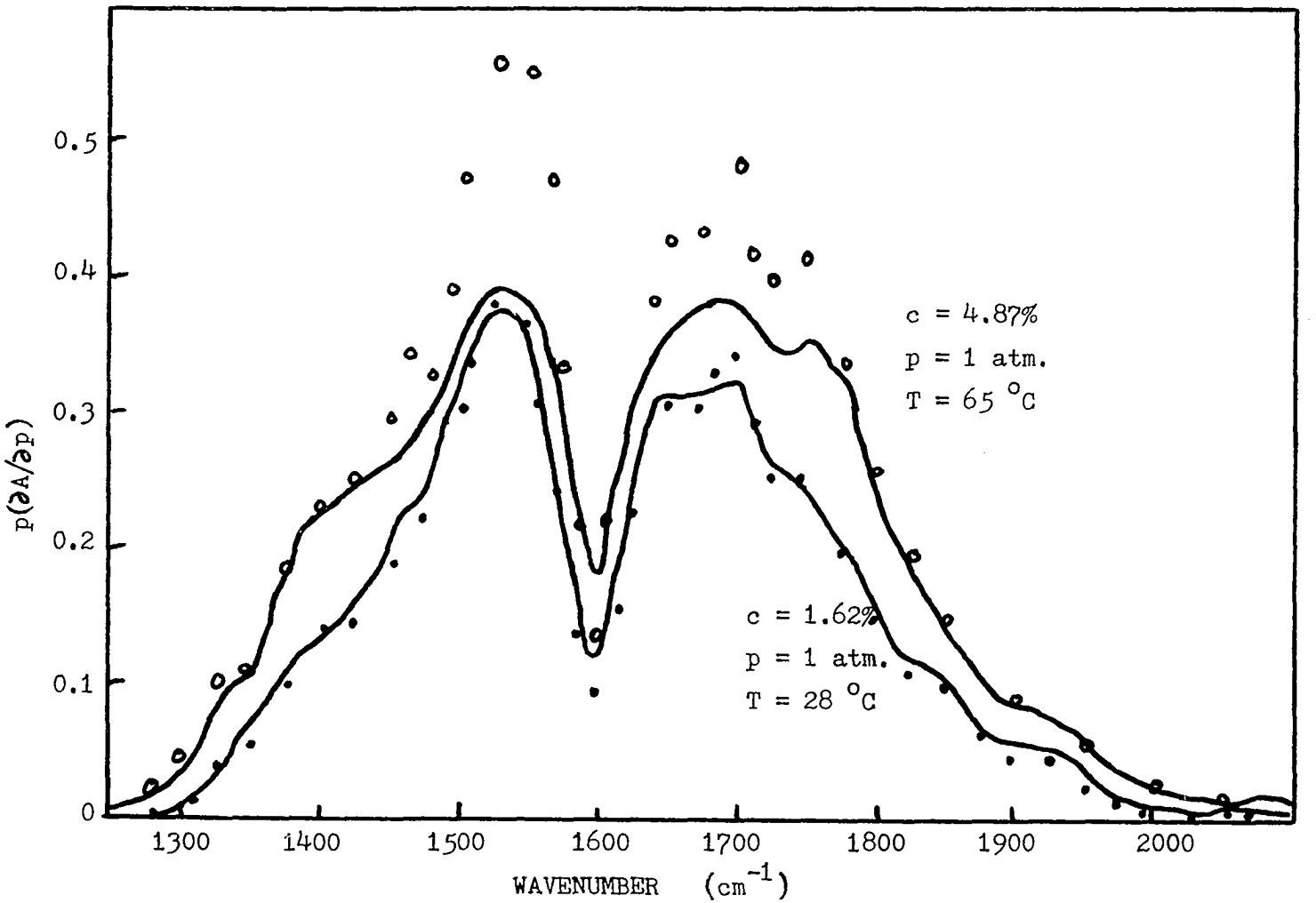


Figure 42. The partial derivative of the absorptance with respect to the pressure at constant concentration and temperature. The calculated values (dots) fit the low concentration experimental curve. The circles differ with the high concentration curve at the peaks of the absorption.

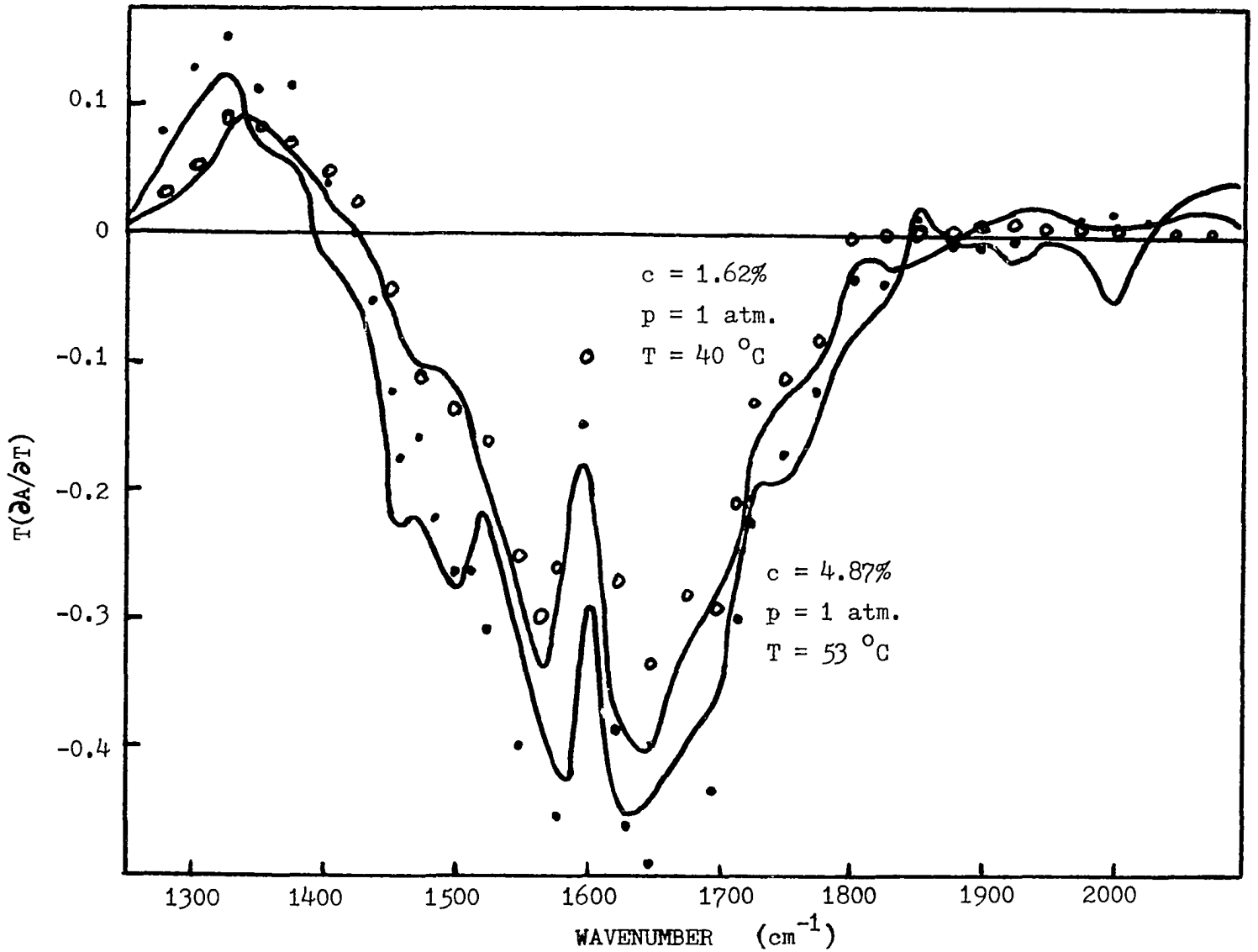


Figure 43. The partial derivative of the absorptance with respect to the temperature at constant concentration and pressure. There is good agreement between the calculated values (circles) and the low concentration experimental curve. There is no large systematic discrepancy between the calculated values (dots) and the high concentration curve.

obtained from 3 or 4 absorption measurements spaced at regular c, p, or T intervals. The averages of the c, p, and T values serve as the reference point.

In figures 44to 47, the calculated values of the second derivatives are indicated with dots for 1 atm, 14.55 °C and various concentrations. The circles indicate calculated values, which are corrected to the actual experimental c, p, and T reference point. These corrections are obtained for a given spectral position by using a power law, $A \propto y^{z(\nu)}$, to express the c, p, and T dependence. The exponent $z(\nu)$ is found by taking the ratio of the calculated first derivative, $y\partial A/\partial y$, and the absorption. Similarly the ratio of the second derivative, $y^2\partial^2 A/\partial y^2$, and the first derivative, $y\partial A/\partial y$, equals $z(\nu) - 1$. In the case of concentration $z(\nu)$ ranges from 0.25 to 0.65, while for pressure $z(\nu)$ varies from 0.5 to 1.0. The temperature dependence, which changes sign, must certainly be examined for each spectral point. Because the power law is approximate, both sets of calculated points, uncorrected (dots) and corrected (circles), should be considered. In the former the derivative is less uncertain, while in the latter the c, p, and T reference point is appropriate to the experiment.

In figure 48 the absorber mass and concentration are such that the calculation can be expected to be accurate. The experimental curve by Burch, et al.[12] indeed fits the calculation (circles). For this curve the integrated absorption is 160 cm^{-1}, while for our calculated spectrum it is 164 cm^{-1}.

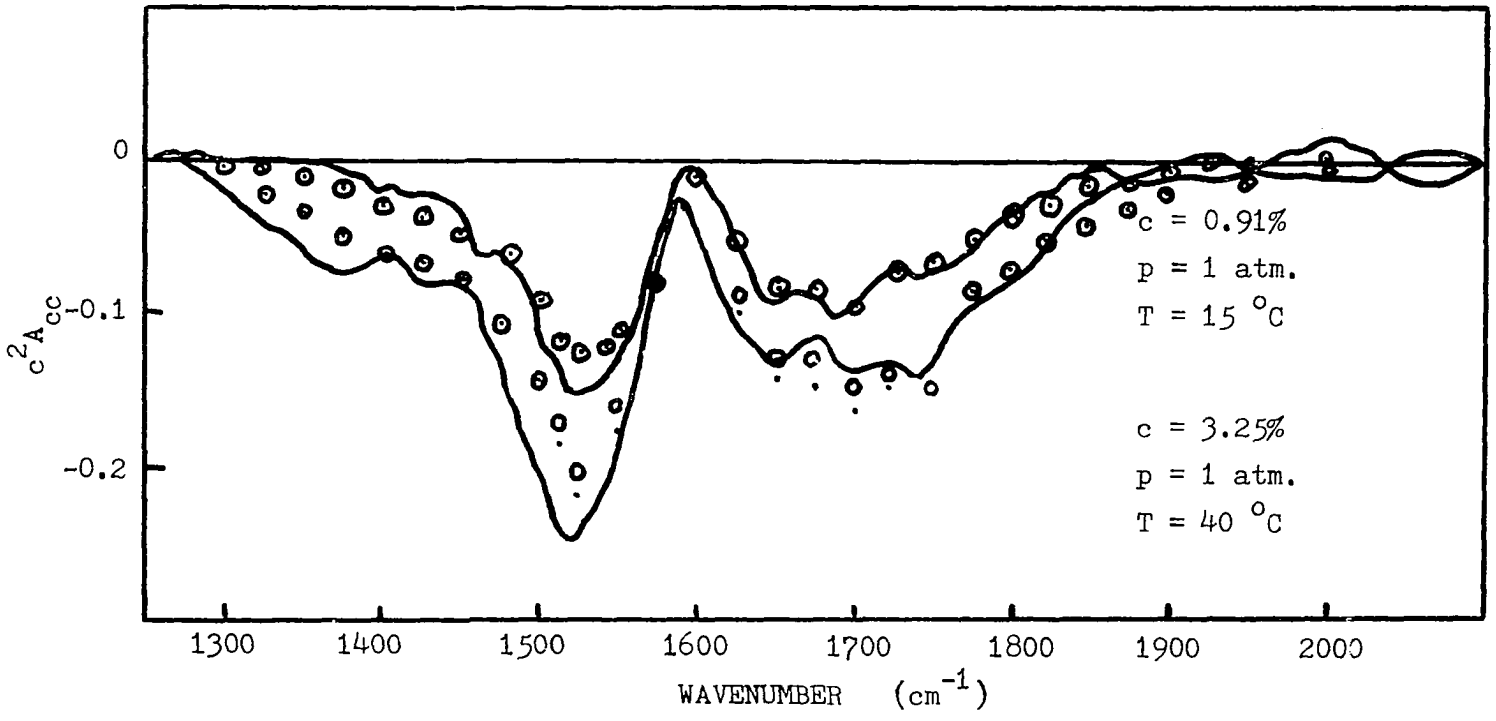


Figure 44. The second partial derivatives of the absorptance with respect to concentration at constant pressure and temperature. At low concentration there is good agreement with the calculation (circles). The difference of the calculated values and the high concentration curve is still within the error estimate.

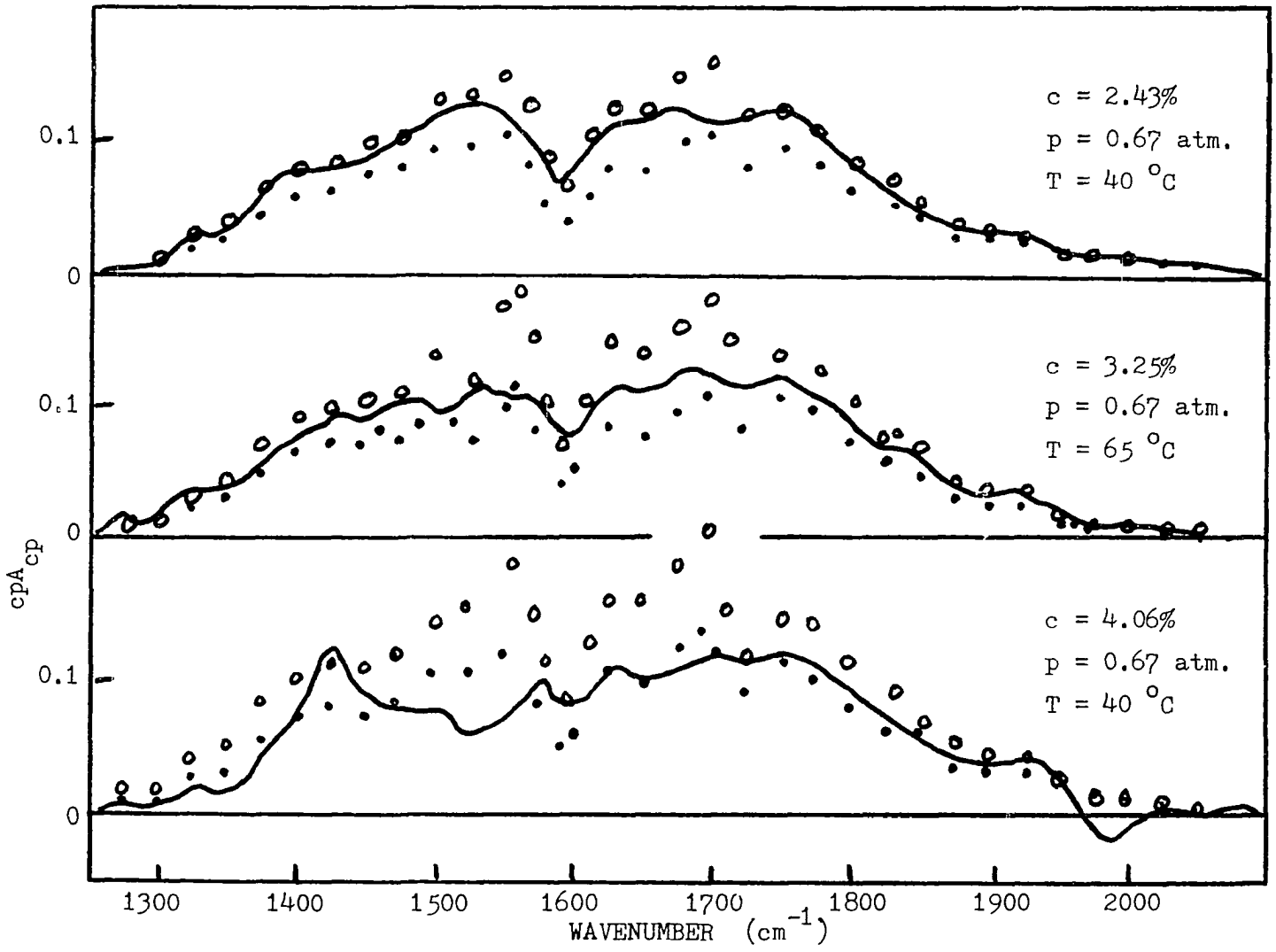


Figure 45. The second partial derivative with respect to concentration and pressure. At low concentration the calculation fits within the error estimate. At the highest concentration the discrepancy is due to calculation errors.

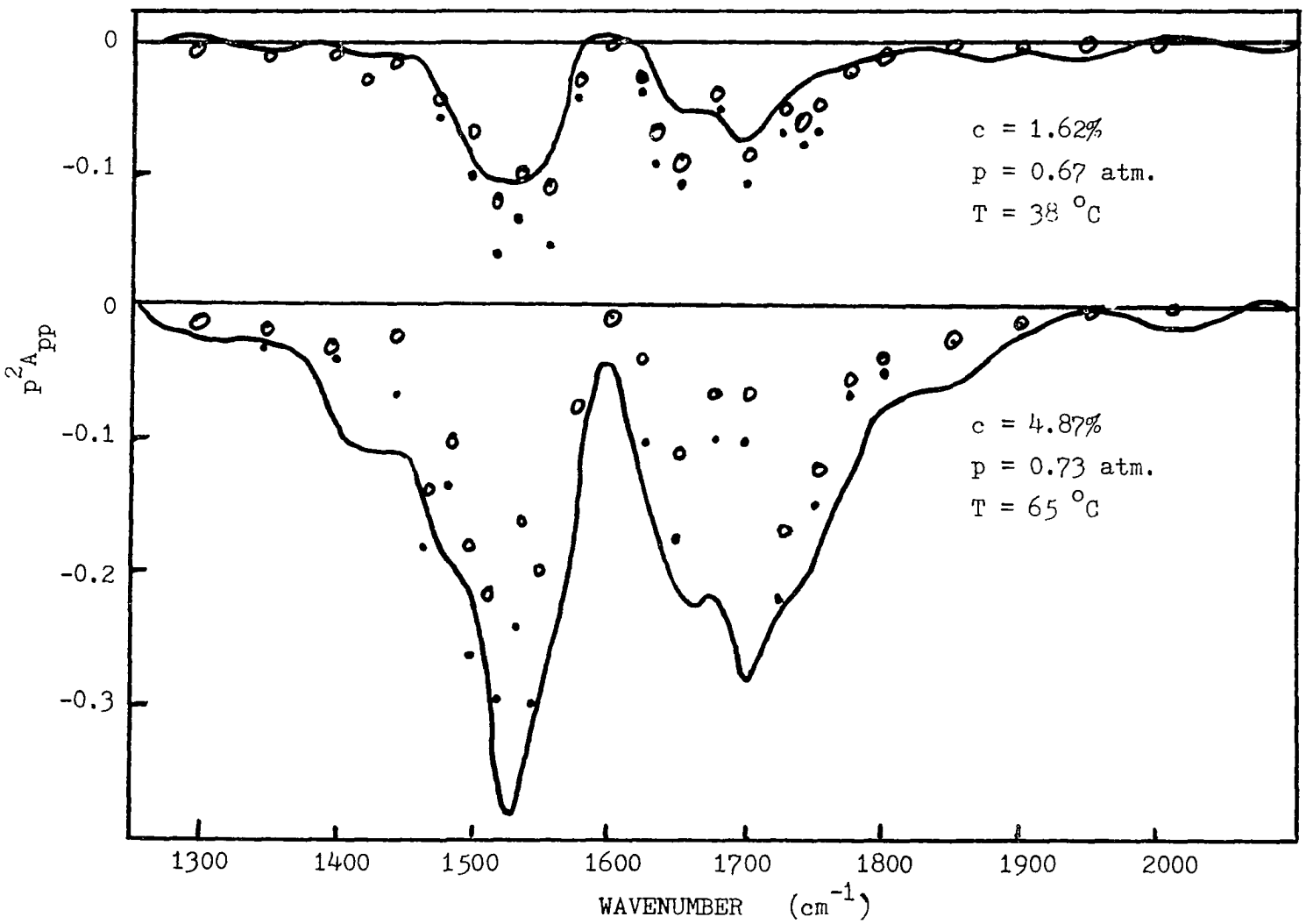


Figure 46. The second partial derivative of the absorptance with respect to pressure at constant concentration and temperature. At low concentration agreement exists with the calculated values (circles). At the high concentration in the center of the band the calculation (circles) does not agree within the expected error.

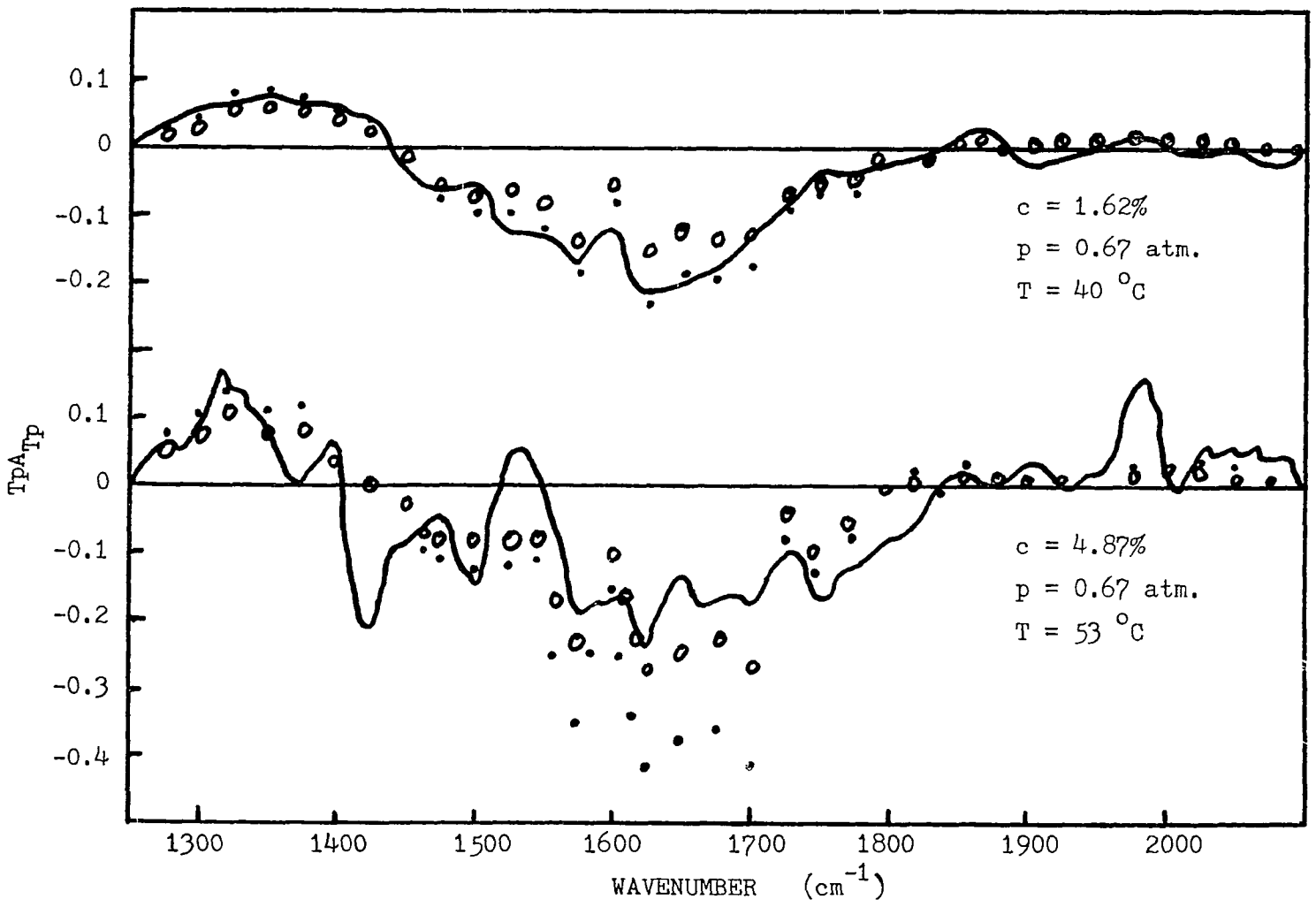


Figure 47. The second partial derivative of the absorptance with respect to pressure and temperature. The error-peaks in the lower experimental curve can be expected, because we use a small relative base of $\Delta T/T = 1/12$. For the high concentration, in the center of the band, the calculation of the pressure derivative is subject to an additional error.

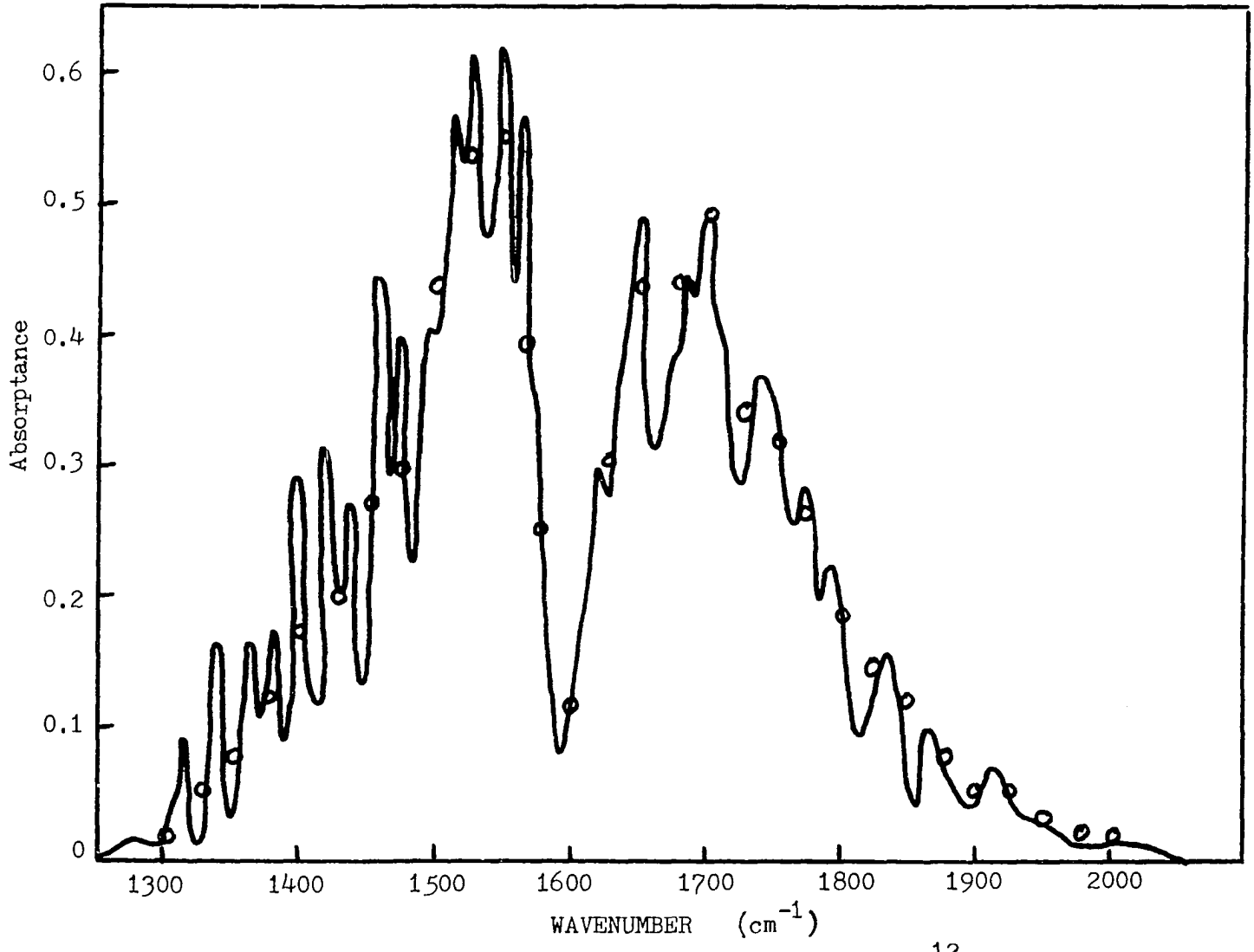


Figure 48. Experimental absorptance curve by Burch, et al.[12], for absorber mass 0.0018 gm/cm^2 and 1.017 atm. The circles represent our calculation for this mass and pressure at 15 °C, degraded to 25 cm^{-1}. Burch's experimental curve is degraded to about 10 cm^{-1}.

E. Conclusions

As the spectra of the absorption derivatives show, the thermodynamic parameters have rather different effects at various locations. For example, near a wavenumber of 1400 cm^{-1} and in the region of 1800 - 1900 cm^{-1} the dependence upon T is minimal. On the other hand near 1325 cm^{-1} the relative effect of T exceeds that of c and p. This same dependence can also be noted for $\partial^2 A/\partial T \partial p$. Moreover, at least for a low absorber mass, $\partial^2 A/\partial p^2$ is small in the wings of the band. Therefore $\partial^2 A/\partial c \partial p$ is significant in the wing and can in principle be used for a measurement of c. These derivatives are related to the c, p, or T dependence of the adiabatic pressure derivative, which occurs in the description of turbulence. The use of particular spectral regions to obtain information about c, p, and T from these derivatives has been suggested by Krause, et al.[21]

Evidently, the first and second derivative spectra can be obtained with a fairly simple instrument.[22] We also show that if the absorptance is below 0.6, a calculation based on individual rotational line parameters can give derivative spectra with sufficient accuracy. We omitted the extra effect due to self-broadening. For a concentration below 3 per cent this does not significantly affect our conclusions, however, above 4 per cent it will have to be considered.

Many aspects of work in the infrared have been emphasized in recent years. It has found uses ranging from detecting clear air turbulence (CAT) to studies in space astronomy. Some aspects have strong scientific appeal while others relate to the impact of

technology on the quality of life.

It has been reported for the atmosphere that a correlation may exist between the water vapor concentration and the extent of turbulence.[23] If this is true, in order for an airplane to be able to avoid CAT, it only needs an infrared sensitive device to continuously monitor water vapor concentrations in the intended path of the aircraft. The detection of CAT could be sensed from distances exceeding 60 miles, allowing the aircraft ample time to avoid the hazard.

Concerning the applications of the infrared in astronomy, two aspects may be mentioned. First there is the study of planetary surfaces enabling one to deduce the composition of the planet's atmosphere as well as the effective temperature of the radiating surface.[24] For example, as early as 1932 reflected light from the surface of Venus was studied. More recently worldwide attention has been focused on the Moon and Mars. Secondly there have been major efforts made to ultilize infrared in gaining knowledge about stars and galaxies. For so long it was thought that stars were too hot to emit radiation excesses in this part of the electromagnetic spectrum. It was a surprise when it was first discovered that some stars emit substantial infrared radiation.[25] Galaxies also are of interest here since, for example, galactic centers have been observed in the infrared while all visible light was extinguished because of the intervening galactic material.

APPENDIX I

SPECTROSCOPIC UNITS

Wavenumber is frequency/velocity of light, or wavenumber is λ^{-1} in units of cm^{-1}.

Line strength S as defined by equation (7) has the units of frequency per absorber path length or $sec^{-1}(gm/cm^2)^{-1}$. When we use wavenumber rather than frequency, then S has the units of cm/gm.

Because half-width α depends inversely on the mean molecular collision time, its units would be sec^{-1}. Again, using the wavenumber the units of α are cm^{-1}.

Precipitable water u is the amount of water contained in a gaseous column of unit cross section and therefore has the units of gm/cm^2.

APPENDIX II

EQUIPMENT LIST

1. Monochromator
   Model 218, 0.3 meter
   McPherson Instrument Corporation
   Acton, Massachusetts

2. Humidity Chamber ($\pm$ 1% RH, $\pm$ 0.5 ^{o}C dry bulb)
   Model VP-100AT-1
   Blue M Electric Company
   Blue Island, Illinois

3. Flowmeters (10-1900 ml/min air, 2%accuracy)
   Roger Gilmont Instruments, Inc.
   Great Neck, New York

4. Compressor (Vacuum) Pump
   Model MB-21
   Metal Bellows Corporation
   Sharon, Massachusetts

5. Dew Point Hygrometer (Accuracy $\pm$ 1.5 ^{o}F dew point)
   Model 880
   EG & G Cambridge Systems, Inc.
   Environmental Equipment Division
   Waltham, Massachusetts

6. Photoelectric Manometer Controller
   Mano-Watch Model MW-1
   I^2R
   Instruments for Research and Industry
   Cheltenham, Pennsylvania

7. Cooling Unit (0.15 ^{o}C control)
   Model PCC-13A-3
   Blue M Electric Company
   Blue Island, Illinois

8. Pressure Gauges (Bourdon Tube Type) (0.1% of full scale accuracy)
   Model CM
   Heise Bourdon Tube Company, Inc
   Newton, Connecticut

9. Infrared Detector (HgCdTe)
   Vacuum Flask Style 520S
   Windows: IRtran II
   Santa Barbara Research Center
   Goleta, California

10. Preamplifier, Lock-in Amplifier
    Model 213 Model 220
    Princeton Applied Research Corporation
    Princeton, New Jersey

REFERENCES

1. S. Broersma and W. L. Walls, J. Opt. Soc. Am. 64, 1111 (1974).
2. C. Gordon Little, Bull. Am. Meteorol. Soc. 53, 936 (1972).
3. Ibid. p.944.
4. W. M. Elsasser, Heat Transfer by Infrared Radiation in the Atmosphere, (Howard University Press, Cambridge, Mass., 1942).
5. F. R. Krause, W. O. Davies and M. W. P. Cann, AIAA Journal 7, 587 (1969).
6. M. J. Fisher and F. R. Krause, J. Fluid Mech. 28, 705 (1967).
7. M. M. Wolff, J. Geophys. Res. 71, 2743 (1966).
8. Barney J. Conrath, J. Geophys. Res. 74, 3347 (1969).
9. John N. Howard and Robert M. Chapman, J. Opt. Soc. Am. 42, 423 (1952).
10. P. Varanasi and C. R. Prasad, J. Quant. Spectrosc. Radiat. Transfer 10, 65 (1970).
11. W. S. Benedict, H. H. Claassen and J. H. Shaw, J. Res. National Bureau Standards 49, 91 (1952).
12. Darrell E. Burch, David Gryvnak, Edgar B. Singleton, Wilbur L. France and Dudley Williams, AF 19(604)-2633, The Ohio State University (1960).
13. Jerald R. Izatt, Hajime Sakai and William S. Benedict, J. Opt. Soc. Am. 59, 19 (1969).
14. Gerhard Herzberg, Infrared and Raman Spectra, (D. Van Nostrand Company, Princeton, New Jersey, 1945), p.280.

15. J. T. Houghton and S. D. Smith, Infrared Physics, (Oxford University Press, 1966), p.46.

16. W. S. Benedict and R. F. Calfee, ESSA Professional Paper 2 (U.S. Government Printing Office, 1967).

17. M. W. P. Cann, Rev. Sci. Instr. 40, 595 (1969).

18. D. J. Lysobey, Ph. D. Thesis, University of Oklahoma (1972).

19. Handbook of Chemistry and Physics, 49th edition, Robert C. Weast (ed.), 1968.

20. G. N. Plass and H. Yates, Handbook of Military Infrared Technology, W. L. Wolfe (ed.), 1965, p.245.

21. F. R. Krause and J. B. Stephens, NASA TMX - 53711 (1967) p.297.

22. P. E. Hendrickson, W. L. Walls, and S. Broersma, Rev. Sci. Instr. 44, 347 (1973); P. E. Hendrickson, W. L. Walls, and S. Broersma, J. Opt. Soc. Am. 64, 1119 (1974).

23. Peter Kuhn, Newsweek, January 17, (1977) p.42.

24. Houghton and Smith, Infrared Physics, p.293.

25. V. Manno and J. Ring, Infrared Detection Techniques for Space Research, (D. Reidel Publishing Company, Dordrecht-Holland,1971), p.5.